Towards an *in vitro* model for age-related macular degeneration: Characterization of human induced pluripotent stem cell derived retinal pigment epithelial cells in 2D and 3D cultures

Dissertation

zur Erlangung des Grades eines

Doktors der Naturwissenschaften

der Mathematisch-Naturwissenschaftlichen Fakultät

und

der Medizinischen Fakultät

der Eberhard-Karls-Universität Tübingen

vorgelegt

von

Lena Mesch

aus Tübingen, Deutschland

2021

Tag der mündlichen Prüfung: 22.11.2021

Dekan der Math.-Nat. Fakultät: Prof. Dr. Thilo Stehle

Dekan der Medizinischen Fakultät: Prof. Dr. Bernd Pichler

1.Berichterstatter: Prof. Dr. Stefan Liebau

2.Berichterstatter: Prof. Dr. Peter Loskill

Prüfungskommission: Prof. Dr. Stefan Liebau

Prof. Dr. Peter Loskill

Prof. Dr. Meltem Avci-Adali

Prof. Dr. Ulrich Rothbauer

Erklärung / Declaration:

Ich erkläre, dass ich die zur Promotion eingereichte Arbeit mit dem Titel

Towards an *in vitro* model for age-related macular degeneration: Characterization of human induced pluripotent stem cell derived retinal pigment epithelial cells in 2D and 3D cultures

selbständig verfasst, nur die angegebenen Quellen und Hilfsmittel benutzt und wörtlich oder inhaltlich übernommene Stellen als solche gekennzeichnet habe. Ich versichere an Eides statt, dass diese Angaben wahr sind und dass ich nichts verschwiegen habe. Mir ist bekannt, dass die falsche Abgabe einer Versicherung an Eides statt mit Freiheitsstrafe bis zu drei Jahren oder mit Geldstrafe bestraft wird.

I hereby declare that I have produced the work entitled

Towards an *in vitro* model for age-related macular degeneration: Characterization of human induced pluripotent stem cell derived retinal pigment epithelial cells in 2D and 3D cultures

submitted for the award of a doctorate, on my own (without external help), have used only the sources and aids indicated and have marked passages included from other works, whether verbatim or in content, as such. I swear upon oath that these statements are true and that I have not concealed anything. I am aware that making a false declaration under oath is punishable by a term of imprisonment of up to three years or by a fine.

Tübingen, den …….. ……..

Unterschrift/Signature

Summary

The human retina is a complex tissue within the human eye and essential for the sense of sight. Retinal diseases, such as age-related macular degeneration (AMD) or retinitis pigmentosa (RP) affect or destroy the sense of vision and impair the quality of life of patients drastically. As currently for many retinal diseases there are only few, or no treatment options available and animal models recapitulate the pathology of those diseases poorly. Therefore, adequate *in vitro* models of the human retina and the supporting retinal pigment epithelium (RPE) are urgently required.

In AMD, pathological changes do not exclusively involve cells of the neural retina, but initial disease manifestation takes place within the retinal pigment epithelium (RPE) and its near surroundings. Therefore, various protocols for the differentiation of RPE cells from human pluripotent stem cells (hPSCs) have been developed in recent years, showing the generation of mature and functional RPE cells.

In this thesis, two distinct approaches for the differentiation of hiPSC-RPE have been applied and were subsequently investigated for several essential characteristics of RPE cells. These essential RPE hallmarks included molecular characteristics, pigmentation, and morphology. Overall analysis demonstrated that both approaches equivalently generated RPE cells of good quality.

Nevertheless, RPE cells which are cultured on plastic surfaces in 2D pose several disadvantages, as those conditions promote e.g. transdifferentiation or detachment from the culture plate. Consequently, long-term cultivation over several month to years remains difficult. In this thesis, those drawbacks were aimed to overcome by implementing a novel three-dimensional RPE organoid (RPEorg) approach. RPE organoids were differentiated simultaneously with retinal organoids and cultured for more than 300 days.

A basic characterization of early (day 80-100), intermediate (day 191) and aged (day 280-360) RPEorg was performed by immunostainings and qRT-PCR analysis. RPEorg expressed several common RPE markers, some of them strongly increasing with age. Deeper analyses of RPEorg showed ultrastructural signs of mature RPE cells, such as apical microvilli and tight junctions, as well as melanosomes. Functionality of RPE cells comprised in RPEorg was demonstrated by phagocytosis of bovine photoreceptor outer segments (POS). Overall, maturation of RPE cells with age could be observed.

As a next step, RPE organoids were investigated for age-related changes in the context for AMD. Therefore, RPEorg were stained for drusen-associated proteins, such as APOE and TIMP3, lipids and hydroxyapatite. Those data were supported by qRT-PCR analysis and showed presence and

partly upregulation of several disease relevant markers with aging. Additionally, transmission electron microscopy revealed ultrastructural signs of drusen formation in aged RPEorg.

To summarize, RPEorg are a suitable model for mature RPE and allows for investigations of age-associated changes related to AMD. Long-term cultivation of RPEorg enables studies of early stages of disease manifestation and drusen formation, which renders it suitable for pathomechanistic as well as drug developmental studies.

Zusammenfassung

Die menschliche Retina ist ein komplexes Gewebe auf der Rückseite des Augapfels und grundlegend für den Sehsinn. Erkrankungen der Retina, wie zum Beispiel Altersabhängige Makuladegeneration (AMD) oder Retinitis Pigmentosa (RP) beeinträchtigen oder Zerstören den Sehsinn und verschlechtern dadurch die Lebensqualität der Patienten erheblich. Da es momentan für viele retinale Erkrankungen nur wenige oder gar keine Behandlungsmöglichkeiten gibt und Tiermodelle die Pathologie solcher Erkrankungen nur unzureichend darstellen können, werden geeignete *in vitro* Modelle der menschlichen Retina und des unterstützenden Retinalen Pigment Epithels (RPE) dringend benötigt.

Bei AMD betreffen die pathologischen Veränderungen nicht nur die Zellen der neuralen Retina, sondern die anfängliche Manifestation findet in den Zellen des RPE und seiner direkten Umgebung statt. Innerhalb der letzten Jahre wurden daher verschiedene Protokolle zur Differenzierung von RPE Zellen aus humanen indizierten pluripotenten Stammzellen (hiPSZ) entwickelt und bringen reife und funktionelle RPE Zellen hervor. In der vorliegenden Arbeit wurden zwei Ansätze zur Produktion von RPE Zellen aus hiPSZ verwendet und die RPE Zellen anschließend in Bezug auf wichtige RPE Charakteristika analysiert. Als wesentliche Charakteristika wurden die Pigmentierung und Morphologie der Zellen untersucht, sowie Immunfärbungen und qRT-PCR von wichtigen RPE Markern durchgeführt. Dabei zeigte sich, dass beide Ansätze RPE Zellen vergleichbarer Qualität generieren.

Die zwei-dimensionale Kultivierung auf RPE auf Plastikoberflächen hat jedoch einige Nachteile, da diese mit der Zeit das Ablösen von der Zellkulturplatte oder die Transdifferenzierung von RPE Zellen begünstigen. Dadurch ist eine Langzeit Kultivierung über mehrere Monate oder sogar Jahre schwierig. Um diese Nachteile zu überwinden, wurde in dieser Arbeit ein neuartiger drei-dimensionaler RPE Organoid (RPEorg) Ansatz verfolgt. RPE Organoide wurden mit Retina Organoiden zusammen differenziert und für mehr als 300 Tage kultiviert.

Eine umfangreiche Charakterisierung von frühen (Tag 80-100), mittelalten (Tag 191) und gealterten (Tag 280-360) RPE Organoiden wurde mithilfe von Immunfärbungen und qRT-PCR Analysen durchgeführt. RPEorg exprimieren einige klassische RPE Marker, die teilweise mit zunehmendem Alter der Organoide stärker exprimiert wurden. Zusätzlich konnten ultrastrukturelle Zeichen von reifem RPE identifiziert werden, wie beispielsweise apikale Mikrovilli und Tight Junctions, sowie Melanosomen. Die Funktionalität der RPE Zellen konnte durch Phagozytose von bovinen Photorezeptor-Außensegmenten gezeigt werden. Generell konnte eine Reifung der RPE Zellen mit zunehmendem Alter beobachtet werden.

Im nächsten Schritt wurden RPE Organoide auf altersbedingte Veränderungen im Zusammenhang mit AMD untersucht. Dafür wurden Immunfärbungen und Live-Imaging für Drusen-assoziierte Proteine, wie zum Beispiel APOE und TIMP3, Lipide und Hydroxyapatit durchgeführt. Die Daten wurden weiterhin durch qRT-PCR Analysen unterstützt und zeigten die Expression und teilweise Hochregulation von einigen krankheits-assoziierten Markern mit steigendem Alter der RPEorg. Elektronenmikroskopische Bilder zeigten außerdem ultrastrukturelle Anzeichen von Drusen Bildung in gealterten RPEorg.

Zusammenfassend sind RPEorg ein geeignetes Modellsystem für reifes RPE und ermöglichen Untersuchungen von altersbedingten Veränderungen im Zusammenhang mit AMD. Die Langzeit-Kultivierung von RPEorg ermöglicht Studien von frühen Stadien der Krankheitsentwicklung und Drusen Bildung, wodurch sie sich sehr gut für pathomechanistische Studien und für die Entwicklung von Arzneistoffen eignen.

Table of Contents

List of Abbreviations

AA	Antibiotics-antimycotics
AF	Autofluorescence
AMD	Age-related macular degeneration
APOE	Apolipoprotein E
APP	Amyloid precursor protein
ATP	Adenosine triphosphate
BEST1	Bestrophin-1
BRDM	B27-based retinal differentiation medium
BrM	Bruch's membrane
CDL	Chemically defined lipid
cDNA	Complementary DNA
CFH	Complement factor H
CO_2	Carbon dioxide
CRYAA/B	Crystallin Alpha A/B
d	Day
DAPI	4′,6-diamidino-2-phenylindole
Dkk-1	Dickkopf WNT signaling pathway inhibitor 1
DMEM	Dulbecco's modified eagle medium
DNA	Deoxyribonucleic acid
dNTP	Dideoxynucleotide
EB	Embryoid body
ECM	Extracellular matrix
EGF	Epidermal growth factor
EtOH	Ethanol
FBS	Fetal bovine serum
FGF	Fibroblast growth factor
FITC	Fluorescein isothiocyanate
GAPDH	Glyceraldehyde 3-phosphate dehydrogenase
GFR	Growth-factor reduced
h	Hour
HAP	Hydroxyapatite
hESC	Human embryonic stem cell
hiPSC	Human induced pluripotent stem cell
HSA	Human serum albumin

ITS	Insulin-transferrin-sodium selenite supplement
IPM	Interphotoreceptor Matrix
LRAT	Lecithin Retinol Acyltransferase
mRNA	Messenger RNA
MG	Matrigel
min	Minutes
MITF	Microphthalmia-associated transcription factor
MMLV-RT	Moloney murine leukemia virus reverse transcriptase
NEAA	Non-essential amino acids
NIC	Nicotinamide
NR	Neural retina
OS	Outer segments
OsO_4	Osmium Tetroxid
O_2	Oxygen
O/N	Overnight
PBS -/-	Phosphate buffered saline w/o calcium and magnesium
PCR	Polymerase chain reaction
PFA	Paraformaldehyde
pH	Potentia hydrogenii
PMEL	Premelanosome protein
POS	Photoreceptor outer segment
PRC	Photoreceptor cell
qRT-PCR	Quantitative real-time PCR
RA	Retinoic acid
RO	Retinal organoid
RNA	Ribonucleic acid
RPE	Retinal pigment epithelium
RPE-DM	RPE differentiation medium
RPEorg	RPE spheroid
RPE65	RPE-specific 65 kDa protein
rpm	Revolutions per minute (1/min)
RPS9	Ribosomal Protein S9
RT	Room temperature
SERPINF1	Serpin family F member 1
TEM	Transmission electron microscope
TGF	Transforming growth factor

TIMP3	Tissue inhibitor of metallopeptidase 3
TJ	Tight junction
T-X	Triton-X
VTN	Vitronectin
w/o	Without
ZO-1	Zonula occludens-1
%	Percentage
°C	Degree Celsius
2D	Two-dimensional
3D	Three-dimensional

List of Tables

List of Figures

1 Introduction

1.1 Anatomy of the human eye and retina

The human eye is an essential sensory organ which enables us to perceive our environment visually. The structure of the eye is complex and can be divided into three main layers (Figure 1-1 a). The external layer is surrounding the eyeball and consists of the transparent cornea and the sclera. The proximate intermediate layer contains iris and ciliary body in the front and the choroid, also called the vascular layer of the eye, in the back. The third, internal layer is the retina, which is responsible for light sensing and signal transmission. When a light beam enters the eye, it passes cornea, pupil, lens and vitreous body before reaching the retina, where the signal is taken up by the sensory cells of the retina, namely photoreceptors [1].

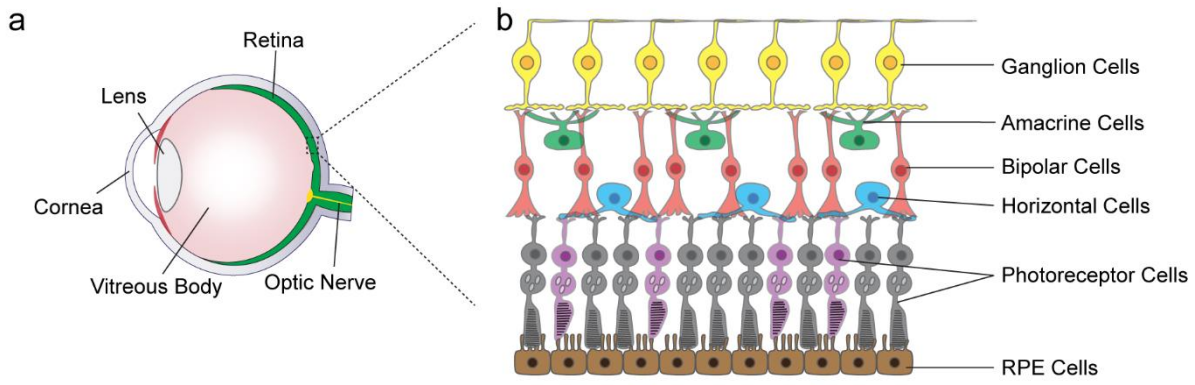

Figure 1-1: Structure of a human eye and enlargement of the retina.
A cross section visualizes the three main layers of the human eye (a): Sclera and cornea form the external layer, iris and ciliary body are components of the intermediate layer and the internal layer consists of the retina (enlarged in b). The retina itself is stratified in a defined order from ganglion cells, amacrine cells, bipolar cells, horizontal cells, photoreceptor cells and retinal pigment epithelial (RPE) cells (from the inside outwards).

The human retina is 200-500 µm thick and 30-40 mm in diameter [2]. The retina is inverse, which means that the ganglion cells are oriented towards the inner part of the eye, while the photoreceptor (PR) cells are located outermost in the retina, in close contact to the retinal pigment epithelium (RPE) and the choroid. Consequently, the light beam has to first pass all the other layers of the retina before reaching the light sensory PR cells.

The retina itself can be morphologically subdivided in ten layers (Figure 1-1 b). From the outside to the inside, or from choroid to vitreous, the first layer is the RPE cell layer. It is not only responsible for nourishment of the neural retina (NR) and phagocytosis of PR outer segment discs,

but also essential for the maintenance of the visual cycle [3]. In essence, the RPE cell layer is a supporting structure for the neural retina, which itself comprises the subsequent nine layers.

Outer segments (OS) and inner segments (IS) of the photoreceptor cells form the second layer of the retina, followed by the outer limiting membrane (OLM), which separates the IS of PR cells from their nuclei. The adjacent outer nuclear layer (ONL) includes the nuclei and cell bodies of PR cells. In the outer plexiform layer (OPL), rods and cones form synapses with bipolar cells and horizontal cells. The subsequent inner nuclear layer (INL) contains nuclei of amacrine cells, bipolar cells, horizontal cells and Müller glia. In the inner plexiform layer (IPL), bipolar cells and ganglion cells build synapses to transfer the signal and additionally, amacrine cells form connections and modify the signal before it is transmitted to the brain. In the ganglion cell layer (GCL), the nuclei of ganglion cells are located, while their axons form the optic nerve itself in the optic nerve fiber layer (OFL). The final layer is the inner limiting membrane (ILM), which separates the neural retina from the vitreous [2], [4], [5].

The light sensory cells of the retina are photoreceptor cells, more specifically achromatic rods and chromatic cones. The outer segments of photoreceptor cells contain the wave-length specific visual pigments L (long-wave = red)/M (middle = green)/S (short = blue)-opsin (cones) and rhodopsin (rods), which are activated by light absorption and initiate the phototransduction cascade. As a result, an electrical signal is generated and transmitted towards bipolar, amacrine and horizontal cells. Those three cell types are defined as interneurons and do not only transmit, but also process the signal for e.g., noise reduction or amplification. Subsequently, the adapted signal is transferred to the ganglion cells. The converging long axons from the ganglion cells form the optic nerve, which finally conducts the electrical stimuli to the brain [6].

The distribution of photoreceptor cell types is not consistent across the whole retina. While in the periphery mostly rods receive the light signal, the density of cones is extremely high in the light focus of the retina, the macula. Within the macula, the fovea is located, which is exclusively covered with cones, also carrying the highest density of PR cells and thus the location of the most focused vision on the retina. Of note, many animals, such as rabbits or pigs, possess a foveal streak instead, which is enriched with cones but still contains rods. Also, RPE cells have their highest density in the macula, in order to adjust to the high metabolism of PR cells. They are also quite small compared to cells in the periphery and have a darker pigmentation [7], [8].

1.2 The retinal pigment epithelium

The retinal pigment epithelium is the outermost layer of the vertebrate retina, framed by photoreceptor cells and the interphotoreceptor matrix (IPM) on the apical side and the Bruch's membrane (BrM) and choriocapillaris on the basal side. "Five p's" have been suggested to describe the most essential characteristics of RPE cells: they are post-mitotic, polygonal, polarized, pigmented and phagocytic [9]. The apical microvilli are in close contact to the outer segments of photoreceptor cells, allowing for a variety of interactions between PR and RPE. On its basal side, the RPE carries invaginations, so called basal infoldings [10], [11]. The basal membrane of the RPE, however, is the innermost of five layers of the Bruch's membrane (BrM), followed by inner collagenous layer, elastic layer, outer collagenous layer, and the basement membrane of the choriocapillaris. The BrM is 2 to 4 µm thick in adults, provides physical stability and enables the transport of nutrients between choriocapillaris and RPE cells. The tight junctions of RPE cells ensure its functionality as a component of the outer blood-retinal-barrier, essential for protection and homeostasis for the retina itself [3], [12]. The morphological characteristics of RPE cells give hints to their comprehensive functions within the human retina (reviewed by [3]) (Figure 1-2).

Light absorption

The strong pigmentation of RPE cells hints to the most obvious function of RPE: the absorption of light, which does not only improve the optical quality but also protects the neural retina from photo-oxidative energy [13]. The RPE is continuously exposed to photo-oxidative energy, apically from the neural retina and on the basal side from an excess of oxygen from the choroid. Moreover, phagocytosis of photoreceptor outer segments (POS) provokes the formation of reactive oxygen species [14].

To protect RPE and the NR against damage, the absorption of light is initially performed by melanin in melanosomes of RPE cells [3], [8]. Additionally, lipofuscin granules, aggregates of lipids and proteins, have been suggested to initially improve light absorption and thus improve visual function. Nevertheless, in the ageing eye the amount of electron-dense melanin-granules decreases and less dense lipofuscin granules accumulate drastically and become toxic for the RPE. This leads to a loss of pigmentation of the RPE with age and a decreased ability for light absorption [8]. In addition to pigments, cells are protected by enzymatic and non-enzymatic antioxidants, as well as intrinsic repair mechanisms for DNA, lipids, and proteins [8], [10].

Transepithelial transport

As component of the outer blood-retinal barrier, the RPE is responsible for the bidirectional transport of metabolites, ions and fluid between the choroid and the PR cells. The tight junctions between adjacent RPE cells thereby ensure a proper barrier function [15], [16].

Nutrients, which are required for an intact metabolism and function of PR cells, such as glucose and 22:6ω3 fatty acid are taken up by the RPE and delivered to the PR cells. Therefore, RPE cells express several glucose transporters, such as GLUT1 and GLUT3 [17]–[19]. The transport processes from retina to blood side mainly involve water and ions, e.g. Cl^-, K^+, Na^+, HCO_3^-. Several enzymes and transporters, such as Na^+/K^+-ATPase and $Na^+/K^+/2Cl^-$ co-transporter perform a continuous adjustment of the conditions and thus ensure buffering of ions, fluid transport and regulation of the pH [3], [8], [20].

Secretion

RPE cells continuously communicate with photoreceptor cells and choroid by secreting growth factors and signaling molecules. Those are amongst others, ATP, fas-ligand (fas-L), fibroblast growth factors (FGF), transforming growth factor-ß (TGF-ß), insulin-like growth factor-1 (IGF-1), ciliary neurotrophic factor (CNTF), platelet-derived growth factor (PDGF), vascular endothelial growth factor (VEGF), interleukins, tissue inhibitor of matrix metalloprotease (TIMP) and pigment epithelium-derived factor (PEDF) [3], [20], [21]. PEDF is a neurotrophic factor, which is released towards the apical side of the RPE and supports the retina by preventing apoptosis in injury and ischemia [22]–[24]. VEGF and TIMP are secreted basolateral and support the structure of endothelium and choroid [25]. However, VEGF and TIMP3 also play a role in retinal diseases, such as age-related macular degeneration [26].

The visual cycle

When a photon activates the phototransduction cascade, 11-cis retinal changes its conformation to all-trans retinal. As the photoreceptor outer segments do not contain the required enzymes for its re-isomerization, all-trans retinal enters a regeneration process, which is described as the visual cycle [27], [28]. Initially, isomerized all-trans-retinal is reduced to all-trans-retinol by a retinol dehydrogenase (RDH) and afterwards transported towards the RPE across the subretinal space, assisted by the interphotoreceptor retinoid-binding protein (IRBP). In the RPE, all-trans retinol is modified by the protein complex cellular retinol binding protein (CRBP) in three steps: esterification by the lecithin:retinol acyltransferase (LRAT), re-isomerization to 11-cis by RPE65 and oxidation to 11-cis retinal by the retinol dehydrogenase 5 (RDH5). The regenerated 11-cis

retinal is finally diffusing back to the outer segments of PR cells and recombines with opsins, to be able to induce the phototransduction cascade again [29].

Phagocytosis

Due to light exposure and the accumulation of toxic substances during the visual process, the photoreceptor outer segments (POS) are constantly destructed; especially the tips of POS show high concentrations of toxic material [10], [30]. To maintain their functionality, they are constantly renewed by shedding the outer segment discs and further uptake and processing of POS discs by phagosomes of the RPE. The mechanism is under circadian control and further coordinated between RPE and PR by specific recognition signals [31], [32]. CD36, $\alpha_V\beta_5$ integrin and receptor-tyrosine kinase c-mer (MerTK) are involved in the regulation of binding, internalization, and phagocytosis of POS in RPE [33]–[35]. After digestion, essential molecules are redelivered to PR cells, while unwanted end-products are drained off over the choriocapillaris [10], [36].

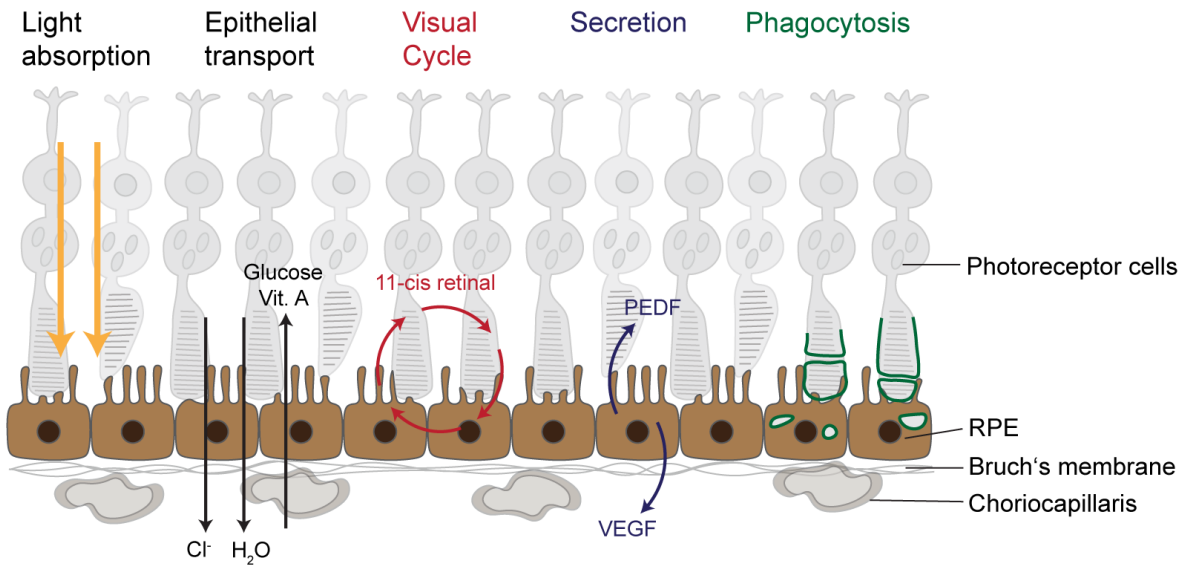

Figure 1-2: Functions of the retinal pigment epithelium.
RPE cells are responsible for light absorption, transepithelial transport between photoreceptor cells and choroid, regeneration of retinal in the visual cycle, secretion of several factors and phagocytosis of photoreceptor outer segment discs.

1.3 Development of the neural retina and the retinal pigment epithelium

The human retina is developing from the neuroectoderm, as a part of the diencephalon. Originating from the neural plate, two optic vesicles, expressing visual system homeobox protein 2 (VSX2) and microphthalmia-associated transcription factor (MITF), evaginate bilaterally and subsequent invagination leads to the formation of optic cups [37], [38]. In this process, lens placode and cornea arise from the initial ectoderm, while neural retina and RPE evolve from the neural tube as two layers opposed to each other [39]. Thereby, the distal part comprises the RPE and the inner, apical part the NR (Figure 1-3). The connections from optic vesicles to the forebrain are defined as optic stalks. While MITF expression drops in the future NR, due to its contact with the lens ectoderm, the future RPE stays MITF positive. The initial lumen between NR and RPE, which is filled with interphotoreceptor matrix, is decreasing during development as the two layers are approaching each other [39], [40]. Nevertheless, during development the designated RPE domains are partly still able to differentiate towards NR, for example in case of a disruption in NR development [41]. Transdifferentiation from RPE towards NR can even happen in mature RPE [42].

At the optic vesicle stage, neural progenitors in the neocortex start to generate retinal neurons and Müller cells in a highly conserved order [43]. Laterally oriented cells, such as HCs, ACs and GCs, as well as cones differentiate first [39], [44]. Vertically orientated cells, to be specific BCs, Müller cells and rods are developing afterwards and form connections between laterally and vertically orientated cells. The lumen of the optic stalk is progressively filled by GC fibers and thereby develops towards the optic nerve. Photoreceptor cell maturation is one of the final processes and is characterized by the formation of outer segments (OS). Additionally, the specification of human PR to rods and three cone-types is induced by CRX, NRL, OTX2 and TRß2 [44], [45].

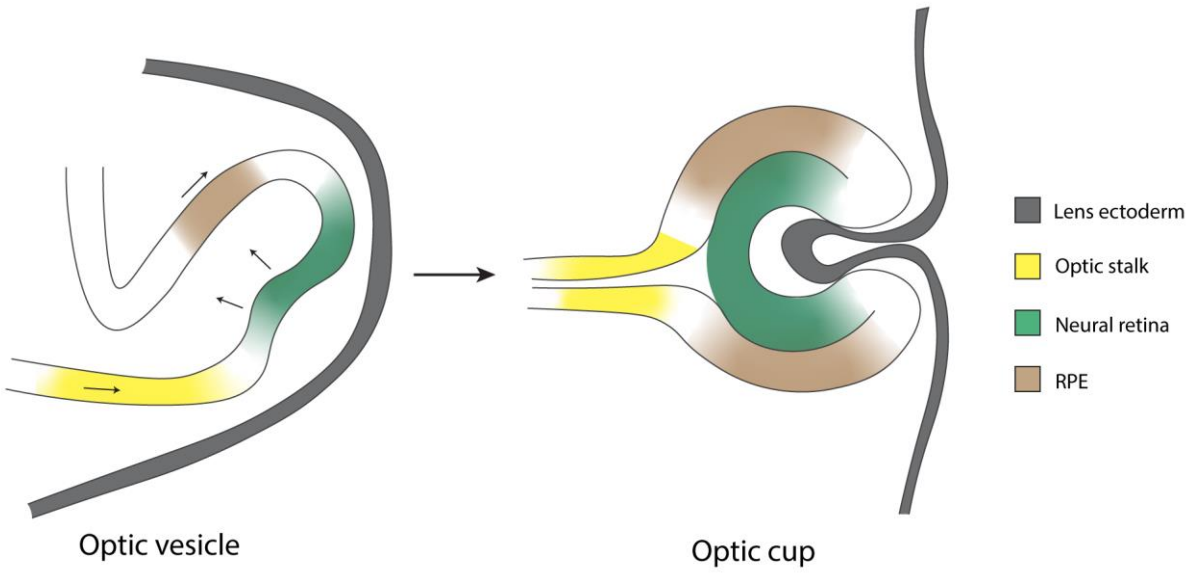

Figure 1-3: Development of retina and retinal pigment epithelium.
The optic vesicles pinch off from the neural tube, invaginate and form the optic cups. The neural tube forms neural retina, retinal pigment epithelium (RPE) and optic stalk. The ectoderm develops lens and cornea.

The development of the retinal pigment epithelium is regulated by several factors, among which the most important are the microphthalmia-associated transcription factor (MITF) and the homeodomain-containing transcription factor (OTX2) [46].

Initially, MITF and OTX2 are expressed across the entire optic vesicle, while at later stages they can only be found in the RPE region of the optic cup. Therefore, in the NR region, MITF is downregulated by VSX2, which is stimulated by FGF [47], [48]. Presumably, MITF is not only regulated by VSX2, but they influence each other during development. Additionally, OTX2 is presumed to downregulate FGF and SOX2 expression to trigger RPE cell fate [49]. Further factors and pathways, such as Pax6, Wnt, hedgehog, BMP4, retinoic acid, Notch and Vax are suggested to support RPE differentiation and maintenance [42].

Maturation of the RPE towards a pigmented epithelium with apical to basolateral polarity is induced by activation of a tyrosinase promoter which indicates the beginning of melanogenesis [50], [51] and is typically assessed by classical maturation markers, such as RPE65, or by ultrastructural analyses [52]. Further, it is strongly affected by interactions with the neural retina through the Interphotoreceptor Matrix (IPM) [40]. While MITF activates the genes for pigmentation and multiple RPE functions, also the Bruch's membrane (BrM) evolves. The five-layered BrM is built below the RPE, which can produce most of the extracellular matrix (ECM)

components of the BrM [53]. Polarization of RPE cells is characterized by the development of microvilli and the expression of specific proteins and transporters, as well as the formation of tight junctions (see chapter 0). While maturation of PR cells is characterized by the formation and extension of OS, RPE cells react by extending their apical microvilli, which in the end frame the OS of PR cells [3]. In general, the development of NR and RPE proceeds in close interaction by regulation of transcription factors or secretion of growth factors [54].

1.4 Stem cell-based in vitro models of the retina and the retinal pigment epithelium

Besides animal models, immortalized cell lines or primary cells, stem cell-based models have gained in importance for studies of the retina in recent years. Stem cells are defined by their potential for self-renewal and differentiation to specialized cells. While totipotent stem cells can produce an entire organism including the extraembryonic tissue, pluripotent stem cells can differentiate to all three embryonic germ layers, to be precise, ectoderm, endoderm and mesoderm. Due to their potential for self-renewal, the availability of pluripotent stem cells is basically unlimited. Stem cells can be derived from animals, as well as from humans, depending on the aim of the current study and on their availability.

Pluripotent stem cells include embryonic stem cells (ECs) and induced pluripotent stem cells (iPSCs). Embryonic stem cells have been widely used in research, especially mouse ECs, but their acquisition is complex and ethically problematic [55]. The generation of new human EC lines is even prohibited in several countries. Therefore, the introduction of induced pluripotent stem cells (iPSCs) by Takahashi and Yamanaka in 2006, was a huge milestone in the field of stem cell research [56]. They presented a method, capable to reprogram all somatic cells of the body by introducing four transcription factors OCT3/4, SOX2, c-MYC and KLF4. The possibility to generate iPSCs from easily accessible (adult) cells, such as fibroblasts or keratinocytes, and their ability to differentiate into multiple cell types, makes them a popular and powerful model system in research [57]–[59].

1.4.1 Model systems of the retina

As discussed above, pluripotent stem cells are highly suited for the generation of *in vitro* models of the neural retina and the retinal pigment epithelium. The first two-dimensional approaches focused on intervening in classical signaling pathways by adding exogenous signaling molecules or inhibitors [60], [61]. Thereby, identity of retinal cells was confirmed by specific marker

expression. Nevertheless, those protocols only comprised individual cell types and lacked proper organization and maturation.

The step towards 3D retina models in suspension was supposed to overcome those drawbacks. Initial studies showed the differentiation of retinal progenitors and retinal cell types as a "default stage" during neural differentiation, suggesting that after priming PSCs towards the neural lineage, retinal cells arise without addition of other modulating factors [62]. This was followed by the development of free-floating optic-cup-like structures from mouse ESCs [63] and optic-vesicle-like structures from human hiPSCs [64]. In the following years, protocols for the differentiation of retinal organoids (ROs) were continuously optimized, whereby two of them should be particularly mentioned.

Nakano *et al.* 2012 [65] used various factors e.g., for the modulation of Wnt and Hedgehog pathways in an entirely three-dimensional protocol. Optic vesicles thereby directly arise from EBs and mature towards well-developed retinal organoids. In contrast, Zhong et al. 2014 [66] did not use signaling pathways modulators for their differentiation, but performed a unidirectional neural differentiation, resulting in the development of retinal fields adjacent to adherently plated EBs, which were manually detached and formed spheroidal retinal organoids in suspension. Both protocols require a manual selection and enrichment of retinal structures to generate retinal organoids.

The retinal organoids obtained in those studies, contained all relevant retinal cell types, arranged in the appropriate stratified layering, formed functional synaptic interconnections between the different neuronal layers and were light sensitive. However, ROs display several limitations, such as insufficient photoreceptor maturation and no physiological interaction between photoreceptor cells of ROs and RPE cells. In that matter, a human Retina-on-a-Chip was developed which could overcome some of those drawbacks by enabling the co-cultivation of ROs and RPE cells in a microphysiological Organ-on-Chip device [67]. To this day, ROs still lack vascularization or immune cells striving for a more elaborated model of the human retina. As the field of stem cell research is developing rapidly, integration of endothelial cells or immune cells into retinal organoids might soon be achieved.

1.4.2 Model systems of the retinal pigment epithelium

The differentiation of retinal pigment epithelial cells from stem cells was first described by Kawasaki *et al.* 2002, who differentiated dopaminergic neurons from primate ESCs in the presence of exogenous stromal cells and observed large patches of polygonal, pigmented cells expressing Pax6 after 3 weeks of differentiation [68]. Further studies performed a detailed

characterization of such differentiated RPE cells and demonstrated the presence of essential RPE markers, as well as functionality [55], [69]. Additionally, the spontaneous differentiation of RPE cells from hESC cultures in feeder-free conditions was established [70] (reviewed by [55]).

Subsequent protocols for RPE differentiation were aiming to increase the yield of RPE cells and to reduce the differentiation time. Therefore, the essential signaling pathways for RPE development were addressed using Wnt and Nodal antagonists and extended cultivation time [60]. A similar approach was performed by Idelson *et al.* 2009, who demonstrated enriched development of pigmented cells under the influence of nicotinamide (NIC) in a 3D suspension culture of optic vesicles. Addition of TGF-ß and Activin A even enhanced this effect [71].

A combination of basic fibroblast growth factor (bFGF), Noggin, retinoic acid and Sonic Hedgehog led to an increase efficiency of RPE differentiation after 60 days of differentiation [72]. Due to its short differentiation time of only 21 days, a study for the generation of neural retinal progenitors became of special interest, in which IGF-1, Noggin, Dkk-1 and bFGF were applied [73]. By combining those observations, a remarkably short differentiation protocol was established, whereby the supplementation with retinal inducing factors (IGF-1, Noggin, Dkk-1, bFGF) and other factors (nicotinamide, Activin A, SU5402 and vasoactive intestinal peptide) at specific time points resulted in RPE cells, which could be harvested already after 14 days [74].

Like ROs, RPE cells can not only be generated by directed differentiation [75]. Self-formation of RPE cells is commonly observed during retinal organoid differentiation. Thereby, RPE patches can be cultured and expanded adherently, without transferring them to suspension [61], [62]. Also, RO differentiations cultured in suspension develop pigmented 3D RPE spheroids/organoids regularly [65], [66]. An improved protocol for the generation of RPE spheroids even demonstrated a higher purity and efficiency of RPE differentiation [76].

The common protocols for RPE differentiation, if conducted adherently or in suspension, have one thing in common: One of the final steps is the dissociation and further adherent cultivation. RPE cells can thus lose their maturity and characteristic properties and lack a sufficient extracellular matrix. RPE spheroids/organoids, on the other hand, do not need to be passaged, and can be cultured for more a long time. So far, they have been cultured for more than 150 days and characterized for some basic RPE markers [76].

1.5 Age-related macular degeneration

Age-related macular degeneration (AMD) is one of the major causes of blindness among elderly people [77], [78]. It affects the central retina, which is responsible for the fine visual acuity, having the highest density of photoreceptor cells across the retina. Impairments in this area, thus alter the quality of vision drastically [79]. Due to the strong correlation of AMD with aging, it was initially described as senile macular degeneration (SMD). Besides aging, a genetic predisposition, cigarette smoke, obesity and hypertension are major risk factors for AMD [26]. Genes involved are usually responsible for retinal-specific functions, related to the immune system, neovascularization, or lipid metabolism [80]. In addition to visual impairments, patients frequently suffer from mental health issues relating to it. Furthermore, not only the quality of life of patients is affected, but the society must deal with excessive economic costs [81]. Thus, adequate models for a better understanding of the pathomechanisms and the development of treatment strategies are highly required.

Classification and progression

AMD is typically classified into dry and wet AMD. Dry AMD is usually correlated to early stages of the disease and clinically characterized by the presence of drusen, extracellular accumulations of lipid proteins and extracellular matrix components between the RPE and the Bruch's membrane (BrM). Thickening of the BrM, RPE hypertrophy and pigment extrusion can further be observed (Figure 1-4) [82]. Late stages of dry AMD are defined as geographic AMD (GA), in which RPE cells become atrophic and with further progression degenerate. Wet or neovascular AMD is accompanied by the invasion of blood vessels and fluid infiltration, resulting in accumulations of blood and fluid between neural retina and RPE or between RPE and BrM which, in the end, can also lead to RPE detachment [79].

Early stages of AMD, in many cases, do not impact vision drastically, and can remain undiscovered for several years. But AMD is a progressive disease and thus, there is a faster or slower transition towards later stages. As soon as RPE cells start to degenerate, PR cells will at a certain point also be affected due to their close interaction. Additionally, immune cells, such as microglia and monocytes, infiltrate and interact with retinal tissue in AMD [83], [84].

While treatment of dry and geographic AMD remains difficult, there are drugs against neovascular AMD. However, these anti-VEGF therapy remains costly and requires frequent repetitions [85]. A second approach using laser-therapy aims to delay disease progression, but application is delicate and the effect still questionable [86].

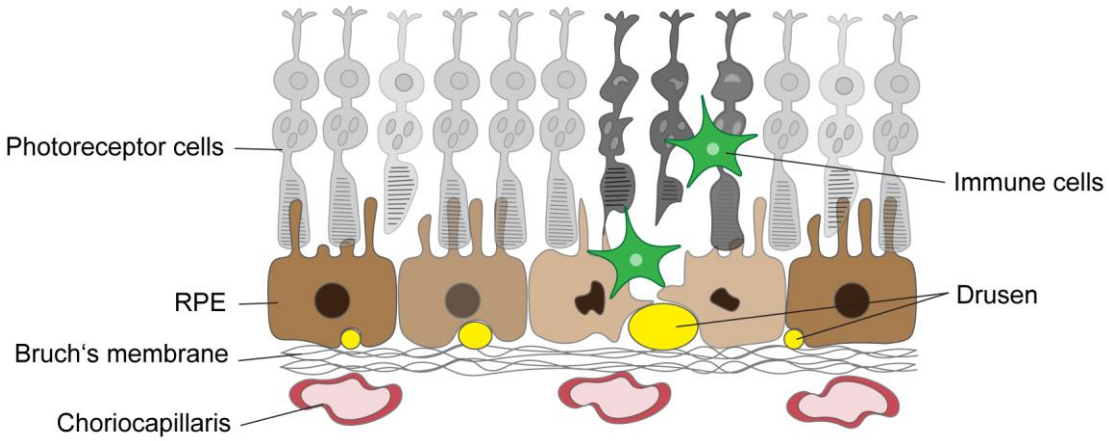

Figure 1-4: Pathological changes in RPE and retina in age-related macular degeneration.
AMD is characterized by thickening of the Bruch's membrane, accumulation of extracellular material, drusen formation, infiltration of immune cells and in late stages by RPE cell and PR cell degeneration.

Molecular and histopathological changes in AMD

Hard drusen, discovered in the normal aging eye and in dry AMD, are small and circular, depict clear boundaries, a homogenous and dense interior and are between 30 to 60 µm in diameter. They are typically found in the periphery of the aging retina and do not necessarily impair visual function [87]. Nevertheless, an increased number of hard drusen can be beneficial for AMD progression towards later stages [88], [89]. Soft drusen, on the other hand, are larger (up to 1 mm in diameter), dome-shaped, filled with membranous debris and do not show distinct borders. Thereby, a correlation between number and size of drusen and disease progression has been observed [89], [90].

The detailed mechanism of drusen formation remains unclear, although the RPE cells are suggested to play an essential role in drusen formation and are even capable to produce components of drusen independently [91]–[93]. On the other hand, more and more components of drusen were revealed in recent studies [94]. It has to be noted that some of the proteins detected in drusen of AMD patients were not discovered in drusen of healthy donors [95].

Tissue inhibitor of metalloproteinases-3 (TIMP3) is commonly found in drusen and is upregulated in AMD [96], [97]. As a member of the TIMP family, TIMP3 usually inhibits matrix metalloproteinases (MMPs) and thus regulates extracellular matrix composition and inhibits angiogenesis (blocking VEGFR) and tumor growth [98]–[100]. Additionally, apolipoprotein E

(APOE) was found to be associated with AMD [101]. In general, APOE is responsible for the transport of lipids through cells, inhibits angiogenesis and has anti-inflammatory and anti-oxidative functions, which could play a role in drusen formation [102], [103].

Furthermore, calcification and crystallization are processes ongoing already in early stages of drusen formation and calcified nodules have been shown to increase the risk for progression towards late stages of AMD [104], [105]. Crystallins are heat shock proteins and have been found in the BrM of AMD patients [106]. Two of them, crystallin alpha A and B (CRYAA and CRYAB), as well as hydroxyapatite (HAP) have been detected in *in vitro* cultures sub RPE deposits [104], [107]–[109].

Furthermore, drusen are partially described as components of a local inflammation process between RPE and BrM, accompanied by activation of the complement system. Involvement of the complement system in drusen biogenesis has been investigated in several studies [110]–[112]. Inherited forms of AMD are frequently caused by mutations in the complement factor H (CFH) gene or further complement factors [113]. In addition, additional complement factors, such as complement factor 3 (C3), complement factor 5 (C5) and complement regulators, such as vitronectin (VTN), are commonly upregulated in AMD [114].

1.6 Distinction between aging and AMD

Age-related changes in the retina, such as RPE and PR degeneration, thickening of the BrM and accumulation of extracellular material and lipids, are quite similar to pathophysiological changes in AMD [8], [115]. As aging is one of the major risk factors for AMD, a strong correlation is apparent. Nevertheless, a distinction between age-related changes and disease is important aiming to understand why not all aging humans develop pathological conditions.

Hard drusen emerge in the aging retina and do not necessarily increase the risk of developing AMD [116]. While in the healthy retina they are mostly located at the periphery, in AMD they can be present in both, peripheral and central retina. In contrast to hard drusen, soft drusen are exclusively found in the macula of AMD retinas [117]. The composition of hard drusen is influenced by their position in the retina but does not indicate if aging or AMD caused their formation [117], [118]. The majority of drusen components and associated factors is detectable in the healthy aged retina, as well as in the AMD retina, whereby their quantity is again clearly higher in AMD retina [96].

In principle, aging can be seen as an intermediate step towards AMD, whereby the pathophysiological changes and factors influence each other and enhance the disease progression more and more. Briefly, in AMD the homeostasis of normal aging gets out of control [115].

1.7 State of the art: Models to study AMD

As pathological changes mainly affect the subcellular space below the RPE and RPE cells can even produce some drusen components themselves, RPE cells are the model of choice investigating development and progression of AMD. Adequate *in vitro* models of retinal pigment epithelial cells are generally highly required, not only for disease modeling of AMD, but also for other related diseases and RPE development.

Animal models often fail to reproduce the complexity of the human eye and are accompanied by ethical concerns. Many mammals like the mouse do not have a macula, which, however, is a key feature in AMD. Additionally, most of the current mouse models can reproduce several characteristics of early AMD, but only few reveal signs of late-stage AMD [119].

However, primary porcine cells cultured on transwell inserts for up to 6 months developed sub-RPE deposits, whose composition was investigated. They contained lipids, hydroxyapatite and showed signs of mineralization [93]. Although their availability is poor, interspecies differences do not occur using primary human RPE cells. Cultured human fetal RPE cells showed formation of

basal deposits, when stressors, such as human serum, were supplemented [120]. Nevertheless, most of the human tissue is acquired from aged people, which show already enhanced progression of aging and AMD and accordingly, early stages of AMD cannot be studied in detail. Cell lines are easier to handle and cheaper than primary cells, but there are not many cell lines of the RPE available and the most common immortalized RPE cell line, ARPE-19, does not sufficiently comply with the properties of human RPE cells *in vivo* [121].

Therefore, usage of hiPSC derived RPE cells became more and more popular in recent years [122]–[125]. The application of hiPSCs has the advantage that not only healthy control tissue can be generated, but also patient derived hiPSCs that can be differentiated towards disease-affected tissue. This was for example deployed by Galloway et al. (2017), who generated RPE from hiPSCs of patients with three dominant macular diseases and observed an increase in drusen-formation, changes in extracellular matrix composition and upregulation of complement genes in patient hiPSC-RPE cultures [126].

RPE cells are typically cultured adherently in cell culture plates, transwell inserts or, most recently, in organ-on-chip devices [67], [93], [122]. Those 2D cultures display several disadvantages, such as transdifferentiation towards a mesenchymal phenotype or detachment from the cell culture plates after several weeks or months in culture. Additionally, enzymatic dissociation is required during the initial seeding process of RPE cells, which can induce a change of metabolism and lead to a loss of pigmentation and polarization [127]–[129].

RPE spheroids, generated from singularized cell suspensions of RPE cells, showed expression of drusen-associated proteins after 2 weeks in culture [130]. Nevertheless, the protocol also requires an initial enzymatic dissociation which can affect the phenotype of RPE cells. Another recent three-dimensional RPE spheroid/organoid approach makes use of self-formation of 3D RPE structures during RO differentiation [76]. This allows long-term cultivation for more than 150 days, provides a pronounced ECM below the outer layer of RPE cells and shows a mature and functional phenotype in RPE cells. However, RPE spheroids have only been studied for some basic RPE markers and not for AMD-associated proteins or age-related differences during cultivation.

1.8 Aim of the work

The aim of this study was the development and characterization of a meaningful *in vitro* model of RPE cells which contains all major RPE hallmarks. The ability of such a model to mimic the basic features of age-related macular degeneration, especially drusen formation, should be tested.

Initially, two approaches for the differentiation of adherent hiPSC-RPE cells were established and compared by assessing morphology and expression of several RPE specific markers. Realizing that adherent cultivation of RPE cells has several disadvantages such as unphysiological ECM due to the culture on plastic surfaces, a 3D approach, the self-formation of 3D RPE structures during RO differentiation was implemented subsequently [76]. RPE organoids were differentiated and cultured for more than 300 days. In depth characterization of RPEorg of different ages was performed via electron microscopy, immunohistochemistry, and qRT-PCR analysis. Functionality of RPE cells in RPEorg was studied applying a phagocytosis assay of photoreceptor outer segments. Finally, RPEorg were examined for the expression and presence of several drusen-associated proteins and lipids, as well as for ultrastructural signs of drusen formation.

2 Material and Methods

2.1 Material

2.1.1 Technical devices

Table 2-1: List of technical devices

Technical devices	Company
Centrifuge Heraeus™ Megafuge 16	Thermo Fisher Scientific, Waltham, MA, USA
Centrifuge Heraeus ™ Fresco 17	Thermo Fisher Scientific, Waltham, MA, USA
Cryostat, Microm HM 560	Thermo Fisher Scientific, Waltham, MA, USA
Fluidigm BioMark™ HD	Fluidigm, South San Francisco, CA, USA
Freezer -20 °C	Liebherr, Biberach, Germany
Freezer -80 °C	Thermo Fisher Scientific, Waltham, MA, USA
Ice machine AF103	Scotsman, Great Blakenham, UK
Incubator 37 °C, Heracell 240i	Thermo Fisher Scientific, Waltham, MA, USA
Microscope FL EVOS	Thermo Fisher Scientific, Waltham, MA, USA
Microscope (Axioskop 2 mot plus)	Zeiss, Oberkochen, Germany
Microscope (Primo Vert)	Zeiss, Oberkochen, Germany
Microscope Confocal (Zeiss LSM 710)	Zeiss, Oberkochen, Germany
Microscope TEM (Zeiss EM 900 transmission electron microscope)	Zeiss, Oberkochen, Germany
Multipipette Stream	Eppendorf, Hamburg, Germany
NanoPhotometer® P330	Implen, München, Germany
Nitrogen Tank, CryoPlus 2	Thermo Fisher Scientific, Waltham, MA, USA
Pipette research plus (2,5 µl ,10 µl, 100 µl, 200 µl, 1000 µl, 5 ml)	Eppendorf, Hamburg, Germany
Pipette F1 Clip-Tip (10 µl, 100 µl, 1000 µl)	Eppendorf, Hamburg, Germany
Pipettus	Hirschmann, Eberstadt, Germany
Sterile Bench, MSC-Advantage	Thermo Fisher Scientific, Waltham, MA, USA
Ultramicrotome Reichert Ultracut S	Leica, Wetzlar, Germany
Vacuum Pump, Integra Vacusafe	Integra Biosciences, Biebertal, Germany
Vortexer	Bender+Hobein, Zürich, Switzerland
Water bath, Lab Line waterbath	Thermo Fisher Scientific, Waltham, MA, USA

2.1.2 Labware and Consumables

Table 2-2: List of labware and consumables

Labware and consumables	Company
6-, 12-, 24-, 48-, 96-well plates (Tissue treated, Non-treated)	Becton Dickinson, New York, NY, USA
96-well V-shaped culture plates	Sarstedt, Nürnbrecht, Germany
Cell scraper	Thermo Fisher Scientific, Waltham, USA
Counting chamber according to Neubauer	NeoLab, Heidelberg, Germany
Coverslips, Menzel (24x24 mm, 24x50 mm)	Thermo Fisher Scientific, Waltham, USA
Cryogenic vial 1.2 ml	Corning, New York, NY, USA
Dako delimiting pen	Dako, Hamburg, Germany
EASY strainer™ (40 µm, 70 µm)	Greiner Bio-One, Frickenhausen, Germany
EASY strainer™ small (40 µm, 70 µm)	Greiner Bio-One, Frickenhausen, Germany
Evo Spring Scissors, curved	Fine Science Tools, Heidelberg, Germany
Fluidigm 48.48/96.96 Dynamic Array IFC	Fluidigm, South San Francisco, CA, USA
Freezing Container Mr. Frosty™	Thermo Fisher Scientific, Waltham, USA
Gloves Peha-Soft nitrile	Hartmann, Heidenheim, Germany
Micro Knife	Fine Science Tools, Heidelberg, Germany
Petri dishes (10 cm, 6 cm, 3,5 cm)	Greiner Bio-One, Frickenhausen, Germany
Pipette tips (10 µl, 100 µl, 200 µl, 1 ml, 5 ml)	Eppendorf, Hamburg, Germany
QiaShredder™ columns	Qiagen, Hilden, Germany
Reaction tubes (15 ml, 50 ml)	Becton Dickinson, New York, NY, USA
Reaction tubes small (0,5 ml, 1,5 ml, 2 ml)	Sarstedt, Nürnbrecht, Germany
Serological Pipettes (5 ml, 10 ml, 25 ml, 50 ml)	Sarstedt, Nürnbrecht, Germany
Sterile filters (0,22 µm, 0,45 µm)	Merck Millipore, Darmstadt, Germany
Super Frost® Plus object slides	R. Langenbrinck, Emmendingen, Germany
Syringes BD Plastikpak 50 ml	Becton Dickinson, New York, NY, USA
Syringes BD 1 ml Insulin Syringe	Becton Dickinson, New York, NY, USA
Tissue-Tek® Cryomold®	Sakura Finetek, Alphen aan den Rijn, NL
µ-Dish 35 mm high	Ibidi, Gräfelfing, Germany

µ-Dish 4-well culture insert	Ibidi, Gräfelfing, Germany
µ-Slide 8-well	Ibidi, Gräfelfing, Germany

2.1.3 Cell culture media

Table 2-3: List of cell culture media

Medium	**Company**
Antibiotic-antimycotic (AA) 100x	Thermo Fisher Scientific, Waltham, MA, USA
CryoStem™	Biological Industries, Beit Haemek, Israel
DMEM, high glucose	Thermo Fisher Scientific, Waltham, MA, USA
DMEM/F12 + GlutaMAX™	Thermo Fisher Scientific, Waltham, MA, USA
Fetal bovine serum (FBS)	Thermo Fisher Scientific, Waltham, MA, USA
GlutaMax™ 100x liquid	Thermo Fisher Scientific, Waltham, MA, USA
KnockOut™-DMEM	Thermo Fisher Scientific, Waltham, MA, USA
Non-essential amino acids (NEAA) 100x	Thermo Fisher Scientific, Waltham, MA, USA
Normal donkey serum (NDS)	Sigma-Aldrich, St. Louis, MO, USA
PeproGrow™ hESC embryonic stem cell media	PeproTech, Hamburg, Germany
Phosphate buffered saline (PBS) w/o calcium and magnesium	Thermo Fisher Scientific, Waltham, MA, USA
Synth-A-Freeze® cryopreservation medium	Thermo Fisher Scientific, Waltham, MA, USA

2.1.4 Chemicals and supplements

Table 2-4: List of chemicals and supplements

Chemical	**Company**
Activin A	Cell Guidance Systems LLC, St. Louis, MO, USA
All-trans retinoic acid	Sigma-Aldrich, St. Louis, MO, USA
Apotransferrin	Serologicals, Atlanta, GA, USA
Araldite® resin	Serva, Heidelberg, Germany
B-27™ without vitamin A	Thermo Fisher Scientific, Waltham, MA, USA
(-)-Blebbistatin	Sigma-Aldrich, St. Louis, MO, USA
Bovine outer segments	InVision BioResources, Seattle, WA, USA
Chemically defined lipid (CDL) concentrate	Thermo Fisher Scientific, Waltham, MA, USA

CHIR99021	Sigma-Aldrich, St. Louis, MO, USA
DAPI (4′,6-diamidino-2-phenylindole)	Thermo Fisher Scientific, Waltham, MA, USA
Dkk-1, human recombinant	Sigma-Aldrich, St. Louis, MO, USA
Dorsomorphin dihydrochloride	Thermo Fisher Scientific, Waltham, MA, USA
Ethanol	Serva, Heidelberg, Germany
Epoxy embedding medium	Sigma-Aldrich, St. Louis, MO, USA
Glutaraldehyde	Electron Microscopy Sciences, Munich, Germany
Heparin sodium salt	Sigma-Aldrich, St. Louis, MO, USA
Human recombinant EGF	Cell Guidance Systems LLC, St. Louis, MO, USA
Human recombinant FGF-2	Cell Guidance Systems LLC, St. Louis, MO, USA
Human serum albumin (HSA)	Biological Industries, Cromwell, CT, USA
Hoechst 33342 solution	Thermo Fisher Scientific, Waltham, MA, USA
IGF-1, human recombinant	PeproTech, Hamburg, Germany
Isopropanol	VWR, Radnor, PA, USA
ITS	BD Biosciences, San Jose, CA, USA
N2 supplement	Thermo Fisher Scientific, Waltham, MA, USA
Nicotinamide	Sigma-Aldrich, St. Louis, MO, USA
Noggin from mouse, recombinant	Sigma-Aldrich, St. Louis, MO, USA
Paraformaldehyde	Roth, Karlsruhe, Germany
Progesterone	Sigma-Aldrich, St. Louis, MO, USA
ProLong™ Gold Antifade Mountant	Thermo Fisher Scientific, Waltham, MA, USA
Propylene oxide	Serva, Heidelberg, Germany
ROCK inhibitor Y-27632	Ascent Scientific, Avonmouth, UK
Sodium cacodylate buffer, pH 7,4	Electron Microscopy Sciences, Munich, Germany
Sucrose	Roth, Karlsruhe, Germany
SU-5402	Sigma-Aldrich, St. Louis, MO, USA
Taurine	Sigma-Aldrich, St. Louis, MO, USA
TGF-ß1	Cell Guidance Systems LLC, St. Louis, MO, USA
Tissue-Tek® O.C.T.™ compound	Sakura Finetek, Alphen aan den Rijn, NL
Trypan Blue solution	Sigma-Aldrich, St. Louis, MO, USA

Uranyl acetate	Serva, Heidelberg, Germany
ß-Mercaptoethanol	Thermo Fisher Scientific, Waltham, MA, USA

2.1.5 Coatings

Table 2-5: List of coatings

Coating	Company
Laminin from EHS sarcoma	Roche, Basel, Switzerland
Laminin from EHS sarcoma	Sigma-Aldrich, St. Louis, MO, USA
Matrigel® hESC-Qualified Matrix	Corning, New York, NY, USA
Matrigel® Growth Factor Reduced (GFR)	Corning, New York, NY, USA
Poly-L-Ornithine 0,01 % solution	Thermo Fisher Scientific, Waltham, MA, USA

2.1.6 Enzymes

Table 2-6: List of enzymes

Enzyme	Company
Accumax™	Sigma-Aldrich, St. Louis, MO, USA
Dispase	Stem Cell Technologies, Vancouver, Canada
TrypLE™ Express	Thermo Fisher Scientific, USA

2.1.7 Antibodies and fluorescence-coupled Proteins

Table 2-7: Primary Antibodies

Antibody target	Dilution	Article number	Company
ApoE	1:150	NB110-60531	Novus, Centennial, CO, USA
C3	1:200	PA5-21349	Thermo Fisher Scientific, USA
C5b9	1:100	NBP1-05120	Novus, USA
Collagen IV	1:50	ab769	Merck Millipore, Germany
CRYAA	1:100	CF505577	OriGene, USA
CRYAB	1:100	CF500680	OriGene, USA
EEA1	1:500	14-9114-82	Thermo Fisher Scientific, USA
EZRIN	1:200	3145S	Cell Signaling, USA
LAMP2	1:50	sc18822	Santa Cruz Biotechnology, USA

LRAT	1:100	LS-C416127-50	LSBio, Seattle, WA, USA
Melanoma gp 100	1:100	ab787	Abcam, Cambridge, MA, USA
MITF	1:500	X1405M	Exalpha Biologicals, USA
RPE65	1:250	ab78036	Abcam, Cambridge, MA, USA
STRA6	1:200	NBP1-83719	Novus, Centennial, CO, USA
TIMP3	1:200	ab61316	Abcam, Cambridge, MA, USA
Ubiquitin	1:100	MAB1510-I-100UG	Merck Millipore, Germany
ZO-1	1:100	33-9100	Thermo Fisher Scientific, USA

Table 2-8: Secondary Antibodies

Antibody	**Type**	**Dilution**	**Company**
Alexa Fluor™ 488	Donkey anti mouse IgG	1:1000	Abcam, Cambridge, MA, USA
Alexa Fluor™ 488	Donkey anti rabbit IgG	1:1000	Abcam, Cambridge, MA, USA
Alexa Fluor™ 488	Donkey anti goat IgG	1:1000	Abcam, Cambridge, MA, USA
Alexa Fluor™ 568	Donkey anti mouse IgG	1:1000	Abcam, Cambridge, MA, USA
Alexa Fluor™ 568	Donkey anti rabbit IgG	1:1000	Abcam, Cambridge, MA, USA
Alexa Fluor™ 568	Donkey anti goat IgG	1:1000	Abcam, Cambridge, MA, USA
Alexa Fluor™ 647	Donkey anti mouse IgG	1:1000	Abcam, Cambridge, MA, USA
Alexa Fluor™ 647	Donkey anti rabbit IgG	1:1000	Abcam, Cambridge, MA, USA
Alexa Fluor™ 647	Donkey anti goat IgG	1:1000	Abcam, Cambridge, MA, USA

Table 2-9: Fluorescence-coupled proteins

Substance	**Dilution**	**Company**
Lectin PNA Alexa Fluor™ 647	1:500	Sigma-Aldrich, St. Louis, MO, USA
Phalloidin Alexa Fluor™ 647	1:500	Sigma-Aldrich, St. Louis, MO, USA

2.1.8 Kits and Assays

Table 2-10: Kits and Assays

Kit	**Company**
RNeasy® Micro Kit	Qiagen, Hilden, Germany
Neurosphere Dissociation Kit (P)	Miltenyi Biotech, Bergisch-Gladbach, Germany

Pierce™ FITC Antibody Labeling Kit	Thermo Fisher Scientific, Waltham, USA

2.1.9 TaqMan™ probes

All TaqMan™ probes were purchased from Thermo Fisher Scientific, Waltham, USA.

Table 2-11: TaqMan™ probes for Fluidigm

Gene	Article number
ApoE	Hs00171168_m1
APP	Hs00169098_m1
BEST1	Hs04397293_m1
C3	Hs00163811_m1
C5	Hs01004342_m1
CFH	Hs00962373_m1
COL4A1	Hs00266237_m1
CRYAA	Hs00166138_m1
CRYAB	Hs00157107_m1
GAPDH	Hs99999905_m1
LRAT	Hs00428109_m1
MITF	Hs01117294_m1
PMEL	Hs00173854_m1
RPE65	Hs01071462_m1
RPS9	Hs02339424_g1
SERPINF1	Hs01106937_m1
STRA6	Hs00980261_g1
TIMP3	Hs00165949_m1
TJP1	Hs01551861_m1
UBC	Hs05002522_g1
VTN	Hs00940758_g1

2.1.10 Software

Table 2-12: Software

Software	Company
Adobe Illustrator	Adobe Systems Software Ireland Limited, Dublin, Republic of Ireland
AxioVision SE64 Rel. 4.9	Zeiss, Oberkochen, Germany
Fluidigm Real-Time PCR Analysis Software v.3.0.2	Fluidigm, San Francisco, USA
ImageJ v1.53c	Wayne Rasband, USA
Microsoft Office	Microsoft Corporation, Redmond, USA
GraphPad Prism 8.4.2	GraphPad Software, San Diego, USA
ZEN 3.3 blue/black	Zeiss, Oberkochen, Germany

2.2 Methods

2.2.1 Cell Culture

Cell culture handling was performed under sterile conditions in a laminar flow hood. Cells were cultured in a humid atmosphere in an incubator at 37 °C and 5 % CO_2. While iPSCs were kept at hypoxia (5 % O_2), ROs and RPE cells were grown under normoxic conditions (20 % CO_2). All cell culture media were heated to RT or 37 °C before usage.

Stem cells used in this study were derived from keratinocytes from healthy human donors, which gave their written consent. The application of human material was authorized by the ethical committee of the University of Tübingen (No. 841/2016BO2) and in accordance with the declaration of Helsinki concerning ethical principles for medical research involving human subjects.

2.2.2 Cultivation of human iPSC

Human iPSC lines for this study were generated by lentiviral reprogramming of human keratinocytes, as described previously [57], [131].

For standard cultivation, hiPSCs were grown as colonies in FTDA medium [132] on 6-well plates coated with 700 µl hESC-qualified matrigel (MG) for 2 h at RT. Medium was changed daily. For passaging at approximately 80 % confluency, used medium was removed and cells were washed with PBS -/-. Then, 500 µl of stem cell dispase solution were incubated for 30 s, followed by two wash steps with PBS -/-. Fresh FTDA medium was added to the well, colonies were gently detached using a cell scraper and collected in a 15 ml reaction tube. Cells were distributed to freshly coated wells in the required density. Differentiated cells were manually removed from the plates with a pipette tip. HiPSCs were cultured up to passage 40.

Table 2-13: FTDA medium

Component	**Amount**
DMEM/F12 + GlutaMAX™	
Human serum albumin (HSA)	1:100
Chemically defined lipids (CDL)	1:100
Antibiotic-antimycotic (AA) 100x	1x
ITS	1:1000
Activin A	5 ng/ml
FGF-2	10 ng/ml

TGF-ß1	0,5 ng/ml
Dorsomorphin	50 nM

2.2.3 Freezing and thawing of hiPSCs

For freezing, hiPSC colonies at 80 % confluency were detached from the plate, according to the protocol for splitting. The collected colonies were centrifuged in a 15 ml reaction tube at 1500 rpm for 2 min. The supernatant was removed, hiPSCs were resuspended in 750 µl CryoStem freezing medium and transferred to a cryovial. All steps must be performed carefully, to not fully dissociate the hiPSC colonies. After the initial freezing of the cryovials in a freezing container filled with isopropanol at -80 °C overnight, cells were moved to the liquid nitrogen for long-term storage at -196 °C.

For thawing, cryovials with frozen hiPSCs were defrosted quickly in a water bath at 37 °C. The completely thawed suspension was immediately transferred to a 15 ml reaction tube with preheated DMEM and centrifuged at 1500 rpm for 2 min. The pellet was carefully resuspended in the required volume of FTDA medium and hiPSCs were plated on a matrigel pre-coated well plate.

2.2.4 Adherent differentiation of retinal pigment epithelial cells

Adherent differentiation of RPE cells, subsequently referred to as adRPE, was carried out according to a previously published protocol [122]. Briefly, on day zero of differentiation a confluent 6-well of hiPSC was split to four 12-wells and switched to RPE differentiation medium (RPE-DM). At the first two days, RPE-DM was supplemented with Noggin (50 ng/ml), Dkk-1 (10 ng/ml), IGF-1 (10 ng/ml) and NIC (10 mM). From day two to four, the concentration of Noggin was reduced to 10 ng/ml and FGF-2 (5 ng/ml) was added to the previous supplements. From day four to six, Dkk-1 and IGF-1 were added in the same concentrations as before and Activin A was supplemented at 100 ng/ml. Then, until day 14 of differentiation, only Activin A (100 ng/ml) and SU-5402 were added to RPE-DM. Medium was changed every two days.

On day 14, cells without RPE-morphology were scratched off the plate using a pipette tip. After rigorous washing with PBS -/-, cells were dissociated using TrypLE and seeded on ten wells of a 24-well plate, which had previously been coated with 0,01 % Poly-L-Ornithine and 20 µg/ml laminin in DMEM. Medium was switched to BRDM (Table 2-16) for the following cultivation period.

Table 2-14: RPE Differentiation medium (RPE-DM)

Component	Amount
DMEM/F12 + GlutaMAX™	96 ml
N2 Supplement 100x	1x (1 ml)
B-27™ without vitamin A 50x	1x (2 ml)
Non-essential amino acids (NEAA) 100x	1x
Antibiotic-antimycotic (AA) 100x	1x

2.2.5 Differentiation of retinal organoids and RPE organoids

Retinal organoids and RPE organoids were differentiated from hiPSC according to a previously published protocol [66] with some modifications [67].

Initially, embryoid bodies (EBs) were generated by dissociating one well of a 6-well plate of hiPSCs with TrypLE for 6-8 min. After stopping the enzymatic reaction with DMEM, the cell suspension was centrifuged (1500 rpm, 2 min) and resuspended in PeproGrow medium containing 10 µM Y-27632 and 10 µM blebbistatin. For EB formation, 15.000 cells per well were distributed on a 96-well V-shaped culture plate and centrifuged (1600 rpm, 4 min) to induce reaggregation of cells. The next day, 80 % of the medium was replaced with N2 medium, the same was carried out on day four of the differentiation. On day seven, EBs were plated on growth-factor-reduced (GFR) MG coated 6-well plates in a density of 32 EBs per well. Medium of the adherent culture was changed daily and switched from N2 to BRDM on day 16.

For detachment of retinal fields on day 24, the adherent cell layer was subdivided into small, regular fragments using a micro knife and detached from the well plate with a cell scraper. The tissue aggregates were collected in a 10 cm petri dish containing 12 ml BRDM. Medium was changed entirely the day after detachment and afterwards half of the medium was changed twice a week. From day 35 BRDM was supplemented with 10 % FBS and 100 µM taurine. Additionally, 1 µM Retinoic acid was added from day 70 to 100, reduced to 0,5 µM from day 100 to 190 and removed afterwards.

Non-retinal tissue was removed from the plate within the first days after detachment and regularly during the subsequent cultivation time. It was separated manually using curved micro scissors, if it was attached to retinal tissue or RPEorg, RPEorg evolved spontaneously during RO differentiation and became clearly visible as irregularly shaped dark organoids between day 40 and 60 of differentiation. ROs and RPEorg were cultivated jointly in a dish until used in experiments.

Table 2-15: N2 medium

Component	Amount
DMEM/F12 + GlutaMAX™	
Sodium selenite	24 nM
Progesterone	16 nM
Human apotransferrin	80 µg/ml
Human recombinant insulin	20 µg/ml
Putrescin	88 µM
Non-essential amino acids (NEAA) 100x	1x
Antibiotic-antimycotic (AA) 100x	1x

Table 2-16: B27-based retinal differentiation medium (BRDM)

Component	Amount
DMEM/F12 + GlutaMAX™ : DMEM	1:1
B-27™ without vitamin A	10 ml
Non-essential amino acids (NEAA) 100x	1x
Antibiotic-antimycotic (AA) 100x	1x

2.2.6 Derivation of adherent retinal pigment epithelial cells from 3D RPE organoids

For the generation of adherently cultured RPE cells from RPEorg, organoids were selected from a dish of retinal differentiation. A minimum number of ten RPEorg was needed to produce an adequate amount of RPE cells. The RPEorg were cut small with micro scissors and non-pigmented areas were removed from the dish, to obtain a population of RPE cells as pure as possible.

Subsequent dissociation of RPE cells was performed either by treating the aggregates with Accumax solution for 60 min at 37 °C or by using the Neurosphere Dissociation Kit (P), following the supplier's manual. In both cases, the cell suspension was resuspended regularly to improve dissociation. The reaction was stopped with DMEM and FBS, the single cell suspension was strained with 70 µm and 40 µm cell strainers and switched to BRDM with supplements. The day of dissociation, BRDM was supplemented with 10 % FBS, 20 ng/ml EGF, 20 ng/ml FGF-2, 2 µg/ml heparin and 10 µM ROCK inhibitor (BRDM++). From the following day, cells were grown in BRDM++ without FBS until they reached confluency.

2.2.7 Cultivation of hiPSC derived retinal pigment epithelial cells

HiPSC derived retinal pigment epithelial cells were usually cultured on tissue-treated cell culture plates, if immunostainings were scheduled, specific polymer µ-dishes were used. For coating, plates were incubated with 0,01 % Poly-L-Ornithine for 2 h at RT, washed with PBS -/- and subsequently 20 µg/ml laminin in DMEM was added for 4 h at 37 °C.

In contrast to other cell types, RPE could be grown in a plate for up to several months and did only need to be split for expansion or if required for experiments. For splitting, adherent RPE cells were washed with PBS -/- and treated with Accumax for 30 min at 37 °C. The single cell suspension was strained (70 µm and 40 µm cell strainer) and after centrifugation (1500 rpm, 2 min) the pellet was resuspended in BRDM++ with 10 % FBS. RPE cells were seeded at a density of ~7,5 x 10^4 cells per cm^2. RPE was further cultured in BRDM++ until cells had grown confluent, afterwards medium was switched to BRDM without supplements. Medium was changed daily.

2.2.8 Phagocytosis assay

Before applying bovine photoreceptor outer segments (POS) to the cells, they were FITC-labeled using the Pierce FITC Antibody Labeling Kit (Thermo Fisher Scientific) following the manufacturer's specifications. Adherent RPE cells (asRPE) were cultured for 14 days on the plate before performing the assay to mature them sufficiently. RPE organoids were used at day 92 (early RPEorg) and day 323 (aged RPEorg) with n=3.

Adherent asRPE cells were incubated with ~ 5 POS per cell and RPE organoids were treated with 1 x 10^6 POS per spheroid for 8 hours at 37 °C. Afterwards, asRPE and RPEorg were washed five times with PBS -/- to remove remaining POS. Cells were fixed and stained according to the standard practice.

2.2.9 Fixation and cryosectioning for immunocytochemistry

Adherent RPE cells were washed with PBS -/- and fixed with 4 % PFA for 20 min at RT. Fixed cells were either stored in PBS -/- with AA at 4 °C or used for immunocytochemistry immediately.

RPE organoids were washed with PBS -/- and fixed with 4 % PFA and 10 % sucrose for 20 min at RT. Afterwards, RPEorg were moved to a 30 % sucrose solution at 4 °C overnight. Within the next few days, the samples were embedded in cryomolds in Tissue-Tek® O.C.T.™ and frozen on a precooled metal block at -80 °C. As soon as frozen, samples were transferred to the -80 °C freezer for storage. Cryosections of RPEorg were generated at the cryostat at -20 °C sample and blade temperature. Samples were cut to slices of 14 µm thickness, collected on object slides for immunostainings and stored at -80 °C.

2.2.10 Immunocytochemistry

While fixed, adherent RPE cells could be used immediately for immunocytochemistry, cryosections were defrosted and rehydrated with PBS -/- for 20 min at RT previously. The further procedure of immunocytochemistry was the same for both sample types and is represented in the following Table 2-17.

Table 2-17: Procedure of immunocytochemistry

Step	Solution	Temperature	Incubation time
Blocking and permeabilization	10 % NDS, 0,2 % T-X in PBS -/-	RT	1 h
1st antibody	10 % NDS, 0,2 % T-X in PBS -/-	4 °C	O/N
Washing	PBS -/-	RT	3 x 5 min
2nd antibody	5 % NDS, 0,1 % T-X in PBS -/-	RT	1 h
Washing	PBS -/-	RT	1 x 5 min
DAPI/Hoechst	PBS -/-	RT	10 min
Washing	PBS -/-	RT	3 x 5 min
Mounting	ProLong™ Gold Antifade		

2.2.11 Transmission electron microscopy

Samples for transmission electron microscopy (TEM) were processed as described previously [133] with some minor modifications. RPEorg were collected and washed with PBS -/-. Fixation was performed in Carnovsky buffer (2,5 % glutaraldehyde, 2 % PFA, 0,1 M sodium cacodylate buffer, pH 7,4) for 2 h at RT. Three wash steps for 10 min in 0,1 M sodium cacodylate buffer were followed by postfixation in 1 % OsO_4 for 1 h at RT. Samples were washed again three times in cacodylate buffer and afterwards dehydrated in 50 % EtOH for 10 min and 70 % EtOH for 10 min. After incubation with uranyl acetate for 1 h at RT, RPEorg were washed with 70 % EtOH for 10 min and 99 % EtOH overnight at 4 °C. The next day, samples were treated three times with acetone for 10 min and three times with propylene oxide for 10 min. Infiltration with Epoxy embedding medium was performed with increasing ratios (25 %, 50 %, 75 %) in propylene oxide for 1 h per condition. Final infiltration was carried out with 100 % Epoxy embedding medium for 2 h at RT in flat molds, before samples were cured for 12 h at 60 °C.

An ultramicrotome was used to cut semithin sections (1 µm) and ultrathin sections (50 nm). Semithin sections were stained with Richardson's solution (0,5 % azure, 0,5 % methylene blue, 1 % borax) to check if the appropriate cutting point for ultrathin sections was reached. Ultrathin

sections were collected on pioloform-coated copper grids and scanned with a Zeiss EM 900 transmission electron microscope.

2.2.12 RNA purification

Total RNA was purified with the Qiagen RNeasy® Micro Kit following the manufacturer's instructions. After washing with PBS -/-, adherent cells or organoids were lysed in 350 µl RLT buffer and centrifuged through a QiaShredder column to achieve complete homogenization.

The RNA was bound to a RNeasy spin column by ethanol addition and subsequently washed with different buffers to remove interfering components. Final elution of RNA was performed with 16 µl RNase free water in RNase free 1,5 ml reaction tubes. RNA content was measured spectrophotometrically.

2.2.13 Fluidigm array

High-throughput gene expression analysis was carried out on the Fluidigm BioMark™. For DNase digestion and cDNA synthesis, 80 ng purified RNA, RT-PCR buffer, dNTPs, hexanucleotide mix, MMLV RT and RNase free H_2O were applied. TaqMan assay probes were used on 48.48/96.96 Dynamic Array plates. Data were analyzed using Microsoft Excel 365 and graphs were created using GraphPad Prism. Relative expression was calculated as a scaled mean of the housekeeping genes GAPDH and RPS9 (Ribosomal Protein S9). Therefore, the subsequent formula was applied:

$$2^{\text{Housekeeping gene for sample x}} = \text{Mean}\left(\frac{2^{\text{GAPDH}_{\text{sample x}}}}{\text{Mean}(2^{\text{GAPDH}_{\text{all samples}}})}, \frac{2^{\text{RPS9}_{\text{sample x}}}}{\text{Mean}(2^{\text{RPS9}_{\text{all samples}}})}\right)$$

2.2.14 Image analysis and autofluorescence recording

For fluorescence intensity quantification (Figure 3-13), the RPE organoid area was manually defined, and intensity was quantified using the Measure plugin of ImageJ.

Autofluorescence recoding in Figure 3-7 and Figure 3-12 was performed using a conventional fluorescence microscope using filter sets for red (Excitation 550/25, Emission 605/70) and green (Ex: 470/40, Em: 525/50) spectra. For Figure 3-10, Figure 3-11 and Figure 3-16, autofluorescence was detected using a confocal microscope (Zeiss LSM 710) with filter sets for green spectrum (Ex: 470/40, Em: 525/50).

2.2.15 Statistical analysis

Statistical analysis was performed in GraphPad Prism, applying Two-sided student's t-test or One-way ANOVA with Bonferroni post-hoc tests. Results are presented as mean values with standard error of the mean (S.E.M). Statistical significance is indicated as: *$p<0.05$, **$p<0.01$, ***$p<0.001$.

3 Results

3.1 Adherently cultured retinal pigment epithelial cells

3.1.1 Differentiation of retinal pigment epithelial cells

Aiming to generate fully mature and functional retinal pigment epithelial cells form hiPSCs, two approaches for RPE differentiation were applied (Figure 3-1) and subsequently, morphology and presence of RPE-specific markers was investigated to inspect the quality of RPE cells, respectively.

In the first approach (Figure 3-1 a), RPE cells were differentiated according to a direct and continuously adherent protocol [122], in the following referred to as adRPE. After the initial splitting of hiPSCs, distinct factors such as IGF, FGF-2, TGF-ß and WNT pathway modulators were applied in different concentrations and for different time spans for the first 14 days to push the hiPSCs towards RPE cell identity (Figure 3-1 c). During this period, a large proportion of cells developed a hexagonal morphology, which is typical for RPE cells. At day 14 of differentiation, all cells which did not exhibit this characteristic morphology were removed from the plate manually and the remaining cells were dissociated and seeded onto a new pre-coated culture plate, regarded as passage 0 (p0) cells. With every other splitting, passage of RPE cells was increased by one (Figure 3-1 d-f). In the following experiments, adRPE cells were used at passage 2.

The second approach (Figure 3-1 b) made use of a 3D retinal organoid differentiation protocol [66] which had been shown to simultaneously generate RPE organoids [76]. For this purpose, embryoid bodies (EBs) were generated from hiPSC colonies and plated on day seven of differentiation (Figure 3-1 g). Applying N2 medium (Table 2-15), cells were directed to a neural fate and started to form retinal fields, appearing as bright regions next to the initial EB (Figure 3-1 h). At day 24, retinal fields were detached and kept in suspension for further cultivation. RPE organoids started to become clearly visible around day 40 of differentiation (Figure 3-1 i). For the generation of an adherent RPE cell layer form RPEorg, organoids were collected, cut into small pieces and non-pigmented areas were removed precisely. After enzymatic dissociation, RPE cells were plated on pre-coated culture plates and defined as passage 0 cells (Figure 3-1 j). Adherent RPE cells generated from RPE organoids are subsequently designated as asRPE. As soon as they reached confluency, their typical hexagonal shape became clearly visible. Furthermore, after several weeks on a culture plate, asRPE cells became strongly pigmented. In this study, asRPE were used at passage 2.

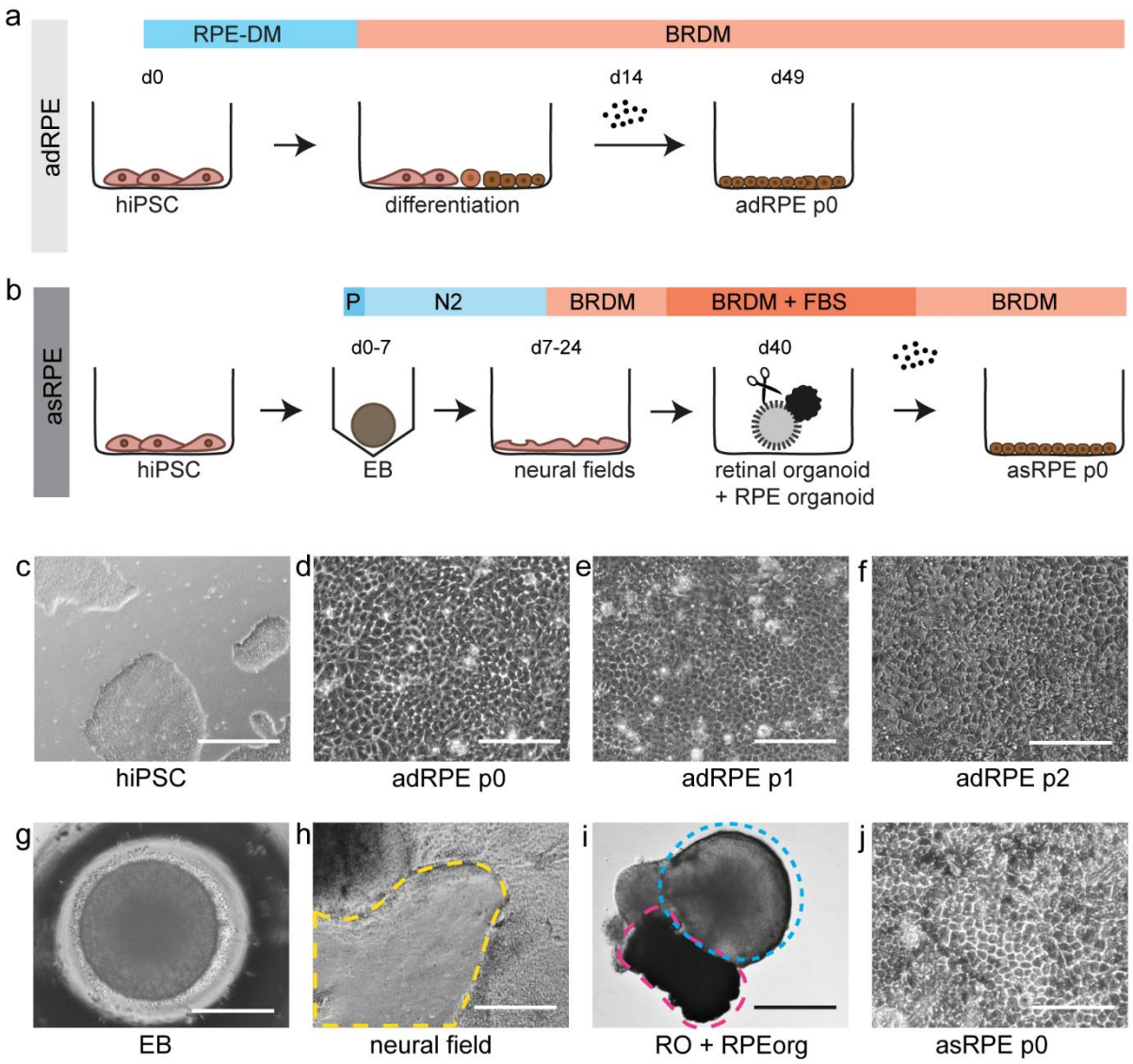

Figure 3-1: Differentiation protocols for adherent retinal pigment epithelial cells.
The differentiation from hiPSCs was either performed adherently towards adRPE (a) or with a 3D retinal organoid differentiation approach (b). Direct differentiation from hiPSCs (c) towards adRPE was performed supplementing specific growth factors. Adherent adRPE cells exhibit the typical hexagonal morphology at passage 0, 1 and 2 (d-f). The 3D retinal organoid approach was initiated producing embryoid bodies from hiPSCs (g), which were subsequently plated and formed neural fields (h, encircled yellow). Detached neural fields developed towards retinal organoids (RO, encircled blue) and RPE organoids (RPEorg, encircled magenta) (i). After selection and dissociation of RPEorg, adherent asRPE cells (j) were obtained. Scale bars: c, g, h, i 500 µm; d, e, f, j 100 µm.

3.1.2 Characterization of adherent retinal pigment epithelial cells

Both approaches for the differentiation of adherent RPE cells, adRPE and asRPE, delivered RPE cells with a characteristic cobblestone-like morphology. For a detailed comparison of the two protocols, adRPE and asRPE cells were investigated via immunohistochemical stainings and gene

expression analyses. As RPE cells require several weeks to mature sufficiently after splitting, they were grown for 28 days on the plates until they were fixed for stainings or harvested for RNA extraction. To avoid inter-donor variation, RPE cells were differentiated from hiPSCs of the same donor.

The typical hexagonal shape could be observed in phase-contrast and brightfield images of both, adRPE and asRPE cells (Figure 3-2 a, b). Apparently adherently differentiated RPE cells were slightly smaller than the ones generated from 3D RPE organoids and appeared to be slightly less pigmented. Pigmentation in adRPE did only increase marginally after up to five months in culture (data not shown).

In immunohistochemical stainings (Figure 3-2 c-o), a robust expression of the RPE-specific 65 kDa protein (RPE65), which is a central enzyme of the visual cycle, could be detected in RPE cells of both differentiation protocols. The presence of an additional visual cycle marker, Lecithin Retinol Acyltransferase (LRAT) was further demonstrated by a strong and uniform signal in adRPE and asRPE cells. The expression of Bestrophin-1 (BEST1), a marker for RPE-specific calcium channels, seemed to be quite comparable in adRPE and asRPE, while the microphthalmia-associated transcription factor (MITF) was detected increasingly in asRPE. Staining for the premelanosome protein (PMEL), as a marker for pigmentation, revealed a typical granular pattern in both, adRPE and asRPE. The presence of two further essential characteristics of RPE could again be demonstrated in both, adRPE and asRPE, using the microvilli marker Ezrin and the tight junction protein 1 (Zonula Occludens-1, ZO-1). In addition, cytoskeleton (more specific F-actin) of the cells was labeled using phalloidin, confirming the cobblestone-like morphology of adRPE and asRPE.

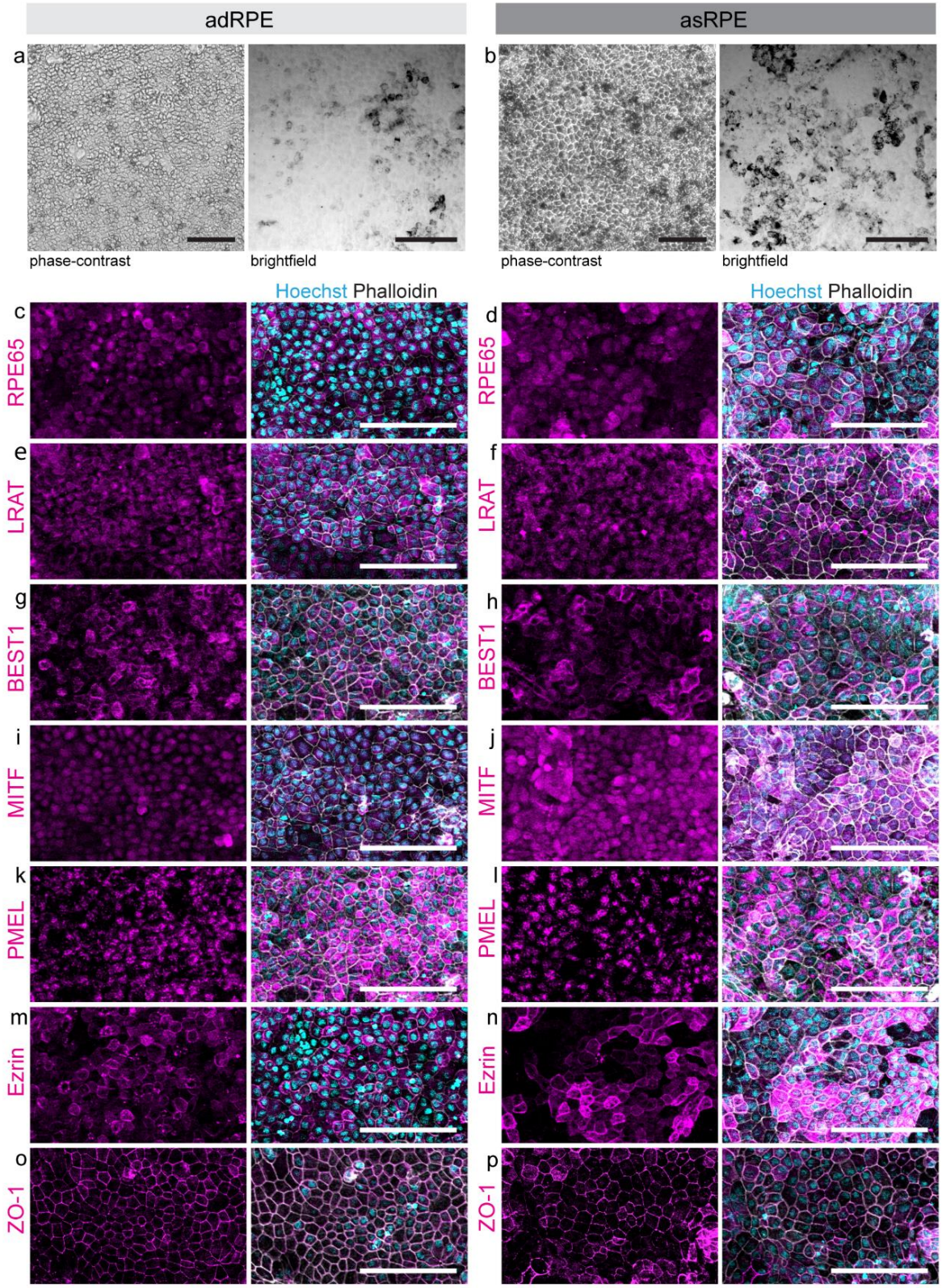

Figure 3-2: Immunohistochemical characterization of adherently cultured RPE cells.
Phase-contrast and brightfield images display morphology and pigmentation of adRPE (a) and asRPE (b). Immunohistochemical stainings of RPE specific markers RPE65 (c, d), LRAT (e, f), BEST1 (g, h), MITF (i, j), PMEL (k, l), Ezrin (m, n) and ZO-1 (o, p) (magenta), co-labeled with phalloidin (white) and Hoechst 33342 (light blue). Images are presented as maximum intensity projections (MIP). Scale bars: 100 µm.

In addition to immunohistochemical stainings, gene expression of RPE specific markers was investigated in adherently differentiated adRPE and organoid derived asRPE. Gene expression analyses revealed a significantly higher expression of *RPE65*, *BEST1*, *MITF* and *PMEL* in adRPE, compared to asRPE (Figure 3-3). The same could be observed for the expression of *serpin family F member 1* (*SERPINF1*), which is secreted by RPE cells and inhibits angiogenesis. The expression of *LRAT* and *COL4A1* (Type IV collagen), a component of the basal membrane, did not reveal significant differences between adRPE and asRPE, although the expression of *COL4A1* was slightly higher in asRPE cells.

To summarize, both differentiation methods generated fully mature RPE cells, which was demonstrated by their typical hexagonal morphology and characteristic pigmentation. Although the expression of RPE-specific markers on protein and mRNA level showed slight differences between adRPE and asRPE, all of them were present. Thus, adRPE, as well as asRPE, are suggested to be suitable in vitro models of the RPE.

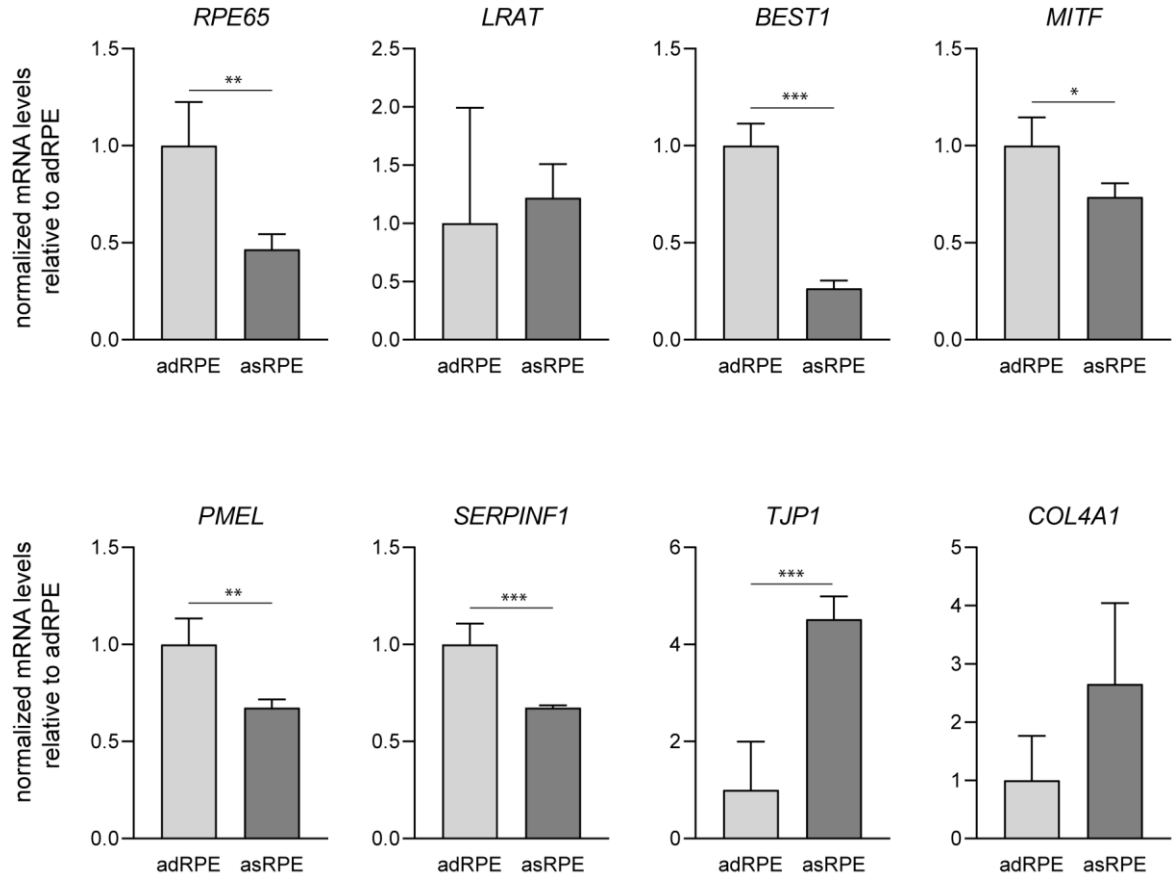

Figure 3-3: mRNA expression of RPE-specific markers in adRPE and asRPE.
RPE cells were cultured for 28 days. Expression was normalized to *GAPDH* and *RPS9* and is displayed relative to adRPE. Bars show means with S.E.M. Significance is *p<0.05, **p<0.01, ***p<0.001 according to Two-sided student's t-test. N = 4 wells per differentiation.

3.2 RPE organoids

3.2.1 Differentiation of RPE organoids

The methodology to differentiate RPE organoids (RPEorg) simultaneously to retinal organoids has been described previously [66], [76]. The concept behind it is to create an environment in which RPE cells can be cultured for an exceptionally long time (up to one year) and with a sufficient ECM. This could potentially not only improve the maturation of RPE cells, but further allow studies of aged RPE cells, which are especially needed for investigations of age-related diseases, such as AMD.

In this study, RPE organoids were differentiated simultaneously to retinal organoids (ROs) (Figure 3-4 a), as described in chapter 3.1.1.. Shortly, EBs were formed from hiPSCs, plated on day seven, emerging neural fields were detached on day 24 of differentiation and cultured in suspension afterwards. RPEorg became visible between day 40 and 60 of differentiation. Due to their strong pigmentation and irregular, amorphous structure (Figure 3-4 d, e), they were easily distinguishable from retinal organoids, which have a bright appearance, a regular shape, and a clear layering (Figure 3-4 b, c). RPEorg were typically attached to ROs or non-retinal tissue, from which they were detached using micro scissors.

In contrast to adherently cultured RPE cells from RPE organoids (asRPE), RPEorg themselves were not dissociated but cultivated in suspension until used for experiments (Figure 3-4 d, e). As the impact of cultivation time on maturation and disease-association was to be investigated, RPEorg were collected at three different ages. In the following, they are referred to as early RPEorg (day 80-100), intermediate RPEorg (day 191) and aged RPEorg (day 280-360). The morphology of early and aged RPEorg of age was indistinguishable from brightfield images (Figure 3-4 d, e).

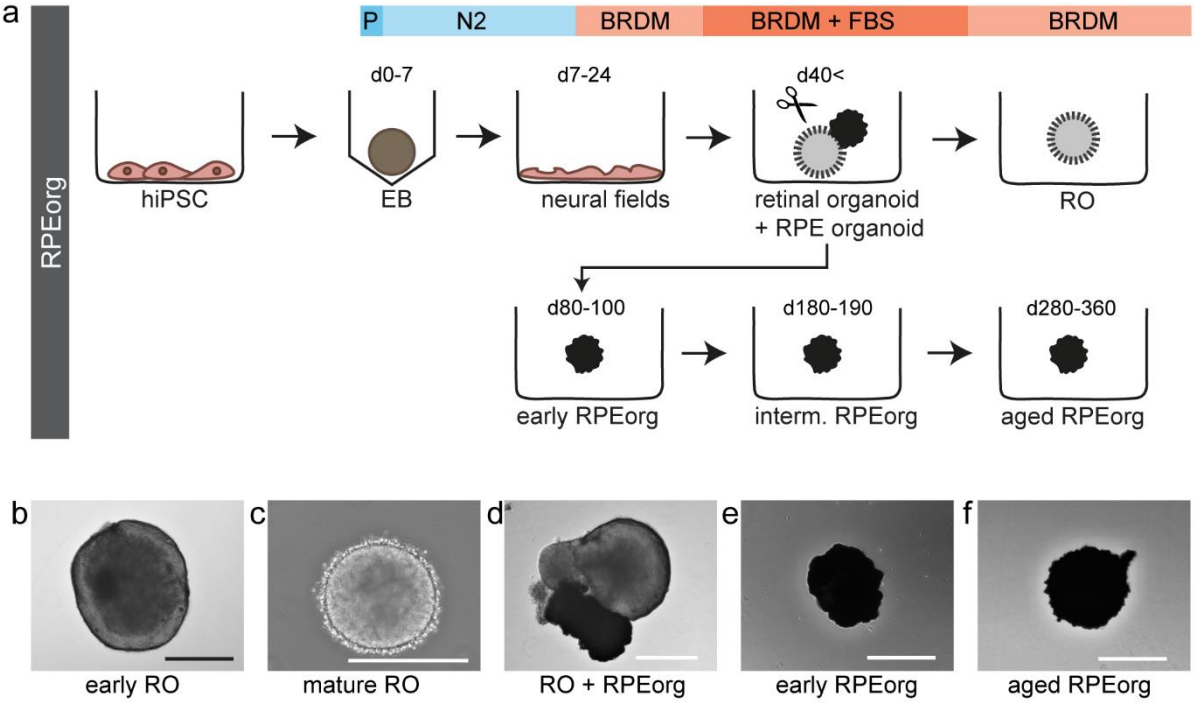

Figure 3-4: Differentiation of 3D retinal pigment epithelial organoids.
RPEorg were differentiated simultaneously with retinal organoids (a). Formation of EBs and neural fields were intermediate steps towards early ROs at day 80 (b) and mature ROs at day 400 (c), RPEorg attached to RO at day 80 (d), as well as early RPEorg at day 80 (e) and aged RPEorg at day 320 (f). Scale bars: 500 µm.

3.2.2 Characterization of RPE organoids

For a more detailed investigation of RPEorg, semithin (1 µm) and ultrathin (50 nm) sections were prepared and examined. Electron microscopy images of early and aged RPEorg showed the presence of several major characteristics of RPE cells, such as apical microvilli, melanosomes, and tight junctions between adjacent cells (Figure 3-5 a-d).

Semithin sections (Figure 3-5 e-j) were stained with Richardson's solution, labeling basophilic and osmiophilic structures in dark blue. RPEorg were mostly framed by a monolayer of RPE cells, which seemed to be polarized, as the nucleus was located at the basal side and dark granules could be observed at the apical side of the monolayer. This could be observed for RPEorg of all ages. Furthermore, some RPEorg displayed cell-free central areas, while in some regions unstructured material, presumably extracellular matrix, or rarely singular cells could be found.

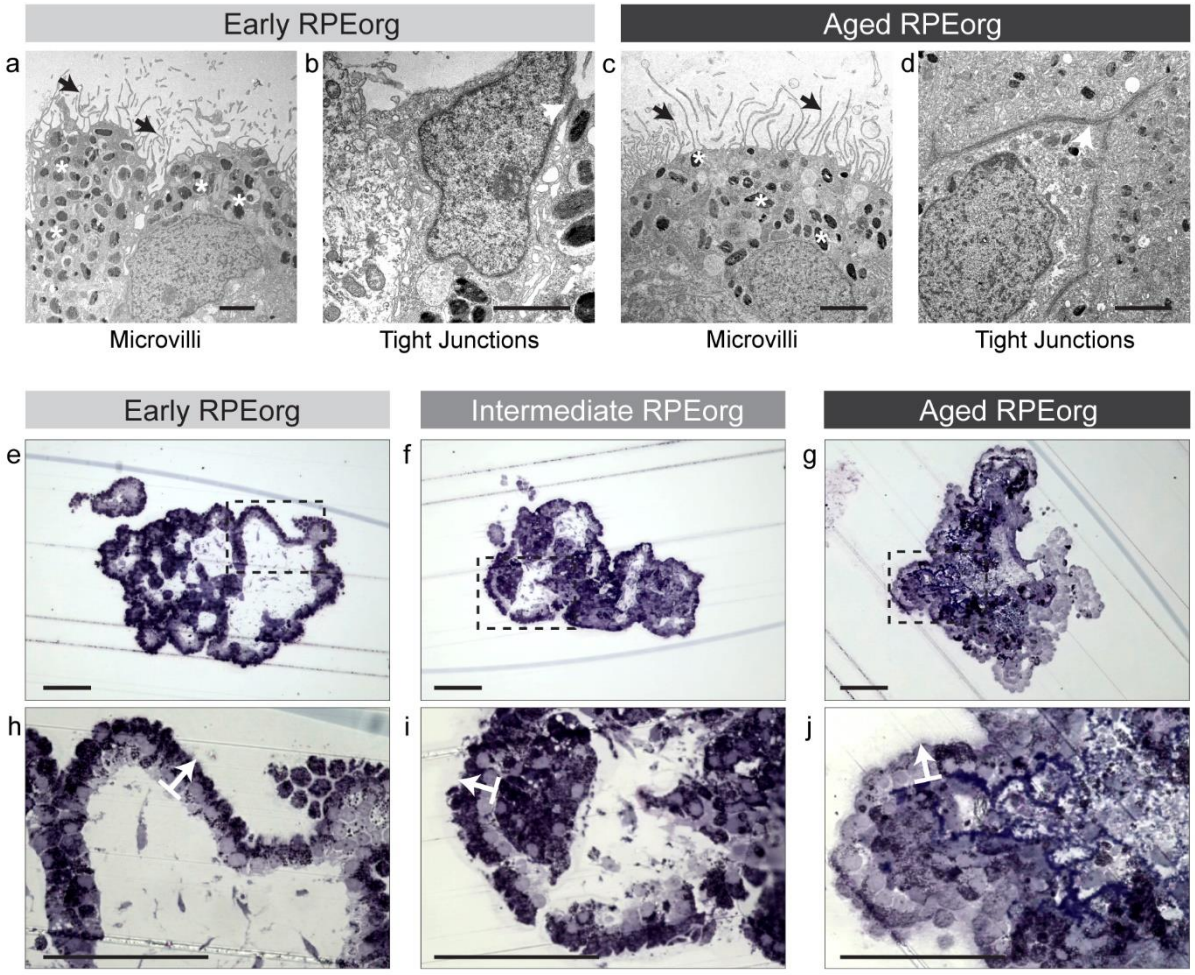

Figure 3-5: (Ultra-)Structural analysis of RPE organoids.
Electron microscopy images (a-d) show apical microvilli (black arrows) and melanosomes (*), as well as tight junctions (white arrows) in early and aged RPEorg. Semithin sections (e-j) were stained with Richardson's solution (0,5 % azure, 0,5 % methylene blue, 1 % borax) and illustrate the outer layer of RPE cells surrounding the RPEorg. White arrows point from basal to apical. Black squares in the overview image show the magnified area depicted in the enlarged image on the bottom, respectively. Scale bars: a-d 2,5 µm; e-j 100 µm.

After investigating the RPE morphology, expression of RPE-specific markers was examined via immunohistochemical stainings of cryosections (Figure 3-6) in early (day 80-90) and aged (day 280-360) RPEorg. The RPE-specific 65 kDa protein (RPE65), which is a maturation marker of RPE, was hardly visible in early RPEorg, while in aged RPEorg it was strongly expressed by the outer cell layer of RPE cells (Figure 3-6 a, b). Both, early and aged RPEorg displayed a clear signal for the premelanosome protein (PMEL) (Figure 3-6 c, d), which plays a central role for pigmentation of cells. Ezrin, labeling microvilli of RPE cells, was expressed at the surface of the outer layer of RPEorg, whereby the apical localization was readily apparent in early and aged RPEorg, seeming to increase slightly in aged RPEorg (Figure 3-6 e, f). Additionally, the tight junction marker zonula occludens-1 (ZO-1) was detected in RPEorg, independently of age (Figure 3-6 g, h).

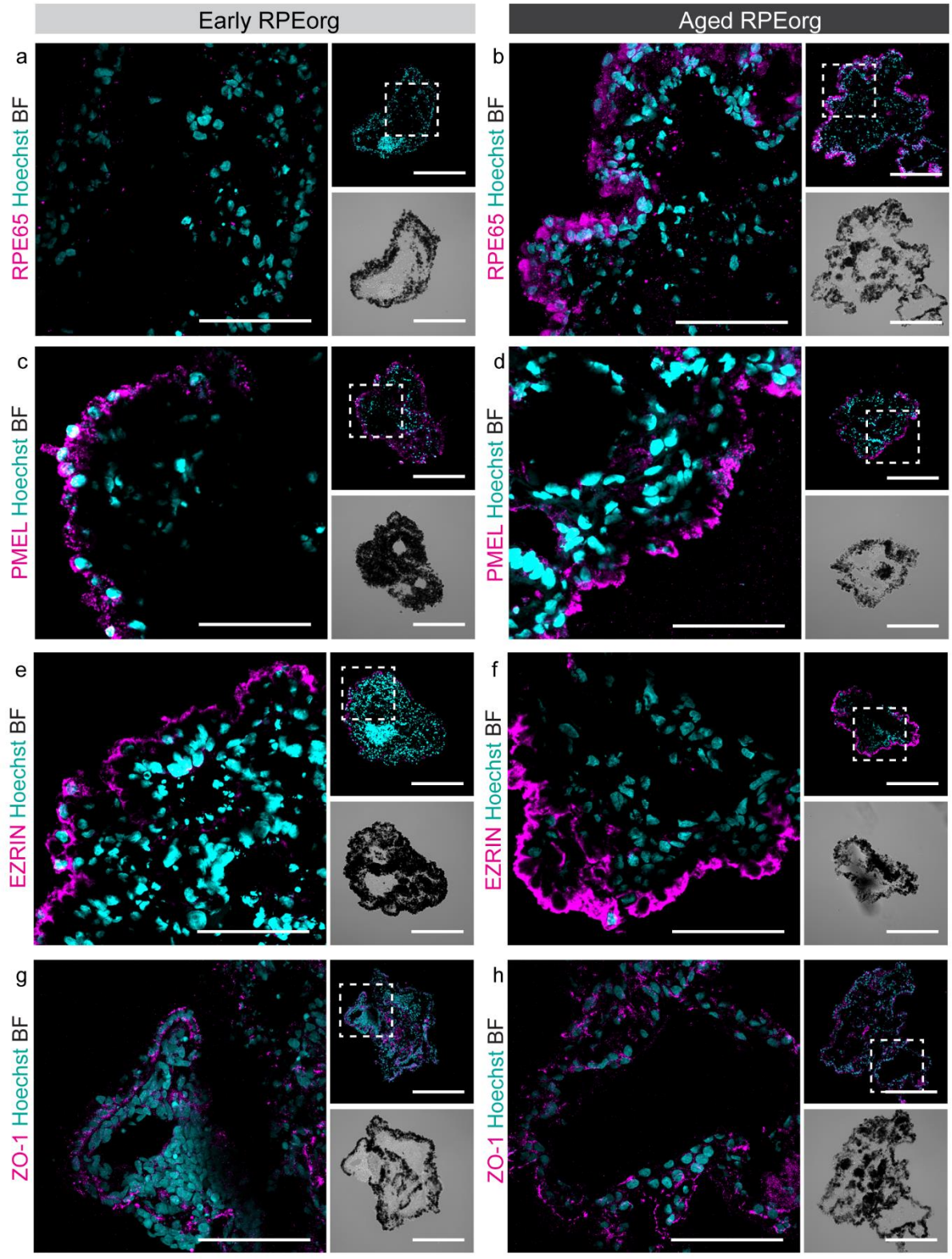

Figure 3-6: Immunohistochemical characterization of early and aged RPE organoids.
Cryosections of RPEorg were stained for RPE markers RPE65 (a, b), PMEL (c, d), Ezrin (e, f) and ZO-1 (g, h) (magenta). Hoechst 33342 = light blue. White squares in the small image show the magnified area depicted in the enlarged image on the left. Images are presented as maximum intensity projections (MIP). Scale bars: enlarged images 50 µm; small images 200 µm.

In addition to the previous characterization of RPEorg, the polarization of RPEorg was to be investigated more precisely, as it is essential for the proper functionality of RPE cells. Ultrastructural analysis of RPEorg had already demonstrated the presence of apical microvilli in early and aged RPEorg (Figure 3-5 a, c).

To illustrate the polarization of RPE cells in RPEorg, Ezrin was chosen as a marker for apical microvilli and Collagen IV as a component of the basal membrane (Figure 3-7 a, b). As autofluorescence of aged RPEorg made reliable co-stainings difficult, all antibodies were applied in a concentration twice as high as usual and autofluorescence in the unstained channel (green AF) was depicted additionally. The resulting co-stainings present a clear apico-basal polarization across the entire RPEorg, in both early and aged RPEorg. Collagen IV was present as a continuous layer at the basal side of the outer cell layer of the RPEorg. Also, Collagen VI was detected only at the basal side in RPEorg in early and aged RPEorg, respectively (Figure 3-7 c, d). In contrast, Ezrin was located on the surface, following also the small evaginations of RPE cells. The central area of the RPEorg below the outer cell layer, was partly cell-free and partly showed clusters of cells, whereby no clear expression of the previous markers for polarization could be reported in the interior.

In conclusion, the major attributes of RPE cells, such as maturation, pigmentation, and tight junctions could be verified in RPEorg by ultrastructural analyses, as well as in immunostainings, partly increasing with age. This does not only demonstrate the identity of RPE cells in RPEorg, but also suggests their maturation and functionality.

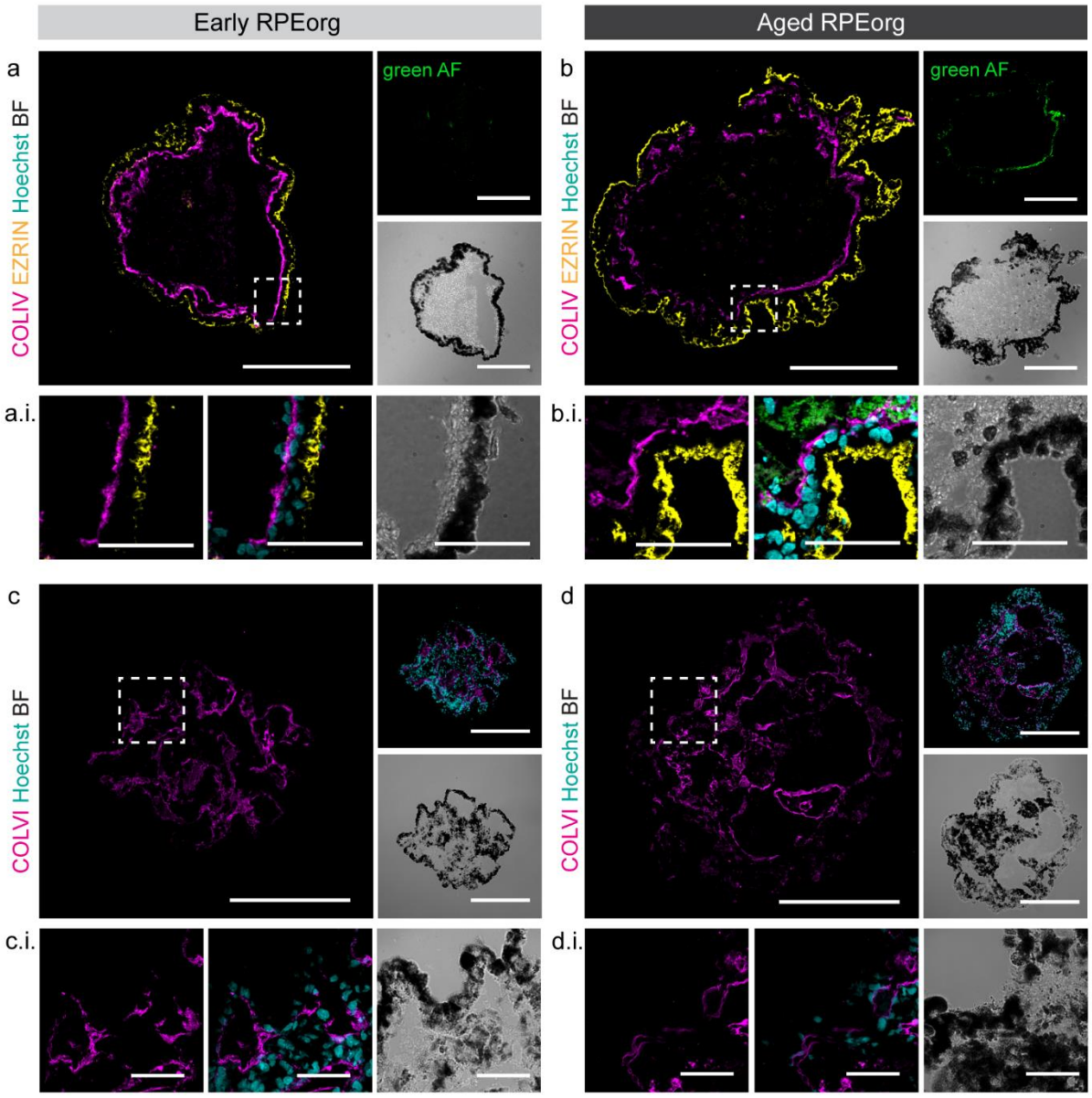

Figure 3-7: Polarization of RPE organoids.
Cryosections of RPEorg were stained for components of the basal membrane, Collagen IV (COLIV) (a, b) and Collagen VI (COLVI) (magenta) (c, d) and the apical microvilli marker Ezrin (yellow). Hoechst 33342 = light blue. White squares indicate the magnified area depicted in the enlarged images (x.i.) on the bottom. Images are presented as maximum intensity projections (MIP). Scale bars: a, b, c, d 200 µm; a.i., b.i., c.i., d.i. 50 µm.

For an in-depth analysis and comparison of RPEorg, gene expression of RPE markers was studied using qPCR (Figure 3-8). In this context, early (day 87-100), intermediate (day 191) and aged RPEorg (day 300-330) RPEorg were additionally compared to four weeks adherently cultured RPE derived from RPEorg (asRPE).

The expression of the visual cycle markers *RPE65* and *LRAT* was significantly higher in aged RPEorg compared to early or intermediate RPEorg and asRPE. These results correspond to previous immunostainings with RPE65 (Figure 3-6) and support the specification of RPE65 as maturation marker of RPE. Additionally, increase of the markers *BEST1*, *MITF* and *SERPINF1* in aged RPEorg was highly significant in comparison to all the other conditions. Interestingly, between asRPE and early or intermediate RPEorg no considerable difference could be observed for *RPE65*, *LRAT* and *SERPINF1*. However, *BEST1* was expressed higher in young and intermediate RPEorg than in asRPE, while *MITF* was expressed lower in young and intermediate RPEorg than in asRPE. Furthermore, expression of the *tight junction protein-1* (*TJP1*) was comparable in asRPE and aged RPEorg, while it was clearly decreased in early and intermediate RPEorg. Expression of the pigmentation marker *PMEL* and the basement membrane component *COL4A1* did not show any clear differences between asRPE and RPEorg, respectively.

To summarize, a major part of RPE markers investigated, displayed a drastic increase in aged RPEorg, suggesting a clear process of maturation with increasing age.

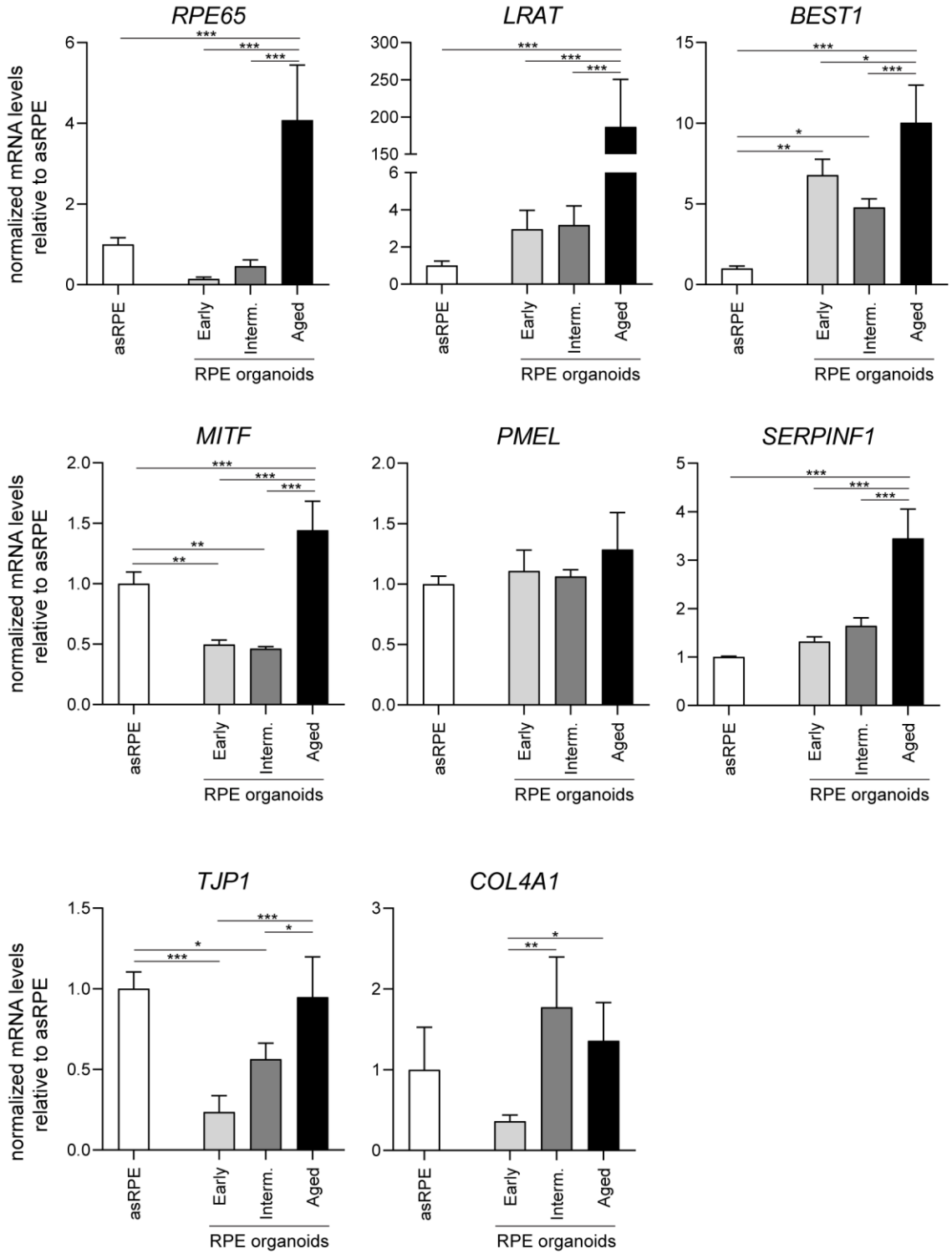

Figure 3-8: Gene expression analysis of RPE organoids.
Expression of RPE characteristic markers was normalized to the housekeeping genes GAPDH and RPS9 and displayed relative to asRPE. Bars show means with S.E.M. Significance is *p<0.05, **p<0.01, ***p<0.001 according to One-way ANOVA with Bonferroni post-hoc test. n=4 RPEorg for asRPE, early RPEorg, intermediate RPEorg and n=12 RPEorg for aged RPEorg.

3.2.3 RPE organoids are functional for phagocytosis

Phagocytosis and digestion of photoreceptor outer segments (POS) which is also linked to the retinal recycling of the visual cycle is one of the main functions of RPE cells. To assess phagocytic functionality of RPE organoids, they were treated with bovine POS, which had been labeled with FITC prior to that.

Immunohistochemistry of RPEorg revealed a signal for FITC in early and aged RPEorg, which co-localized with the signal for rhodopsin, verifying the identity of FITC- positive particles as POS (Figure 3-9 a, b). Autofluorescence in RPEorg could not only be distinguished from FITC-POS by co-localization stainings with rhodopsin, but also the signal pattern did not show the clear plain dots, as FITC-POS did. In untreated control RPEorg, no signal for FITC or rhodopsin staining could be detected (data not shown).

In RPE cells *in vivo*, POS are processed in early endosomes after their uptake, fusing to lysosomes in later stages, in which their degradation is continued [134]. Co-stainings with the early endosome associated protein 1 (EEA1) and the lysosomal membrane protein 2 (LAMP2) showed partly co-localization with FITC-POS, implying the uptake and further digestion of POS in endosomes and lysosomes of functional RPE cells (Figure 3-9 c-f).

As a control for RPEorg, adherent asRPE cells were additionally treated with FITC-POS and showed similar results to RPEorg. The signal of FITC and rhodopsin, EEA1 and LAMP2 displays co-localization (Figure 3-9 g-i). Notably, the amount of FITC-POS is not directly comparable between asRPE and RPEorg images, as the cryosections of RPEorg only display a small part of RPEorg.

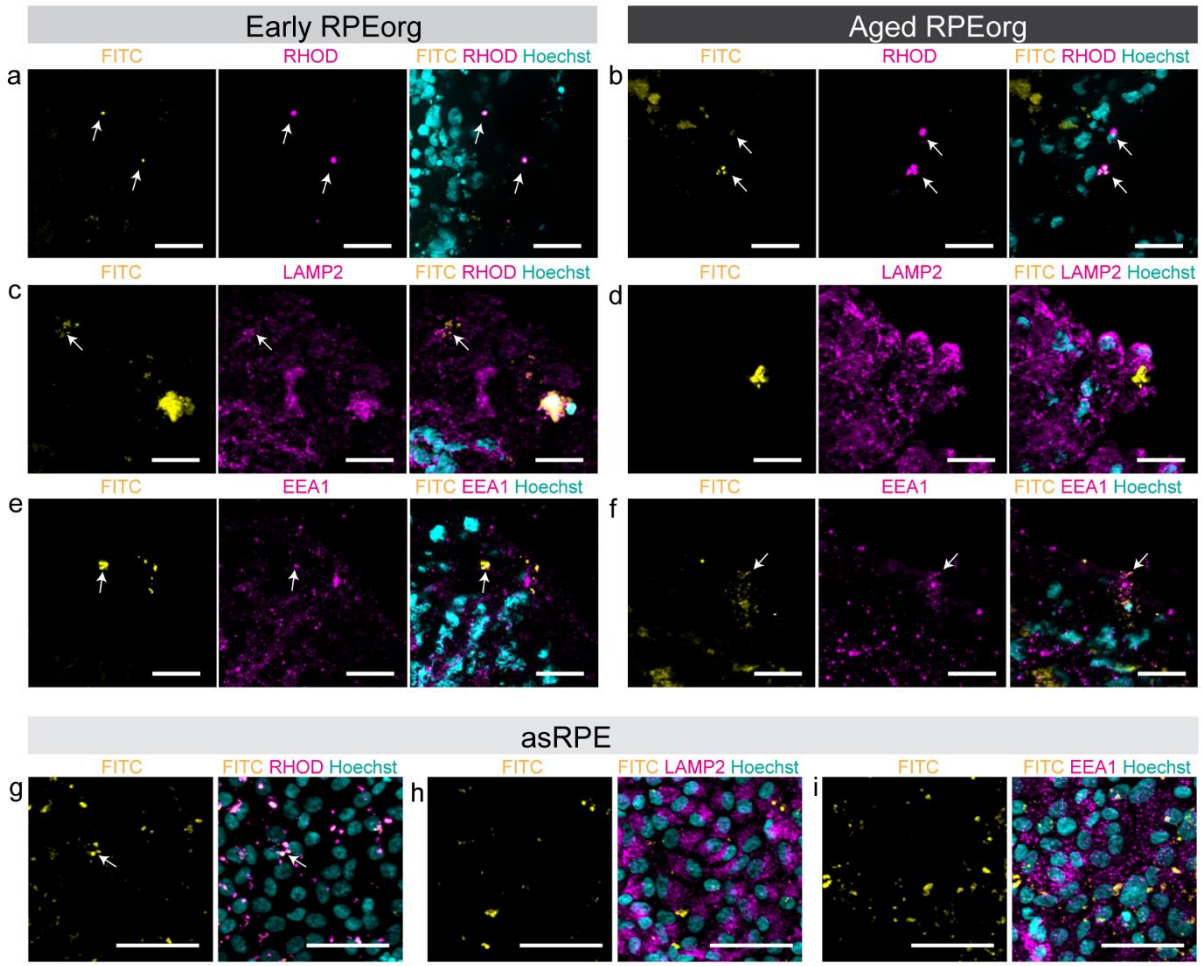

Figure 3-9: RPE organoids are functional for phagocytosis.
RPEorg and asRPE were incubated with FITC-labeled POS (yellow) for 8 h. Cryosections of RPEorg and asRPE were additionally stained for Rhodopsin (RHOD), LAMP2 and EEA1 (magenta). Hoechst 33342 = light blue. Images are presented as maximum intensity projections (MIP). Scale bars: a-f 20 µm; g-i 50 µm.

3.3 AMD association in RPE organoids

3.3.1 RPE organoids express drusen-associated proteins and lipids

After detailed characterization of RPE organoids, their suitability as model system for AMD was examined by investigating the expression of various drusen-associated proteins and lipids.

First, RPEorg were stained for tissue inhibitor of metallopeptidase 3 (TIMP3) and apolipoprotein E (APOE). Immunohistochemistry demonstrated a strong expression of TIMP3 in aged RPEorg, while the signal was hardly visible in early RPEorg (Figure 3-10 a, b). Autofluorescence (red AF) also clearly increased in aged RPEorg. Both, the signal of TIMP3 and red autofluorescence were located basally and showed a similar, but not identical pattern at higher magnification (Figure 3-10 d). Gene expression analysis further confirmed these data and showed a significantly higher

expression of TIMP3 in aged RPEorg compared to asRPE and early and intermediate RPEorg (Figure 3-10 c).

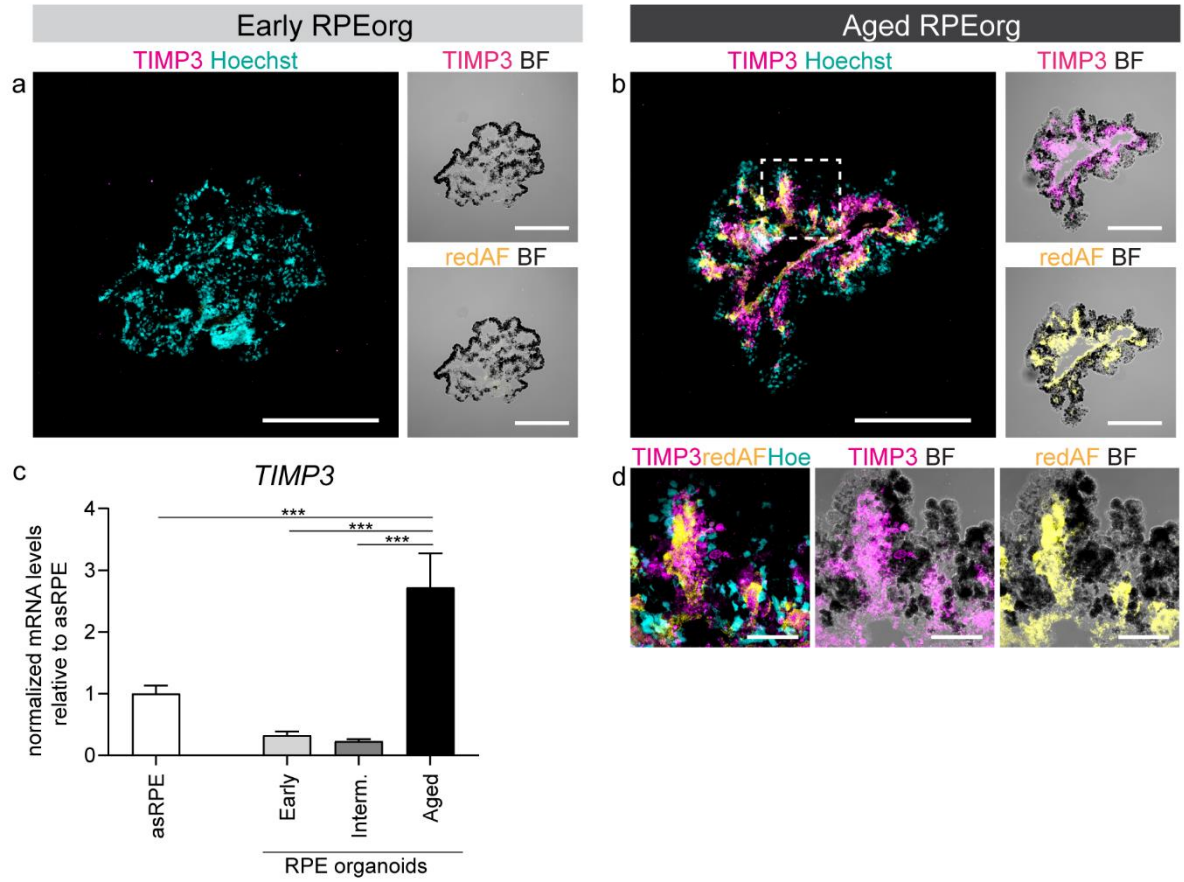

Figure 3-10: RPE organoids express the drusen-associated protein TIMP3.
(a, b, d) Cryosections of RPEorg were stained for TIMP3 (magenta). Hoechst 33342 = light blue. Red AF = yellow. Images are presented as maximum intensity projections (MIP). Scale bars: a, b 200 µm and d 50 µm. White squares in indicate the magnified area depicted in the enlarged images on the bottom (d).
(c) Expression of *TIMP3* was normalized to the housekeeping genes GAPDH and RPS9 and displayed relative to asRPE. Bars show means with S.E.M. Significance is *p<0.05, **p<0.01, ***p<0.001 according to One-way ANOVA with Bonferroni post-hoc test. n=4 RPEorg for asRPE, early RPEorg, intermediate RPEorg and n=12 RPEorg for aged RPEorg.

Additionally, expression of APOE, a frequent component of drusen, was studied. Immunohistochemistry revealed a signal for APOE in both, early and aged RPEorg without notable difference (Figure 3-11 a, b). Gene expression analyses demonstrated a higher expression of *APOE* in aged RPEorg compared to asRPE and an even highly significant increase in aged RPEorg compared to early and intermediate RPEorg (Figure 3-11 c).

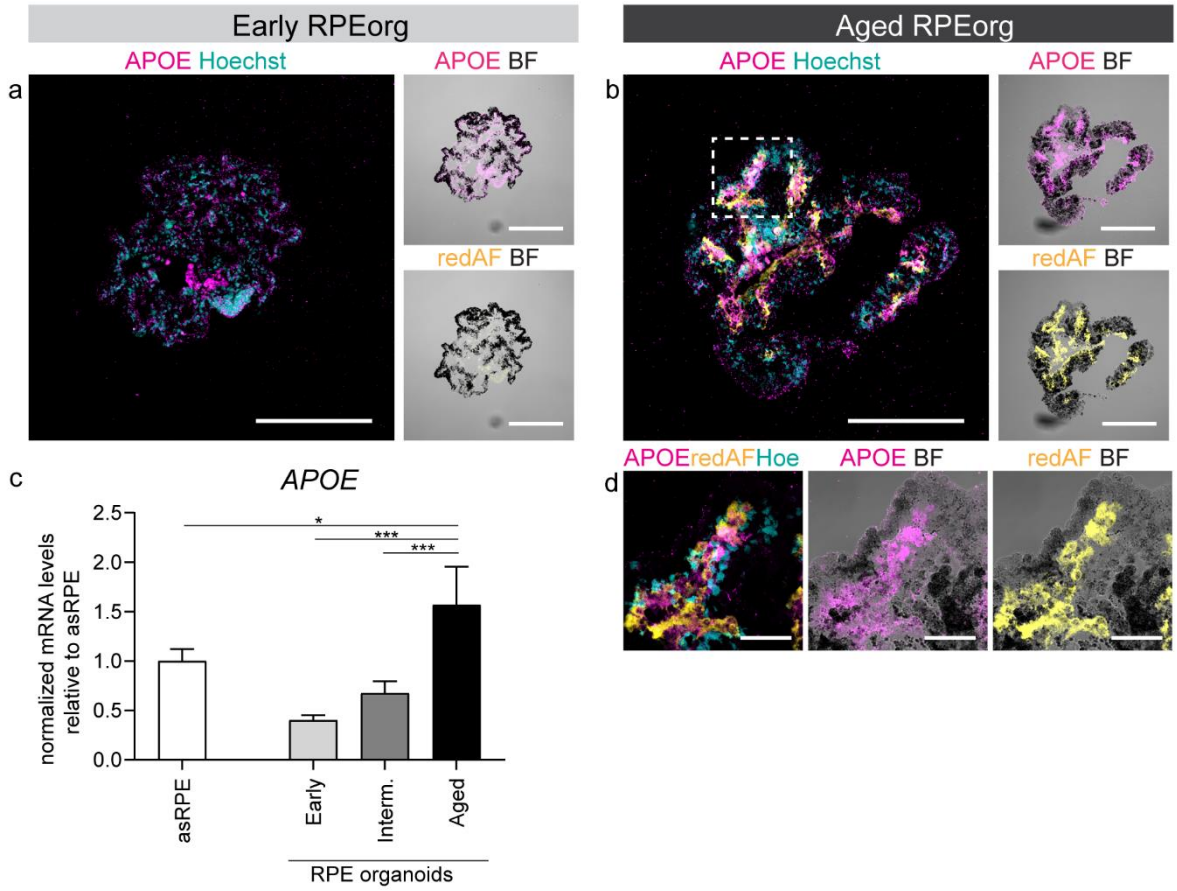

Figure 3-11: RPE organoids express the drusen component APOE.
(a, b, d) Cryosections of RPEorg were stained for APOE (magenta). Hoechst 33342 = light blue. Red AF = yellow. Images are presented as maximum intensity projections (MIP). Scale bars: a, b 200 µm and d 50 µm. White squares in indicate the magnified area depicted in the enlarged images on the bottom (d).
(c) Expression of *APOE* was normalized to the housekeeping genes GAPDH and RPS9 and displayed relative to asRPE. Bars show means with S.E.M. Significance is *p<0.05, **p<0.01, ***p<0.001 according to One-way ANOVA with Bonferroni post-hoc test. n=4 RPEorg for asRPE, early RPEorg, intermediate RPEorg and n=12 RPEorg for aged RPEorg.

The accumulation of neutral lipids in the retina is related to aging and has been observed in the context of AMD [135]. It was examined in whole mount stainings with Nile Red, a red phenoxazone dye. Live cell imaging revealed a signal for Nile Red in early, as well as in aged RPEorg (Figure 3-12 a, b). Thereby, the signal of individual samples was subject to wide fluctuations but did not display a significant difference (Figure 3-13). Additionally, RPEorg were labeled with Osteosense, a hydroxyapatite (HAP) dye, to investigate calcification processes, which are already ongoing in early stages of AMD [105]. The punctiform signal for HAP was present in both, early and aged RPEorg (Figure 3-12 c, d). Surprisingly, quantification of Osteosense revealed a higher signal in early RPEorg (Figure 3-13). Those results demonstrate the presence of neutral lipids as well as

hydroxyapatite in both, early and aged RPEorg and thus show their suitability for further studies in context with AMD.

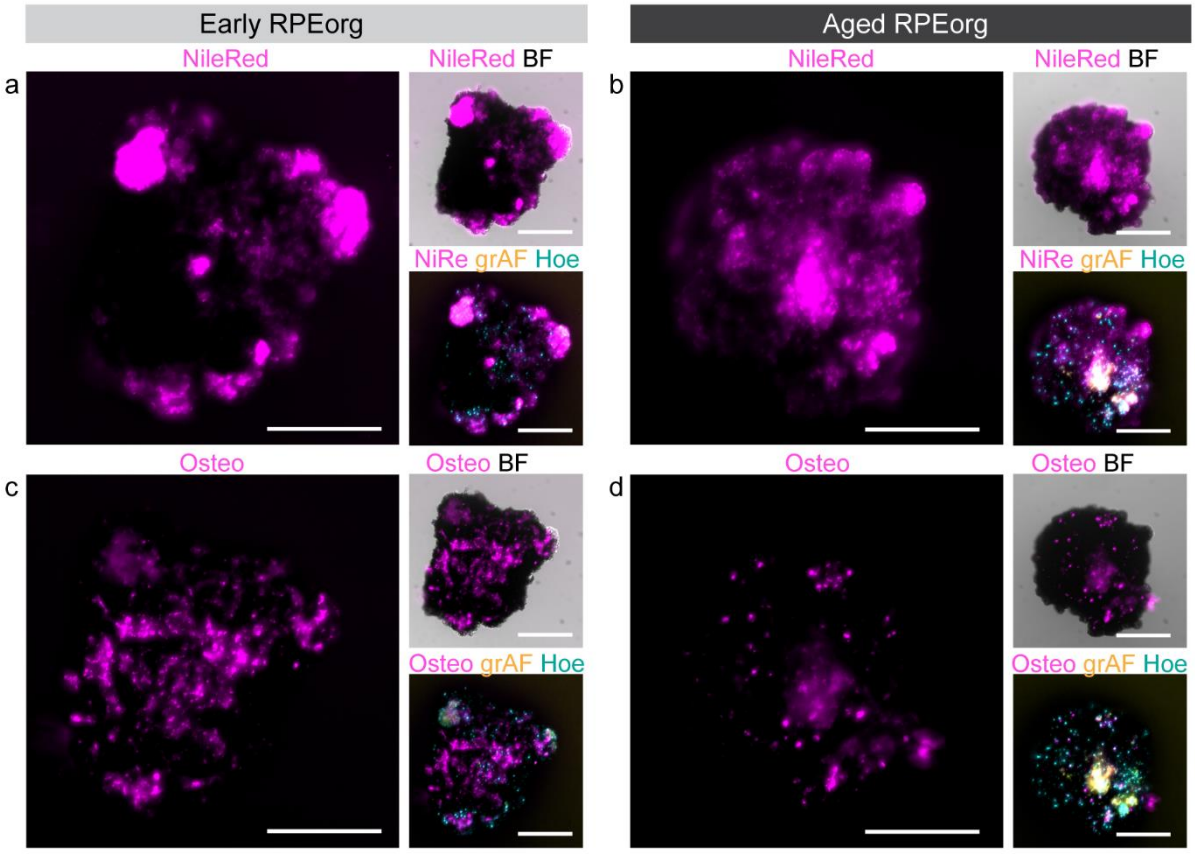

Figure 3-12: RPEorg display signs for neutral lipid accumulation and calcification.
RPEorg were labeled with Nile Red (a, b) and Osteosense (c, d) (both magenta) prior whole mount imaging. Green autofluorescence (grAF) is displayed as a comparison (yellow). Hoechst (Hoe) = blue. Scale bars: 200 µm.

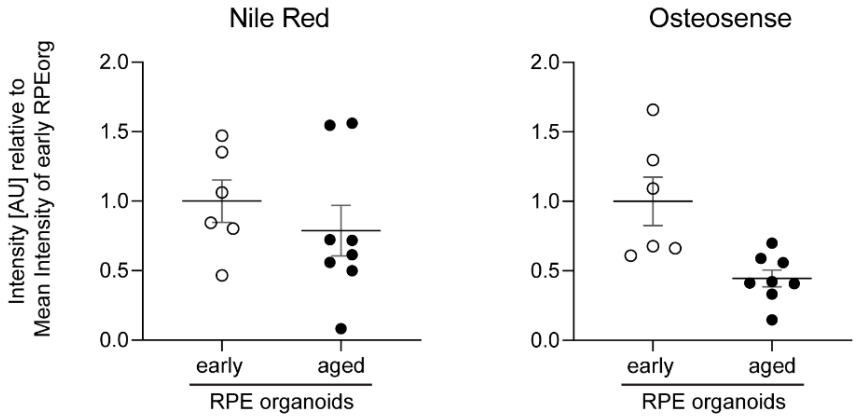

Figure 3-13: Quantification of neutral lipid accumulation and calcification in RPEorg.
Signal for Nile Red and Osteosense is displayed relative to the mean intensity of early RPEorg of each experiment. In total, n = 6 early RPE organoids and n = 8 aged RPE organoids were quantified.

Expression of Crystallin Alpha A (CRYAA) and Crystallin Alpha B (CRYAB), is increased in drusen in AMD, correlating with ongoing calcification processes [106]. Immunostainings of both, CRYAA and CRYAB showed their localization mostly at the inner layers of early and aged RPEorg and seemed to be slightly higher expressed in aged RPEorg compared to early RPEorg (Figure 3-14 a-d). Gene expression of *CRYAA* and *CRYAB* was additionally analyzed using qPCR. Data showed a decrease in *CRYAA* expression with increasing age of RPEorg, but an increase for *CRYAB*. Additionally, adherently cultured RPE (asRPE) showed a relatively high expression of *CRYAA* and *CRYAB* (Figure 3-14 e,f).

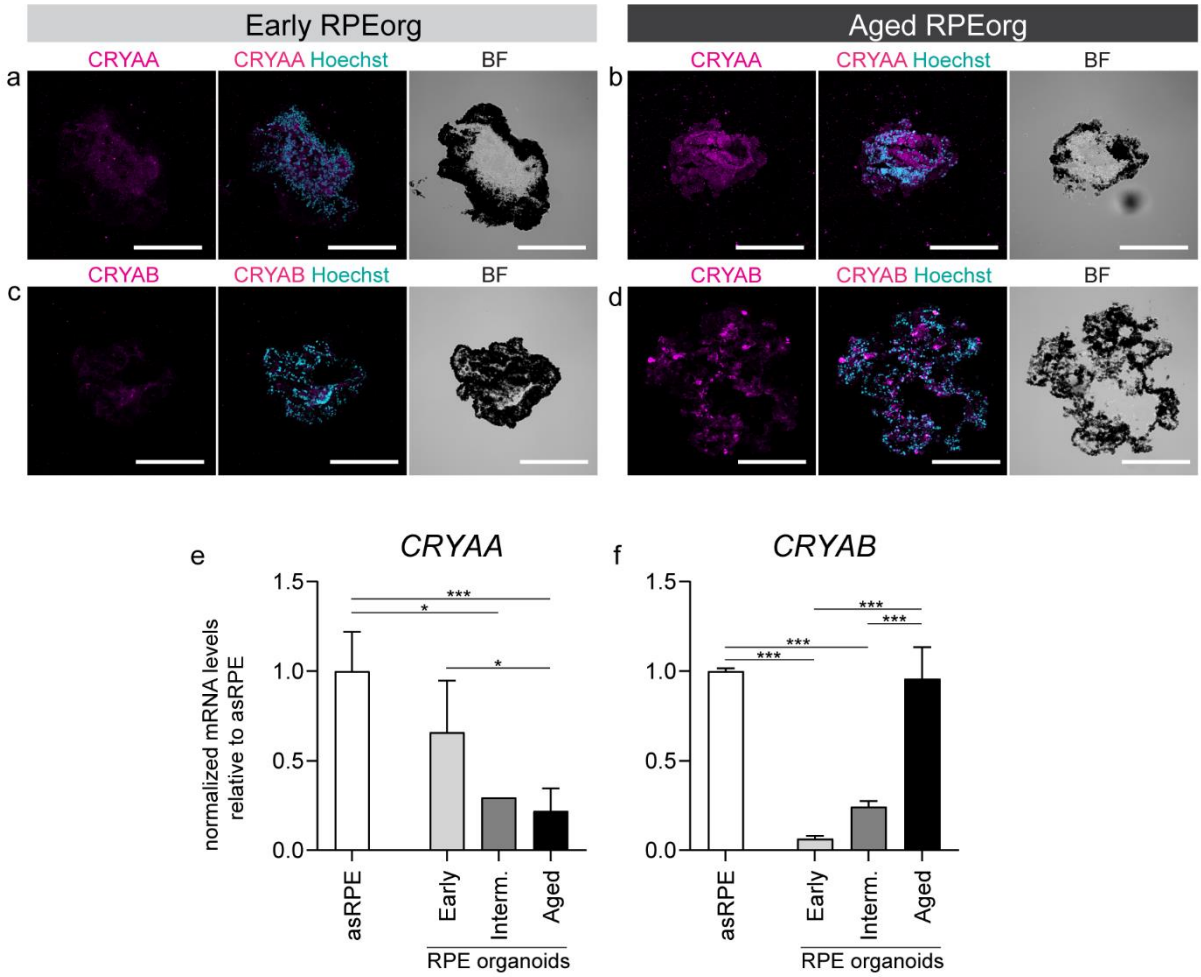

Figure 3-14: RPE organoids display signs of calcification.
(a, b, c, d) Cryosections of RPEorg were stained for CRYAA and CRYAB (magenta). Hoechst = light blue. Images are displayed as maximum intensity projections (MIP). Scale bars: a-d 200 µm.
(e-i) Expression of *CRYAA* and *CRYAB* was normalized to the housekeeping genes GAPDH and RPS9 and displayed relative to asRPE. Bars show means with S.E.M. Significance is *p<0.05, **p<0.01, ***p<0.001 according to One-way ANOVA with Bonferroni post-hoc test. n=4 RPEorg for asRPE, early RPEorg, intermediate RPEorg and n=12 RPEorg for aged RPEorg.

In addition, ubiquitin was present in immunostainings of early and aged RPEorg (Figure 3-15 a, b). Gene expression of *APP, UBC* and *VTN* revealed an increase in aged RPEorg compared to early and intermediate RPEorg, but also displayed high expression in adherent asRPE (Figure 3-15 c-e).

To summarize, the presence of crystallins, as well as APP, UBC and VTN as components of AMD drusen [136] could be demonstrated in early and aged RPEorg in this study, partly increasing with age.

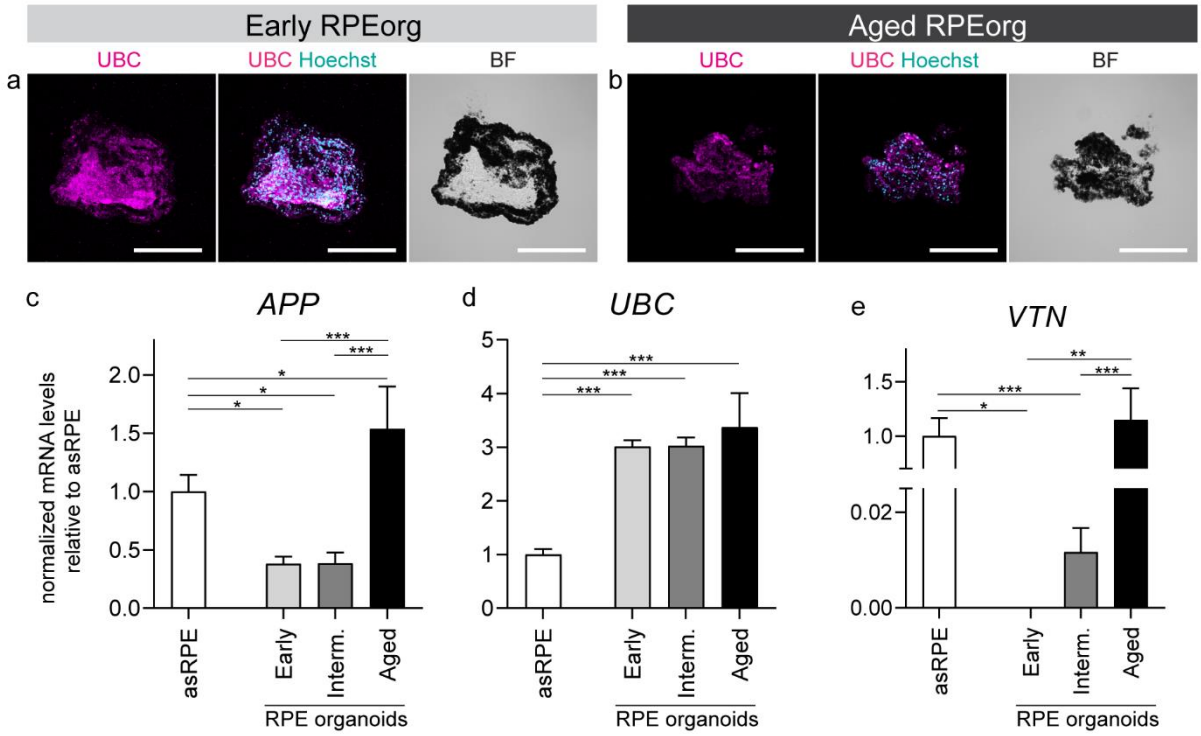

Figure 3-15: RPE organoids express drusen-associated proteins.
(a, b,) Cryosections of RPEorg were stained for UBC (magenta). Hoechst 33342 = light blue. Images are displayed as maximum intensity projections (MIP). Scale bars: a-d 200 µm.
(c-e) Expression of *UBC* and *VTN* was normalized to the housekeeping genes GAPDH and RPS9 and displayed relative to asRPE. Bars show means with S.E.M. Significance is *p<0.05, **p<0.01, ***p<0.001 according to One-way ANOVA with Bonferroni post-hoc test. n=4 RPEorg for asRPE, early RPEorg, intermediate RPEorg and n=12 RPEorg for aged RPEorg.

3.3.2 Expression of complement factors in RPE organoids

Gene expression of the complement factors *C3*, *C5* and *CFH* in RPEorg was further investigated, as inflammation is implicated to be an early event in drusen biogenesis [112], [114]. While *C3* and *CFH* displayed a significantly higher expression in aged RPEorg compared to early and intermediate RPEorg, no clear differences could be detected for *C5* (Figure 3-16 a-c). Interestingly, *C3* showed by far the highest expression in adherently cultured asRPE (Figure 3-16 a).

Additionally, the influence of normal human serum with preserved complement proteins (HS) on C3 expression in RPEorg was studied. Previous studies had shown the increase of complement factors after serum treatment, suggesting precise interactions between serum components and RPE cells, as an essential process in AMD pathogenesis [120], [126]. Therefore, HS was added to the culture medium for 14 days and afterwards cryosections were stained for C3. Results showed C3 expression in both, early and aged RPEorg before HS treatment (Figure 3-16 d-e). Expression of C3 after HS treatment was slightly higher in individual samples (Figure 3-16 f-), nevertheless quantification of the signal in multiple samples did not reveal significant differences between non-treated and HS treated RPEorg (data not shown).

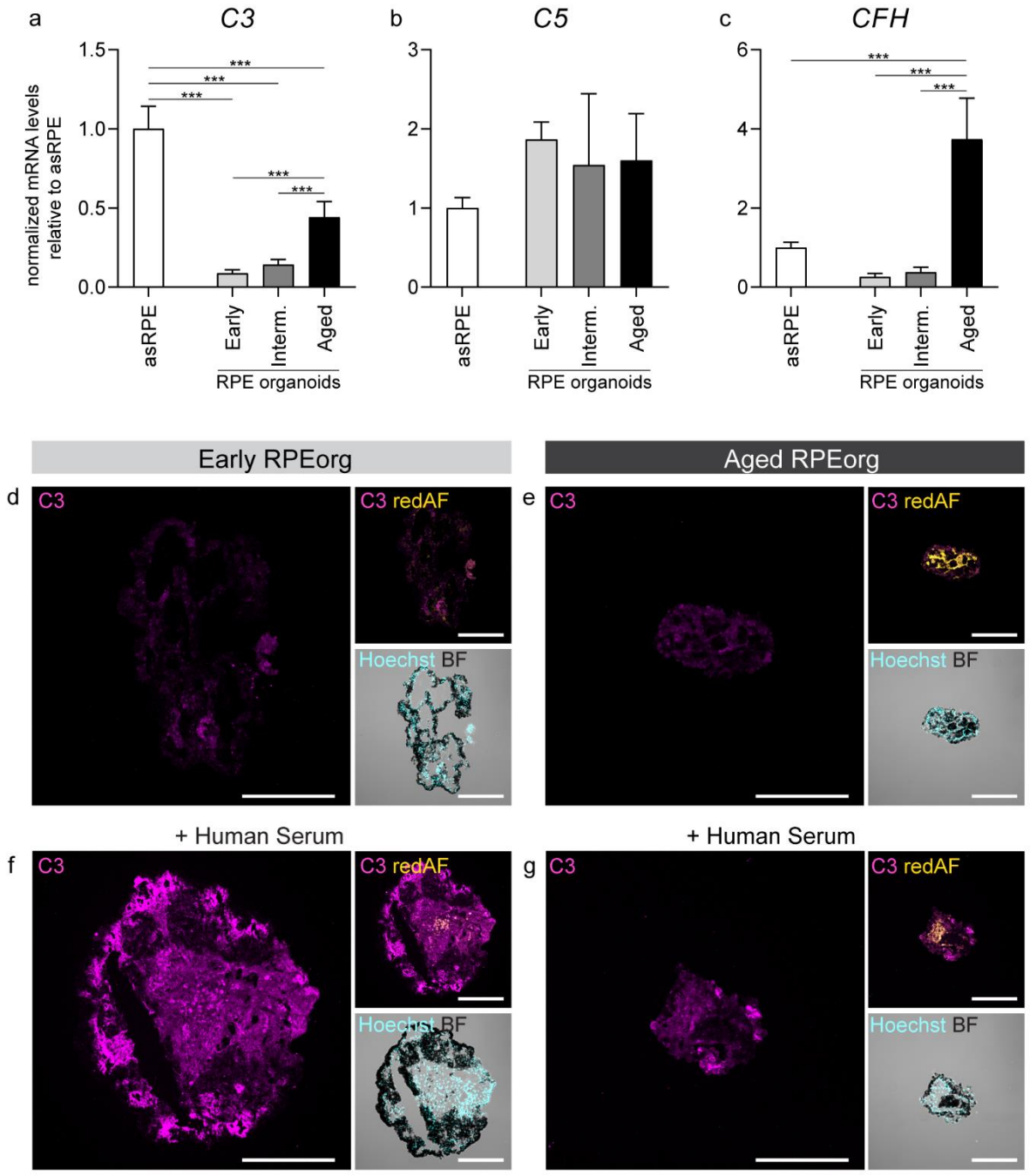

Figure 3-16: Complement factors are expressed in early and aged RPEorg.
(a-c) Expression of *C3, C5* and *CFH* was normalized to the housekeeping genes GAPDH and RPS9 and displayed relative to asRPE. Bars show means with S.E.M. Significance is *p<0.05, **p<0.01, ***p<0.001 according to One-way ANOVA with Bonferroni post-hoc test. n=4 RPEorg for asRPE, early RPEorg, intermediate RPEorg and n=12 RPEorg for aged RPEorg.
(d-g) Cryosections of RPEorg were stained for C3 (magenta). Red AF = yellow. Hoechst 33342 = light blue. Images are displayed as maximum intensity projections (MIP). Scale bars: d-g 200 µm.

3.3.3 Ultrastructural observations of extracellular deposits in aged RPE organoids

To morphologically assess formation of sub-RPE deposition, semithin and ultrastructural samples of RPEorg were investigated. Strong accumulations of dark blue material below the outer RPE cell layer could be observed in semithin sections stained with Richardson's solution, which correlates with basophilic and osmiophilic structures (Figure 3-17 a). This potentially indicates the presence of lipophilic deposition material, which in contrast was absent in early RPEorg (Figure 3-5 e, f, h, i).

Transmission electron microscopy does not only allow for the detection of drusen like material or basal extracellular deposits, but also enables to distinguish between hard and soft drusen [94], [120]. Ultrastructural analysis showed various signs of drusen in aged RPEorg (Figure 3-17 b-h), but almost none in early RPEorg (data not shown). Noteworthy was the presence of homogenous circular structures of high electron density and approximately 1-3 µm diameter (Figure 3-17 b, c), resembling hard drusen [117].

Soft drusen, in contrast, are noticeably larger, less electron-dense and more frequently heterogenous than hard drusen [94], [117]. Thus, larger structures of lower and intermediate electron density in aged RPEorg (Figure 3-17 b, b.i., d), as well as sections filled with granular structures (Figure 3-17 d, e) could be allocated to soft drusen. Basal deposits frequently resemble basement membrane material, as they contain laminin and collagen and thus, are difficult to differentiate [137]–[139]. Nevertheless, basal extracellular accumulations of wide-spaced collagen were particularly striking (Figure 3-17 f, f.i.) and were frequently accompanied by amorphous structures of homogenous electron density, which could present lipoprotein particles and had been described in literature as "lipid lakes" [94], [140]. Finally, several areas filled with vesicular structures (Figure 3-17 h) and membranous debris could be detected in aged RPEorg resembling lipoprotein-derived debris, frequently found in drusen [94], [139], [140].

In conclusion, TEM of aged RPEorg revealed a variety of structures below the outer RPE cell layer resembling components of hard or soft drusen. Notable, those structures were not found in early RPEorg, suggesting a correlation with aging. Consequently, in addition to protein and mRNA studies, the presence of drusen in aged RPEorg could be confirmed on ultrastructural level and demonstrates their suitability as *in vitro* model for AMD.

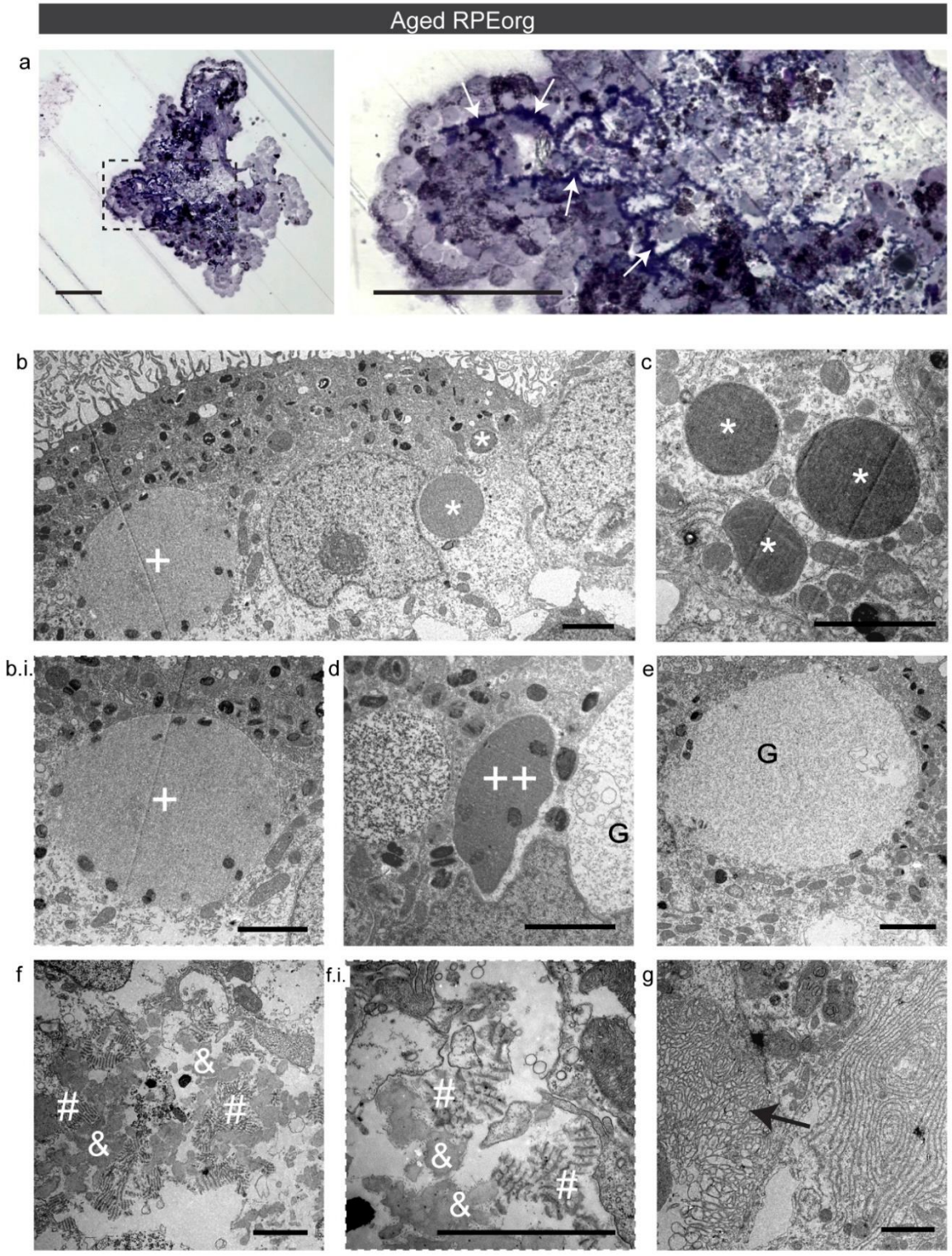

Figure 3-17: Presence and ultrastructure of extracellular deposits in aged RPE organoids.
Semithin sections labeled with Richardson's solution displayed strong accumulations of dark blue material (white arrows) below the outer RPE cell layer (a). Transmission electron microscopy revealed small circular structures of high electron density (*) (b, c), homogenous structures of intermediate electron density (+) (b, b.i.) and structures of higher electron density (++) (d). Additionally, big granular structures (G) (d, e), wide-spaced collagen (#), small, irregular structures (&) of intermediate electron density (f, f.i.) and vesicular structures (black arrow) could be observed. Scale bars: 2,5 µm.

4 Discussion

Although in recent years research is has made significant progress in understanding retinal diseases, such as AMD, many important questions regarding the disease development and progression remain uncleared. Thus, the search for new treatment strategies requires adequate model systems, which resemble the human physiology and sufficiently mimic the disease pathophysiology. The poor transferability to the human physiology and ethical concerns are drawbacks of various animal models, which can be overcome by using 2D or 3D *in vitro* models of the affected cell types, in this case of the RPE.

In the present work, two different approaches for the generation of adherent hiPSC-RPE cells were assessed and both acquired the most important hallmarks of RPE. At the same time, 3D RPE organoids were differentiated and characterized. They did not only possess essential characteristics of mature RPE cells, but also displayed functionality for phagocytosis. To assess the suitability of aged RPE organoids for modelling hallmarks of AMD such as sub-RPE drusen, the presence of AMD-associated proteins and lipids, and in particular complement factors were verified on protein and mRNA level. Additionally, several ultrastructural signs of drusen formation were found in aged RPEorg.

The following points will be discussed subsequently:

1. Differentiation and characterization of adherent RPE cells
2. Characterization of RPE organoids and comparison to classic RPE culture systems
3. Modeling hallmarks of AMD with RPE organoids

4.1 Differentiation and characterization of adherent RPE cells

Cultivation of primary and hiPSC derived RPE is mostly performed adherently on plastic surfaces or porous membranes [72], [122], [141], [142]. The differentiation towards adherent hiPSC-RPE cells can be either (1) performed adherently by adding specific morphogens directly to the hiPSCs, or (2) they can be derived from 3D organoid differentiation protocols, whereby they are only directed towards a neural fate and subsequently arise spontaneously [62], [65], [66]. Consequently, in this study, RPE cells were (1) differentiated adherently (adRPE) and (2) from suspension using a 3D organoid approach in suspension (asRPE). To evaluate, if both methods generate cells which exhibit the major hallmarks of RPE, morphology, immunohistochemistry, and qPCR of typical RPE genes were analyzed.

Both, adRPE and asRPE exhibit the typical hexagonal shape of RPE calls and form a tightly packed monolayer in the dish 28 days after plating. Immunostainings of visual cycle components (LRAT, RPE65), RPE-specific calcium channels (BEST1), MITF as transcription factor for development and function, pigmentation (PMEL), apical microvilli (Ezrin) and tight junctions (ZO-1) verify the presence of RPE-characteristic proteins, which are essential for maturation and functionality in adRPE and asRPE, respectively. A regular, hexagonal pattern of ZO-1, as found in adRPE and asRPE, has been previously shown to correlate with high transepithelial electrical resistance (TEER) values [143]. While immunostainings do not display apparent differences in expression of RPE markers, qPCR data state a clearly higher expression of *RPE65*, *BEST1*, *PMEL* and *SERPINF1* in adRPE. On the other hand, *TJP1* is expressed significantly higher in asRPE, implying an enhanced formation of tight junctions. In the future, additional markers for tight junctions and adherens junctions, such as claudin and occludins, as well as cellular retinaldehyde binding protein (CRALBP), as a visual cycle actor, and NaK-ATPase could be applied for in-depth analysis. Still, the RPE markers investigated in this study, are commonly used to assess quality and functionality of RPE cells and cover the major hallmarks of RPE, such as tight junction formation, polarization, and the visual cycle [143], [144].

Pigmentation has been shown to be a crucial sign for maturation of RPE cells *in vitro*, correlating with the expression of essential genes for RPE function [145]. In the present experiments, adherently differentiated adRPE cells seemed to be slightly less pigmented than asRPE cells after 28 days in culture. Surprisingly, this did not correlate with gene expression of PMEL, which is involved in the maturation of melanosomes and usually associated with pigmentation. Nevertheless, the degree of pigmentation was suggested to not be the most crucial sign for RPE maturation. Bennis et al., showed that only the first appearance of pigmentation correlates with maturation and specific gene expression and further increase of pigmentation does not necessarily improve RPE functionality [146].

Another difference between adRPE and asRPE becomes clear looking at the immunostainings: The morphology of adRPE cells is quite uniform and the cell layer is very homogeneous, while the asRPE cells are a little more variable in size and shape. A possible reason could be the heterogenous composition of RPE organoids, from which the adherent asRPE cells are derived. Nevertheless, limited passaging can enhance the purity of RPE cells *in vitro* [127] and could thus further improve the quality of asRPE in culture.

A major aspect regarding the differentiation of hiPSC-RPE is cultivation time, as RPE cell maturation needs exceptionally long, but is required for sufficient functionality [147]–[149]. Initially, the protocol for adherent differentiation of RPE cells claims to be fast with 14 days of

differentiation time but taking a closer look, the RPE needs to mature for additional 28 to 35 days after initial passaging, which makes a total differentiation time of almost 50 days [122]. RPE cells derived from RPE organoids (asRPE), on the other hand, can be generated earliest around day 50 of differentiation, and could theoretically be used at p0, although subsequent passaging and 7 to 14 days of maturation might be recommendable. Nevertheless, they do not need to mature as long as adRPE, as their maturation can already take place at three-dimensional organoid level. To summarize, the adherent differentiation protocol could be slightly faster (7 to 14 days), which does not make a crucial difference regarding the minimal differentiation time of 50 days.

Both approaches for the differentiation of adherent hiPSC derived RPE cells generate cells which show typical morphology and pigmentation and express relevant RPE markers. Also, tightness of RPE was confirmed for asRPE (data not shown), measuring the diffusion of fluorescently labeled dextrans, a widely used approach to assess barrier integrity [150]. Barrier tightness could further be evaluated by measurements of the transepithelial electrical resistance (TEER), which has been shown to reach >500 $\Omega \cdot cm^2$ *in vitro* [151]–[153]. To conclude, adRPE and asRPE show essential hallmarks of RPE and thus, both are suitable for future *in vitro* studies for disease modeling or drug development.

4.2 Characterization of RPE organoids and comparison to classic RPE culture systems

RPE cells are classically cultured either on plastic surfaces in cell culture plates or in transwell inserts on porous membranes. Transwell cultures are an ideal system to grow polarized cell layers and enable simple measurements of TEER and permeability. In the context of AMD, formation of sub-RPE deposits, as well as the secretion of material in transwell insert pores has been observed in cultures of primary porcine RPE cells [93]. Nevertheless, 2D cultures are not very physiological, as the plastic surfaces impede the formation of a sufficient basal membrane and ECM. Additionally, adherently cultured cells have the tendency to detach from the culture device during long-term cultivation, or frequently transdifferentiate towards a mesenchymal phenotype [154], [155].

3D cultivation of RPE cells has the capability to overcome those drawbacks. There are two ways of generating 3D RPE models. The first approach is the formation of RPE spheroids by aggregation of singularized RPE cells [130], [156]. Those RPE spheroids have been shown to form a differentiated monolayer of RPE cells at the surface, as well as a BrM like structure below [156]. Additionally, drusen formation and expression of many drusen-associated proteins has been described [130]. Nevertheless, the initial dissociation of RPE cells disrupts their mature

phenotype [128]. Therefore, in this study, the second option for generation of 3D RPE models was applied, the self-formation of RPE organoids during RO differentiation [66], [76]. This method does not require enzymatic dissociation steps, which allows the generation of highly mature and well differentiated RPE cells. In addition to their pronounced maturity, RPE organoids allow for an easy observation of pathological processes usually located at the BrM, such as accumulation of extracellular material and drusen formation.

In this study, 3D hiPSC-derived RPE organoids, were cultured for more than 300 days. In-depth characterization of RPEorg of different age demonstrated the presence of major attributes of RPE cells, comparable to a previous study applying the same protocol [76]. In detail, pigmentation, which was already clearly visible by eye, was confirmed by immunostainings and qPCR analysis of the pigmentation associated marker PMEL and electron microscopy images showing the presence of apical melanosomes. Additionally, RPEorg expressed multiple RPE markers for visual cycle function (RPE65, LRAT), calcium channels (BEST1), RPE identity (MITF) and PEDF secretion (SERPINF1), mostly increasing with age.

Polarization has been described to be fundamental for RPE identity and function [3]. Immunostainings and TEM images of RPEorg present a pronounced polarization of the outermost cell layer across the whole RPEorg. In contrast, the interior of the RPEorg contained various areas of disorganized cells, or cell-free areas which partly contained ECM components. The phagocytosis of inner apoptotic cellular components by outer functional RPE cells has previously been described in RPE spheroid cultures and could plausibly also occur in RPEorg [156]. Despite the variances of the interior, the outer RPE cell layer was quite consistent and homogenous among all RPE organoids investigated. In future experiments, single cell RNA sequencing of RPEorg could reveal crucial information on their precise cellular composition and degree of maturation of RPE cells within RPEorg.

In vivo, the BrM is an essential feature of RPE cells, as it provides mechanical support and works as a filtration barrier between RPE and choriocapillaris. The BrM is divided into five layers, the basement membrane of the RPE, the inner collagenous layer, an elastic layer, outer collagenous layer, and basement membrane of the choriocapillaris [157]. Although a clearly defined BrM with all five layers could not be observed by ultrastructural analysis of RPEorg, several components of the BrM were detected. The basal membrane of the RPE showed basal infoldings and vesicular structures in RPEorg, similar to *in vivo* data [158]–[161]. Moreover, multiple accumulations of wide-spaced collagen were detected below the outer RPE layer in RPEorg, correlating to inner and outer collagenous layer of the BrM. Those data are in accordance with previous studies of 3D RPE cultures [76], [156] and are of special interest, as the formation of a basal membrane is frequently

insufficient in 2D RPE models [93], [156]. To summarize, although data on a pronounced stratification of a BrM are still insufficient in RPEorg, multiple components of the BrM could be detected in RPEorg.

Furthermore, the presence of tight junctions in TEM and the expression of the tight junction protein ZO-1 in immunostainings and qPCR implicate the formation of a tight barrier in RPEorg. The barrier properties could moreover be assessed by measurements of the transepithelial electrical resistance or by permeability assays using fluorescently labeled dextran. Nevertheless, measurements of the TEER so far require a monolayer of cells grown in a transwell inlet or, more recently, in Organ-on-Chip devices [76], [162]. In contrast, permeability assays using dextran have already been performed in 3D cultures of vascular or blood-brain barrier organoids [163], [164]. However, the strong pigmentation of RPE and the massive autofluorescence of RPEorg complicates an easy detection of fluorescence in the center of the RPEorg.

Functionality of RPE cells is commonly evaluated by phagocytosis of photoreceptor outer segments (POS) [123], [127]. This has, so far, only been performed in 2D cultures, in which quantification of POS per cell and imaging is straightforward. Translating this concept to 3D cultures, we treated RPEorg of early and aged timepoints with FITC-labeled bovine POS, which both showed for the first time functional phagocytosis in 3D grown cells. A decrease of phagocytic activity has been previously observed in aging and AMD [165]. Thus, in further experiments, quantification of phagocytosed POS would be an appealing approach, to investigate age-related differences in aged 3D cultured RPE cells.

3D RPE organoids showcased in this study revealed several advantages in comparison to 2D adherent RPE cultures. Most crucial, long-term cultivation of RPEorg for more than 300 days enables a comprehensive maturation of RPE cells. Time as the main factor of maturation becomes clear, regarding that expression of several RPE markers increases significantly in aged RPEorg, while early and intermediate RPEorg display levels, which are more similar to adherent asRPE cells. Additionally, after the initial steps of differentiation, cultivation of RPEorg requires much less attention and time compared to adherent RPE cells, as they do not need to be split at all and medium only needs to be changed twice a week. This also lowers the chance of cell detachment by cell coating exhaustion and long-term culture effects.

4.3 Modeling hallmarks of AMD with RPE organoids

The major aim of this study was to investigate the suitability of RPE organoids as a model system for AMD. Characterization of RPEorg already confirmed their RPE identity and functionality. Considering that AMD is strongly associated with aging and most of the pathological changes in AMD are located at the interface between RPE and BrM, an adequate model system should fulfill the following criteria: RPE cells should be mature and functional, long-term cultivation should be possible, and an ECM compartment below the basal membrane mimicking the Bruch's membrane that would allow for large accumulations of extracellular material and deposits. Those criteria can be fulfilled applying 3D RPE organoids. On the other hand, the absence of the choroid is still a drawback that needs to be tackled in the future.

As inhibitor of the matrix metalloproteinase 3, TIMP3 is claimed to play an essential role in thickening of the BrM by regulating the turnover rate of the ECM. In addition, it could regulate choroidal neovascularization by inhibiting VEGFR. TIMP3 has been found to be a major component of hard drusen in normal aging, but also in particular of soft drusen in AMD [95], [96]. In this study, in all assessed RPEorg, TIMP3 expression was massively elevated in aged RPEorg when comparing to early RPEorg. This correlates well with observations that TIMP3 content strongly increases during normal aging in human donor eyes [96]. In addition to the normal aging process, eyes of AMD patients display increased levels of TIMP3 in particular below the RPE cell layer correlating with the fact that TIMP3 is regularly found in soft and hard drusen [96], [115].

Apolipoprotein E (APOE), an abundant component of drusen, was expressed in the inner layers of the RPE organoids and significantly increased in aged RPEorg. APOE mediates the transport of neutral lipids and cholesterol and is assumed to play a role in disease manifestation of AMD [93], [166], [167]. The risk to develop AMD was further shown to correlate with certain polymorphisms of APOE [101], [167].

Next, using Nile red the presence of neutral lipids was assessed. A strong signal for NileRed was observed in some areas of early and aged RPEorg, with the tendency to be stronger in aged RPEorg. Nevertheless, the signal had great individual variations and thus, it is difficult to draw a clear conclusion. In comparison to that, co-localization of NileRed and TIMP3 was found in basal deposits in hiPSC-RPE transwell cultures [126]. Additionally, solid particles and pools of neutral lipids were detected by TEM in drusen of AMD patients. indicating that neutral lipids are a major component of drusen [168]. Future in depth component analysis of the sub-RPE accumulation of RPEorg could reveal whether lipid-rich material also plays are role in this model.

In addition to lipid accumulation, crystallization and calcification have been observed already in early disease stages and shown to accelerate disease progression in AMD [95], [104], [105]. This was consistent with the expression of crystallin's (CRYAA, CRYAB) in early and aged RPEorg. Further, hydroxyapatite (HAP) spherules have been frequently found in aging RPE and are associated with a variety of drusen proteins [93], [108]. Labeled with Osteosense, patches of HAP could be demonstrated in early and aged RPEorg, indicating their early appearance during drusen biogenesis. This is in accordance with findings in adherently cultured porcine RPE, in which HAP spherules could be detected after 90 days of culture [93].

Not surprisingly, complement pathways play an important role in AMD and have been shown to be expressed in extracellular drusen [111], [136]. Additionally, mutations in several complement genes have been described as risk factors for AMD [115]. While *C3* and *CFH* gene expression significantly increased in aged RPEorg, *C5* expression did not change drastically.

While the accumulation of drusen had previously been shown to occur without external stressors *in vitro*, serum treatment did not only enhance drusen formation, but also changed drusen composition including an increased expression of complement proteins [120], [126]. The presence of complement proteins in drusen of AMD patients supports the hypothesis that they originate from an alternative source, then the RPE itself [120]. To assess, whether normal human serum with preserved complement proteins (HS) would lead to an accumulation of active complement system components in RPEorg culture, HS was added to the cultures for 2 weeks and C3 expression was investigated subsequently. An increase of C3 expression could be observed in some of the HS-treated RPEorg, nevertheless the signal varied strongly. It should be noted, that due to their structure, RPEorg were treated with HS from the apical side, while *in vivo*, blood serum components reach the RPE cells basally. The injection of HS to the center of the RPEorg could create a more physiological model and thus, mimic complement protein accumulation in AMD drusen more precisely.

Although recent studies show that aged hiPSC-RPE cells can produce sub-RPE deposits autonomously [126], the application of exogenous stressors to the culture medium has been frequently used to enhance the disease phenotype in AMD models. Those include photoreceptor outer segments (regular or photo-oxidized) [169], components thereof, such as the bisretinoid N-retinylidene-N-retinylethanolamine (A2E), or blue light exposure [170], [171]. Also, smoke extract has been applied to RPE cultures, as smoking is a major risk factor for AMD [172], [173]. Although we could already observe signs of aging and AMD association in aged RPE organoids without any supplementation, treatment with exogenous stressors, could clearly enhance the disease phenotype and improve the model system.

The exogenous stressors mentioned are partly associated with oxidative stress and hypoxia, which are frequently described in AMD pathology [130], [166], [174], [175]. In this regard, it would be of great interest, to assess the oxygen and metabolic conditions of the interior of the RPEorg. Since the center of the RPEorg is separated from direct culture medium contact by a tight layer of RPE cells on the outer rim, it may cause hypoxic and hypometabolic environment. Furthermore, due to the structure of RPE organoids and the missing choriocapillaris at the basal side of the RPE cells, waste products and cellular debris cannot be cleared by the blood stream but instead potentially accumulate inside of the RPEorg. This could enhance accumulation of toxic waste products and therefore increase the occurrence of pathological changes and creates a pathophysiological milieu. Interestingly, this might be in line with AMD-like conditions where compound diffusion is hampered by a thickened BrM [115].

One striking feature observed in aged RPEorg was the accumulation of autofluorescent material (in green and red spectrum) at the basal side of the RPE. The appearance of autofluorescence is not only observed in RPE cells *in vitro*, but fundus autofluorescence imaging is routinely used in the clinic to determine the stage of disease in AMD [176], [177]. Thereby, autofluorescence is suggested to be mainly caused by intracellular lipofuscin granules, which increase in AMD, but at the same time are a sign of normal aging [115], [178]. In aged RPE organoids, autofluorescence was strongly enhanced, while only slightly detected in early RPEorg. Interestingly, the autofluorescent patterns did not fully co-localize with other tested drusen markers such as TIMP3, supporting the findings of earlier studies, which suggest that intracellular lipofuscin is different from extracellular drusen-like deposits [94]. In addition to lipofuscin, autofluorescence in RPE cultures can be caused by the Bruch's membrane and drusen themselves [179], [180]. Consequently, autofluorescence in red and green spectra complicates the procedure for immunostainings. To avoid an overlap between autofluorescence (in green and red spectrum) and antibody signal, almost all immunostainings in this study were performed using a 647 nm secondary antibody. A possible solution for this issue provides treatment of the tissue with Sudan Black, which has been shown to quench tissue autofluorescence and has already be used studying RPE and the BrM [181], [182]. Nevertheless, therefore the staining procedure needs to be modified and optimized and the signal of the antibodies themselves can partially be affected.

Although more and more studies focus on the development and composition of drusen in AMD, an easy and clear method to distinguish between age-related hard drusen and harmful soft drusen is still lacking. Ultrastructural analyses so far give the best hints for precise histopathological investigations [93], [94], [126]. Semithin sections of RPEorg stained with Richardson's solution, revealed a strong accumulation of dark blue material below the outer RPE layer mostly in aged

RPEorg. As blue staining correlates with basophilic and osmiophilic material, this indicates the presence of lipid material, relating with findings in aging and AMD affected RPE [115].

More detailed observations and correlations were conducted via transmission electron microscopy. Numerous small, spheroidal structures of high electron density were found in aged RPEorg and closely resemble hard drusen [117]. Due to their dense structure, they are probably more resistant to damage occurring during sample preparation and thus are clearly identifiable in comparison to soft drusen. However, the size of hard-drusen like structures in RPEorg does by far not gain the size of hard drusen *in vivo*, which reach up to 60 µm in diameter [117], [183]. Soft drusen are usually bigger and less homogenous, which led to the conclusion, that bigger electron dense structures in aged RPEorg and resembled soft drusen [94]. Clusters of collagenous material and membranous debris and vesicles were difficult to distinguish from components of the BrM, but due to their concentrated occurrence they were suspected to be components of extracellular material or soft drusen occurring in AMD [87], [94], [126], [183]. A specific fluorescent marker, filipin, is widely used to determine the presence of esterified cholesterol in amorphous structures which have been assigned to macular soft drusen [118], [139]. Those, so-called lipid lakes, have also been detected in aged RPEorg. To summarize, signs of both, hard and soft drusen, could be noticed in RPEorg. It must be noted that the ultrastructural changes described, have been observed in aged RPEorg, but scarcely in early RPEorg, implicating a strong correlation with aging.

In summary, long-term cultured RPEorg presented several drusen hallmarks although no additional stressors have been added and bona fide healthy cell lines have been used for this study. The usage of hiPSCs for RPE organoid generation, however, permit a wide range of opportunities for AMD modeling. For instance, iPSCs can be generated from healthy donors, as well as from patients, carrying genetic risk factors for AMD or mutations that can cause early-onset macular degeneration associated with drusen. In addition, CRISPR-Cas technology allows for genetic manipulation in hiPSCs [184], [185]. In this way, disease-correlated mutations can be corrected or inserted, and the isogenic controls obtained enable an adequate comparison between healthy and disease affected cells. Patient derived hiPSCs have already been used to generate RPE models of retinal diseases, such as AMD [126], [127], [186], and would provide better insights in development and pathophysiology of AMD in the present RPE organoid model.

Drusen pathogenesis is quite complex, and even though RPE cells are able to produce drusen-associated proteins and lipids independently, interactions with additional cell types, such as endothelial cells from the choriocapillaris or immune cells, play an important role in AMD. Protocols for the differentiation of endothelial cells or microglia cells from hiPSCs even provide the possibility to combine cells from the same donor [187], [188]. While co-cultivation with

adherent RPE cells often requires special equipment, such as transwell inserts or Organ-on-Chip devices, co-cultivation with RPE organoids in suspension is assumed to be much easier.

To summarize, RPEorg investigated show several characteristics associated with aging and AMD, partly increasing in aged RPEorg compared to early RPEorg. In further studies the disease phenotype could be enhanced by applying external stressors or using patient-derived hiPSCs and a deeper understanding of disease mechanisms could be gained by establishing co-culture systems with additional cell types involved in AMD. The RPE organoids described in this study provide a powerful model system for a better understanding of disease development in AMD and thus, facilitates the identification of new drug targets for AMD.

5 Bibliography

[1] H. Kolb, “Gross Anatomy of the Eye,” *Webvision: The Organization of the Retina and Visual System*, 1995. http://www.ncbi.nlm.nih.gov/pubmed/21413392.

[2] H. Kolb, *Simple Anatomy of the Retina*. 1995.

[3] O. Strauss, “The Retinal Pigment Epithelium in Visual Function,” *Physiological Reviews*, vol. 85, no. 3, pp. 845–881, Jul. 2005, doi: 10.1152/physrev.00021.2004.

[4] M. Hoon, H. Okawa, L. della Santina, and R. O. L. Wong, “Functional architecture of the retina: Development and disease,” *Progress in Retinal and Eye Research*, vol. 42. Elsevier Ltd, pp. 44–84, 2014, doi: 10.1016/j.preteyeres.2014.06.003.

[5] C. S. McCaa, “The eye and visual nervous system: anatomy, physiology and toxicology,” *Environmental Health Perspectives*, vol. Vol. 44, pp. 1–8, 1982, doi: 10.1289/ehp.82441.

[6] H. Kolb, “How the Retina Works: Much of the Construction of an Image Takes Place in the Retina Itself through the Use of Specialized Neural Circuits,” *American Scientist*, vol. 91, no. 1, 2003.

[7] D. M. Snodderly, M. M. Sandstrom, I. Y. F. Leung, C. L. Zucker, and M. Neuringer, “Retinal pigment epithelial cell distribution in central retina of rhesus monkeys,” *Investigative Ophthalmology and Visual Science*, vol. 43, no. 9, 2002.

[8] M. Boulton and P. Dayhaw-Barker, “The role of the retinal pigment epithelium: Topographical variation and ageing changes,” *Eye*, vol. 15, no. 3, 2001, doi: 10.1038/eye.2001.141.

[9] F. Mazzoni, H. Safa, and S. C. Finnemann, “Understanding photoreceptor outer segment phagocytosis: Use and utility of RPE cells in culture,” *Experimental Eye Research*, vol. 126, pp. 51–60, Sep. 2014, doi: 10.1016/j.exer.2014.01.010.

[10] D. Bok, “The retinal pigment epithelium: A versatile partner in vision,” in *Journal of Cell Science*, 1993, vol. 106, no. SUPPL. 17, pp. 189–195, doi: 10.1242/jcs.1993.supplement_17.27.

[11] A. D. Marmorstein, S. C. Finnemann, V. L. Bonilha, and E. Rodriguez-Boulan, “Morphogenesis of the retinal pigment epithelium: Toward understanding retinal degenerative diseases,” in *Annals of the New York Academy of Sciences*, Oct. 1998, vol. 857, no. 1, pp. 1–12, doi: 10.1111/j.1749-6632.1998.tb10102.x.

[12] M. A. Fields, L. v. del Priore, R. A. Adelman, and L. J. Rizzolo, "Interactions of the choroid, Bruch's membrane, retinal pigment epithelium, and neurosensory retina collaborate to form the outer blood-retinal-barrier," *Progress in Retinal and Eye Research*, vol. 76. Elsevier Ltd, p. 100803, May 01, 2020, doi: 10.1016/j.preteyeres.2019.100803.

[13] B. M. Carlson, "Special Senses—Vision and Hearing," *The Human Body*, pp. 177–207, Jan. 2019, doi: 10.1016/B978-0-12-804254-0.00007-7.

[14] M. v. Miceli, M. R. Liles, and D. A. Newsome, "Evaluation of oxidative processes in human pigment epithelial cells associated with retinal outer segment phagocytosis," *Experimental Cell Research*, vol. 214, no. 1, 1994, doi: 10.1006/excr.1994.1254.

[15] Y. Ban and L. J. Rizzolo, "Differential regulation of tight junction permeability during development of the retinal pigment epithelium," *American Journal of Physiology - Cell Physiology*, vol. 279, no. 3 48-3, 2000, doi: 10.1152/ajpcell.2000.279.3.c744.

[16] K. Konari, N. Sawada, Y. Zhong, H. Isomura, T. Nakagawa, and M. Mori, "Development of the blood-retinal barrier in vitro: Formation of tight junctions as revealed by occludin and ZO-1 correlates with the barrier function of chick retinal pigment epithelial cells," *Experimental Eye Research*, vol. 61, no. 1, 1995, doi: 10.1016/S0014-4835(95)80063-8.

[17] Y. Ban and L. J. Rizzolo, "Regulation of glucose transporters during development of the retinal pigment epithelium," *Developmental Brain Research*, vol. 121, no. 1, pp. 89–95, May 2000, doi: 10.1016/S0165-3806(00)00028-6.

[18] S. I. Harik *et al.*, "Glucose transporters are abundant in cells with 'occluding' junctions at the blood-eye barriers," *Proceedings of the National Academy of Sciences of the United States of America*, vol. 87, no. 11, pp. 4261–4264, 1990, doi: 10.1073/pnas.87.11.4261.

[19] N. G. Bazan, W. C. Gordon, and E. B. Rodriguez de Turco, "Docosahexaenoic acid uptake and metabolism in photoreceptors: Retinal conservation by an efficient retinal pigment epithelial cell-mediated recycling process," *Advances in Experimental Medicine and Biology*, vol. 318. Springer, Boston, MA, pp. 295–306, 1992, doi: 10.1007/978-1-4615-3426-6_26.

[20] R. H. Steinberg, "Interactions between the retinal pigment epithelium and the neural retina," *Documenta Ophthalmologica*, vol. 60, no. 4, pp. 327–346, Oct. 1985, doi: 10.1007/BF00158922.

[21] H. Tanihara, M. Inatani, and Y. Honda, "Growth factors and their receptors in the retina and pigment epithelium," *Progress in Retinal and Eye Research*, vol. 16, no. 2. Pergamon, pp. 271–301, Apr. 01, 1997, doi: 10.1016/S1350-9462(96)00028-6.

[22] M. Cayouette, S. B. Smith, S. P. Becerra, and C. Gravel, “Pigment epithelium-derived factor delays the death of photoreceptors in mouse models of inherited retinal degenerations,” *Neurobiology of Disease*, vol. 6, no. 6, pp. 523–532, 1999, doi: 10.1006/nbdi.1999.0263.

[23] N. Ogata *et al.*, “Pigment epithelium derived factor as a neuroprotective agent against ischemic retinal injury,” *Current Eye Research*, vol. 22, no. 4, pp. 245–252, 2001, doi: 10.1076/ceyr.22.4.245.5506.

[24] S. P. Becerra, R. N. Fariss, Y. Q. Wu, L. M. Montuenga, P. Wong, and B. A. Pfeffer, “Pigment epithelium-derived factor in the monkey retinal pigment epithelium and interphotoreceptor matrix: Apical secretion and distribution,” *Experimental Eye Research*, vol. 78, no. 2, pp. 223–234, 2004, doi: 10.1016/j.exer.2003.10.013.

[25] A. N. Witmer, G. F. J. M. Vrensen, C. J. F. van Noorden, and R. O. Schlingemann, “Vascular endothelial growth factors and angiogenesis in eye disease,” *Progress in Retinal and Eye Research*, vol. 22, no. 1. Prog Retin Eye Res, pp. 1–29, Jan. 2003, doi: 10.1016/S1350-9462(02)00043-5.

[26] N. G. Lambert *et al.*, “Risk factors and biomarkers of age-related macular degeneration,” *Progress in Retinal and Eye Research*, vol. 54. Elsevier Ltd, pp. 64–102, Sep. 01, 2016, doi: 10.1016/j.preteyeres.2016.04.003.

[27] W. Baehr, S. M. Wu, A. C. Bird, and K. Palczewski, “The retinoid cycle and retina disease,” *Vision Research*, vol. 43, no. 28. Elsevier Ltd, pp. 2957–2958, 2003, doi: 10.1016/j.visres.2003.10.001.

[28] D. A. Thompson and A. Gal, “Vitamin A metabolism in the retinal pigment epithelium: genes, mutations, and diseases,” *Progress in Retinal and Eye Research*, vol. 22, no. 5, pp. 683–703, Sep. 2003, doi: 10.1016/S1350-9462(03)00051-X.

[29] P. D. Kiser, M. Golczak, A. Maeda, and K. Palczewski, “Key enzymes of the retinoid (visual) cycle in vertebrate retina,” *Biochimica et Biophysica Acta - Molecular and Cell Biology of Lipids*, vol. 1821, no. 1. Biochim Biophys Acta, pp. 137–151, Jan. 2012, doi: 10.1016/j.bbalip.2011.03.005.

[30] S. Beatty, H. H. Koh, M. Phil, D. Henson, and M. Boulton, “The role of oxidative stress in the pathogenesis of age-related macular degeneration,” *Survey of Ophthalmology*, vol. 45, no. 2, 2000, doi: 10.1016/S0039-6257(00)00140-5.

[31] M. M. LaVail, “Circadian nature of rod outer segment disc shedding in the rat,” *Investigative Ophthalmology and Visual Science*, vol. 19, no. 4, 1980.

[32] M. M. LaVail, "Outer segment disc shedding and phagocytosis in the outer retina," *Transactions of the Ophthalmological Societies of the United Kingdom*, vol. 103, no. 4. 1983.

[33] S. W. Ryeom, J. R. Sparrow, and R. L. Silverstein, "CD36 participates in the phagocytosis of rod outer segments by retinal pigment epithelium," *Journal of Cell Science*, vol. 109, no. 2, pp. 387–395, Feb. 1996, doi: 10.1242/jcs.109.2.387.

[34] S. C. Finnemann, "Focal adhesion kinase signaling promotes phagocytosis of integrin-bound photoreceptors," *EMBO Journal*, vol. 22, no. 16, pp. 4143–4154, Aug. 2003, doi: 10.1093/emboj/cdg416.

[35] S. C. Finnemann and R. L. Silverstein, "Differential roles of CD36 and αvβ5 integrin in photoreceptor phagocytosis by the retinal pigment epithelium," *Journal of Experimental Medicine*, vol. 194, no. 9, pp. 1289–1298, 2001, doi: 10.1084/jem.194.9.1289.

[36] C. Bibb and R. W. Young, "Renewal of fatty acids in the membranes of visual cell outer segments," *Journal of Cell Biology*, vol. 61, no. 2, 1974, doi: 10.1083/jcb.61.2.327.

[37] S. Fuhrmann, *Eye morphogenesis and patterning of the optic vesicle*, vol. 93, no. C. 2010.

[38] J. Hyer, J. Kuhlman, E. Afif, and T. Mikawa, "Optic cup morphogenesis requires pre-lens ectoderm but not lens differentiation," *Developmental Biology*, vol. 259, no. 2, 2003, doi: 10.1016/S0012-1606(03)00205-7.

[39] T. D. Lamb, S. P. Collin, and E. N. Pugh, "Evolution of the vertebrate eye: Opsins, photoreceptors, retina and eye cup," *Nature Reviews Neuroscience*, vol. 8, no. 12. Nature Publishing Group, pp. 960–976, Dec. 2007, doi: 10.1038/nrn2283.

[40] F. Gonzalez-Fernandez and J. I. Healy, "Early expression of the gene of interphotoreceptor retinol-binding protein during photoreceptor differentiation suggests a critical role for the interphotoreceptor matrix and retinal development," *Journal of Cell Biology*, vol. 111, no. 6 I, 1990, doi: 10.1083/jcb.111.6.2775.

[41] J. Rymer and C. F. Wildsoet, "The role of the retinal pigment epithelium in eye growth regulation and myopia: A review," *Visual Neuroscience*, vol. 22, no. 3. Vis Neurosci, pp. 251–261, May 2005, doi: 10.1017/S0952523805223015.

[42] S. Fuhrmann, C. Zou, and E. M. Levine, "Retinal pigment epithelium development, plasticity, and tissue homeostasis," *Experimental Eye Research*, vol. 123, pp. 141–150, 2014, doi: 10.1016/j.exer.2013.09.003.

[43] C. Dehay and H. Kennedy, "Cell-cycle control and cortical development," *Nature Reviews Neuroscience*, vol. 8, no. 6. 2007, doi: 10.1038/nrn2097.

[44] R. Ohsawa and R. Kageyama, "Regulation of retinal cell fate specification by multiple transcription factors," *Brain Research*, vol. 1192. Elsevier, pp. 90–98, Feb. 04, 2008, doi: 10.1016/j.brainres.2007.04.014.

[45] A. Swaroop, D. Kim, and D. Forrest, "Transcriptional regulation of photoreceptor development and homeostasis in the mammalian retina," *Nature Reviews Neuroscience*, vol. 11, no. 8, pp. 563–576, 2010, doi: 10.1038/nrn2880.

[46] J. R. Martínez-Morales *et al.*, "OTX2 activates the molecular network underlying retina pigment epithelium differentiation," *Journal of Biological Chemistry*, vol. 278, no. 24, pp. 21721–21731, Jun. 2003, doi: 10.1074/jbc.M301708200.

[47] M. T. T. Nguyen and H. Arnheiter, "Signaling and transcriptional regulation in early mammalian eye development: A link between FGF and MITF," *Development*, vol. 127, no. 16, 2000.

[48] D. J. Horsford, M. T. T. Nguyen, G. C. Sellar, R. Kothary, H. Arnheiter, and R. R. McInnes, "Chx10 repression of Mitf is required for the maintenance of mammalian neuroretinal identity," *Development*, vol. 132, no. 1, 2005, doi: 10.1242/dev.01571.

[49] A. Nishida *et al.*, "Otx2 homeobox gene controls retinal photoreceptor cell fate and pineal gland development," *Nature Neuroscience*, vol. 6, no. 12, 2003, doi: 10.1038/nn1155.

[50] J. v. Forrester, A. D. Dick, P. G. McMenamin, F. Roberts, and E. Pearlman, *The eye: Basic sciences in practice*. 2015.

[51] G. Jeffery, "The retinal pigment epithelium as a developmental regulator of the neural retina," *Eye (Basingstoke)*, vol. 12, no. 3, 1998, doi: 10.1038/eye.1998.137.

[52] H. L. May-Simera *et al.*, "Primary Cilium-Mediated Retinal Pigment Epithelium Maturation Is Disrupted in Ciliopathy Patient Cells," *Cell Reports*, vol. 22, no. 1, pp. 189–205, Jan. 2018, doi: 10.1016/J.CELREP.2017.12.038.

[53] P. A. Campochiaro, J. A. Jerdan, and B. M. Glaser, "The extracellular matrix of human retinal pigment epithelial cells in vivo and its synthesis in vitro," *Investigative Ophthalmology and Visual Science*, vol. 27, no. 11, pp. 1615–1621, 1986, Accessed: Jun. 03, 2021. [Online].

[54] I. Grierson, P. Hiscott, P. Hogg, H. Robey, A. Mazure, and G. Larkin, "Development, repair and regeneration of the retinal pigment epithelium," *Eye (Basingstoke)*, vol. 8, no. 2, pp. 255–262, 1994, doi: 10.1038/eye.1994.54.

[55] K. Achberger, J. C. Haderspeck, A. Kleger, and S. Liebau, "Stem cell-based retina models," *Advanced Drug Delivery Reviews*, vol. 140. Elsevier B.V., pp. 33–50, Feb. 01, 2019, doi: 10.1016/j.addr.2018.05.005.

[56] K. Takahashi and S. Yamanaka, "Induction of Pluripotent Stem Cells from Mouse Embryonic and Adult Fibroblast Cultures by Defined Factors," *Cell*, vol. 126, no. 4, pp. 663–676, Aug. 2006, doi: 10.1016/j.cell.2006.07.024.

[57] L. Linta *et al.*, "Rat embryonic fibroblasts improve reprogramming of human keratinocytes into induced pluripotent stem cells," *Stem Cells and Development*, vol. 21, no. 6, pp. 965–976, Apr. 2012, doi: 10.1089/scd.2011.0026.

[58] T. Aasen *et al.*, "Efficient and rapid generation of induced pluripotent stem cells from human keratinocytes," *Nature Biotechnology*, vol. 26, no. 11, 2008, doi: 10.1038/nbt.1503.

[59] Y. H. Loh *et al.*, "Generation of induced pluripotent stem cells from human blood," *Blood*, vol. 113, no. 22, 2009, doi: 10.1182/blood-2009-02-204800.

[60] F. Osakada *et al.*, "Toward the generation of rod and cone photoreceptors from mouse, monkey and human embryonic stem cells," *Nature Biotechnology 2008 26:2*, vol. 26, no. 2, pp. 215–224, Feb. 2008, doi: 10.1038/nbt1384.

[61] M. J. Phillips *et al.*, "Blood-Derived Human iPS Cells Generate Optic Vesicle–Like Structures with the Capacity to Form Retinal Laminae and Develop Synapses," *Investigative Ophthalmology & Visual Science*, vol. 53, no. 4, p. 2007, 2012, doi: 10.1167/IOVS.11-9313.

[62] J. S. Meyer *et al.*, "Modeling early retinal development with human embryonic and induced pluripotent stem cells," *Proceedings of the National Academy of Sciences of the United States of America*, vol. 106, no. 39, pp. 16698–16703, Sep. 2009, doi: 10.1073/pnas.0905245106.

[63] M. Eiraku *et al.*, "Self-organizing optic-cup morphogenesis in three-dimensional culture," *Nature*, vol. 472, no. 7341, pp. 51–58, 2011, doi: 10.1038/nature09941.

[64] J. S. Meyer *et al.*, "Optic vesicle-like structures derived from human pluripotent stem cells facilitate a customized approach to retinal disease treatment," *Stem Cells*, vol. 29, no. 8, pp. 1206–1218, Aug. 2011, doi: 10.1002/stem.674.

[65] T. Nakano *et al.*, "Self-formation of optic cups and storable stratified neural retina from human ESCs," *Cell Stem Cell*, vol. 10, no. 6, pp. 771–785, 2012, doi: 10.1016/j.stem.2012.05.009.

[66] X. Zhong *et al.*, "Generation of three-dimensional retinal tissue with functional photoreceptors from human iPSCs," *Nature Communications*, 2014, doi: 10.1038/ncomms5047.

[67] K. Achberger *et al.*, "Merging organoid and organ-on-a-chip technology to generate complex multi-layer tissue models in a human retina-on-a-chip platform," *eLife*, 2019, doi: 10.7554/eLife.46188.

[68] H. Kawasaki *et al.*, "Generation of dopaminergic neurons and pigmented epithelia from primate ES cells by stromal cell-derived inducing activity," *Proceedings of the National Academy of Sciences*, vol. 99, no. 3, pp. 1580–1585, Feb. 2002, doi: 10.1073/PNAS.032662199.

[69] M. Haruta *et al.*, "In Vitro and In Vivo Characterization of Pigment Epithelial Cells Differentiated from Primate Embryonic Stem Cells," *Investigative Ophthalmology & Visual Science*, vol. 45, no. 3, pp. 1020–1025, Mar. 2004, doi: 10.1167/IOVS.03-1034.

[70] I. Klimanskaya, J. Hipp, K. A. Rezai, M. West, A. Atala, and Dr. R. Lanza, "Derivation and Comparative Assessment of Retinal Pigment Epithelium from Human Embryonic Stem Cells Using Transcriptomics," *https://home.liebertpub.com/clo*, vol. 6, no. 3, pp. 217–245, Oct. 2004, doi: 10.1089/CLO.2004.6.217.

[71] M. Idelson *et al.*, "Directed Differentiation of Human Embryonic Stem Cells into Functional Retinal Pigment Epithelium Cells," *Cell Stem Cell*, vol. 5, no. 4, pp. 396–408, Oct. 2009, doi: 10.1016/J.STEM.2009.07.002.

[72] A. Zahabi *et al.*, "A new efficient protocol for directed differentiation of retinal pigmented epithelial cells from normal and retinal disease induced pluripotent stem cells," *Stem Cells and Development*, vol. 21, no. 12, 2012, doi: 10.1089/scd.2011.0599.

[73] D. A. Lamba, M. O. Karl, C. B. Ware, and T. A. Reh, "Efficient generation of retinal progenitor cells from human embryonic stem cells," 2006, Accessed: Jul. 19, 2021. [Online]. Available: www.pnas.orgcgidoi10.1073pnas.0601990103.

[74] D. E. Buchholz, B. O. Pennington, R. H. Croze, C. R. Hinman, P. J. Coffey, and D. O. Clegg, "Rapid and Efficient Directed Differentiation of Human Pluripotent Stem Cells Into Retinal

Pigmented Epithelium," *STEM CELLS Translational Medicine*, vol. 2, no. 5, pp. 384–393, May 2013, doi: 10.5966/sctm.2012-0163.

[75] D. E. Buchholz *et al.*, "Derivation of Functional Retinal Pigmented Epithelium from Induced Pluripotent Stem Cells," *STEM CELLS*, vol. 27, no. 10, pp. 2427–2434, Oct. 2009, doi: 10.1002/STEM.189.

[76] S. Liu *et al.*, "Self-formation of RPE spheroids facilitates enrichment and expansion of hiPSC-derived RPE generated on retinal organoid induction platform," *Investigative Ophthalmology and Visual Science*, vol. 59, no. 13, pp. 5659–5669, Nov. 2018, doi: 10.1167/iovs.17-23613.

[77] J. R. Evans, A. E. Fletcher, and R. P. L. Wormald, "28 000 Cases of age related macular degeneration causing visual loss in people aged 75 years and above in the United Kingdom may be attributable to smoking," *British Journal of Ophthalmology*, vol. 89, no. 5, pp. 550–553, May 2005, doi: 10.1136/bjo.2004.049726.

[78] R. R. A. Bourne *et al.*, "Prevalence and causes of vision loss in high-income countries and in Eastern and Central Europe: 1990-2010," *British Journal of Ophthalmology*, vol. 98, no. 5, pp. 629–638, May 2014, doi: 10.1136/bjophthalmol-2013-304033.

[79] K. M. Gehrs, D. H. Anderson, L. v. Johnson, and G. S. Hageman, "Age-related macular degeneration - Emerging pathogenetic and therapeutic concepts," *Annals of Medicine*, vol. 38, no. 7. Taylor & Francis, pp. 450–471, Nov. 01, 2006, doi: 10.1080/07853890600946724.

[80] M. M. DeAngelis *et al.*, "Genetics of age-related macular degeneration (AMD)," *Human Molecular Genetics*, vol. 26, no. R1. Oxford University Press, pp. R45–R50, Aug. 01, 2017, doi: 10.1093/hmg/ddx228.

[81] K. M. Ke, U. Chakravarthy, and C. O'Neill, "Economic cost of age-related macular degeneration: A review of recent research," *Drugs and Aging*, vol. 23, no. 3. 2006, doi: 10.2165/00002512-200623030-00004.

[82] R. W. Young, "Pathophysiology of age-related macular degeneration," *Survey of Ophthalmology*, vol. 31, no. 5. Elsevier, pp. 291–306, Mar. 01, 1987, doi: 10.1016/0039-6257(87)90115-9.

[83] W. Ma, L. Zhao, and W. T. Wong, "Microglia in the outer retina and their relevance to pathogenesis of age-related macular degeneration," in *Advances in Experimental Medicine and Biology*, 2012, vol. 723, pp. 37–42, doi: 10.1007/978-1-4614-0631-0_6.

[84] W. Ma, L. Zhao, A. M. Fontainhas, R. N. Fariss, and W. T. Wong, "Microglia in the mouse retina alter the structure and function of retinal pigmented epithelial cells: A potential cellular interaction relevant to AMD," *PLoS ONE*, vol. 4, no. 11, Nov. 2009, doi: 10.1371/journal.pone.0007945.

[85] T. Wecker *et al.*, "Anti-VEGF injection frequency correlates with visual acuity outcomes in pro re nata neovascular AMD treatment," *Scientific Reports*, vol. 9, no. 1, Dec. 2019, doi: 10.1038/s41598-019-38934-8.

[86] R. H. Guymer *et al.*, "Subthreshold Nanosecond Laser Intervention in Age-Related Macular Degeneration: The LEAD Randomized Controlled Clinical Trial," *Ophthalmology*, vol. 126, no. 6, pp. 829–838, Jun. 2019, doi: 10.1016/j.ophtha.2018.09.015.

[87] C. Balaratnasingam *et al.*, "Cuticular Drusen: Clinical Phenotypes and Natural History Defined Using Multimodal Imaging," *Ophthalmology*, 2018, doi: 10.1016/j.ophtha.2017.08.033.

[88] N. Joachim, P. Mitchell, G. Burlutsky, A. Kifley, and J. J. Wang, "The incidence and progression of age-related macular degeneration over 15 years: The Blue Mountains Eye Study," *Ophthalmology*, vol. 122, no. 12, pp. 2482–2489, Dec. 2015, doi: 10.1016/j.ophtha.2015.08.002.

[89] N. S. Abdelfattah *et al.*, "Drusen volume as a predictor of disease progression in patients with late age-related macular degeneration in the fellow eye," *Investigative Ophthalmology and Visual Science*, vol. 57, no. 4, pp. 1839–1846, Apr. 2016, doi: 10.1167/iovs.15-18572.

[90] F. G. Schlanitz *et al.*, "Drusen volume development over time and its relevance to the course of age-related macular degeneration," *British Journal of Ophthalmology*, vol. 101, no. 2, 2017, doi: 10.1136/bjophthalmol-2016-308422.

[91] M. J. Hogan, "Role of the retinal pigment epithelium in macular disease.," *Transactions - American Academy of Ophthalmology and Otolaryngology*, vol. 76, no. 1, 1972, doi: 10.1016/S0002-7154(72)30135-3.

[92] M. C. Killingsworth, "Age-related components of Bruch's membrane in the human eye," *Graefe's Archive for Clinical and Experimental Ophthalmology*, vol. 225, no. 6, 1987, doi: 10.1007/BF02334166.

[93] M. G. Pilgrim *et al.*, "Subretinal pigment epithelial deposition of drusen components including hydroxyapatite in a primary cell culture model," *Investigative Ophthalmology and Visual Science*, vol. 58, no. 2, pp. 708–719, Feb. 2017, doi: 10.1167/iovs.16-21060.

[94] C. A. Curcio, "Soft drusen in age-related macular degeneration: Biology and targeting via the oil spill strategies," *Investigative Ophthalmology and Visual Science*, 2018, doi: 10.1167/iovs.18-24882.

[95] J. W. Crabb, "The proteomics of drusen," *Cold Spring Harbor Perspectives in Medicine*, vol. 4, no. 7, 2014, doi: 10.1101/cshperspect.a017194.

[96] M. Kamei and J. G. Hollyfield, "TIMP-3 in Bruch's membrane: Changes during aging and in age-related macular degeneration," *Investigative Ophthalmology and Visual Science*, 1999.

[97] A. Ruiz, P. Brett, and D. Bok, "TIMP-3 is expressed in the human retinal pigment epithelium," *Biochemical and Biophysical Research Communications*, vol. 226, no. 2, pp. 467–474, Sep. 1996, doi: 10.1006/bbrc.1996.1379.

[98] B. Anand-Apte, "A review of tissue inhibitor of metalloproteinases-3 (TIMP-3) and experimental analysis of its effect on primary tumor growth," *Biochemistry and Cell Biology*, vol. 74, no. 6, 1996, doi: 10.1139/o96-090.

[99] B. Anand-Apte *et al.*, "Inhibition of angiogenesis by tissue inhibitor of metalloproteinase-3," *Investigative Ophthalmology and Visual Science*, vol. 38, no. 5, 1997.

[100] J. H. Qi *et al.*, "A novel function for tissue inhibitor of metalloproteinases-3 (TIMP3): Inhibition of angiogenesis by blockage of VEGF binding to VEGF receptor-2," *Nature Medicine*, vol. 9, no. 4, pp. 407–415, Apr. 2003, doi: 10.1038/nm846.

[101] B. Y. Ishida *et al.*, "Regulated expression of apolipoprotein E by human retinal pigment epithelial cells," *Journal of Lipid Research*, vol. 45, no. 2, pp. 263–271, Feb. 2004, doi: 10.1194/jlr.M300306-JLR200.

[102] P. J. Browning *et al.*, "Apolipoprotein E (ApoE), a Novel Heparin-binding Protein Inhibits the Development of Kaposi's Sarcoma-like Lesions in BALB/c nu/nu Mice," *Journal of Experimental Medicine*, vol. 180, no. 5, 1994, doi: 10.1084/jem.180.5.1949.

[103] R. K. Tangirala *et al.*, "Reduction of isoprostanes and regression of advanced atherosclerosis by apolipoprotein E," *Journal of Biological Chemistry*, vol. 276, no. 1, 2001, doi: 10.1074/jbc.M003324200.

[104] R. Kannan, P. G. Sreekumar, and D. R. Hinton, "Alpha crystallins in the retinal pigment epithelium and implications for the pathogenesis and treatment of age-related macular degeneration," *Biochimica et Biophysica Acta - General Subjects*, vol. 1860, no. 1. Elsevier B.V., pp. 258–268, Jan. 01, 2016, doi: 10.1016/j.bbagen.2015.05.016.

[105] A. C. S. Tan *et al.*, "Calcified nodules in retinal drusen are associated with disease progression in age-related macular degeneration," *Science Translational Medicine*, vol. 10, no. 466, Nov. 2018, doi: 10.1126/scitranslmed.aat4544.

[106] K. Nakata, J. W. Crabb, and J. G. Hollyfield, "Crystallin distribution in Bruch's membrane–choroid complex from AMD and age-matched donor eyes," *Experimental Eye Research*, vol. 80, no. 6, pp. 821–826, Jun. 2005, doi: 10.1016/J.EXER.2004.12.011.

[107] W. R. Green, "Histopathology of age-related macular degeneration.," *Molecular vision*. 1999.

[108] R. B. Thompson *et al.*, "Identification of hydroxyapatite spherules provides new insight into subretinal pigment epithelial deposit formation in the aging eye," *Proceedings of the National Academy of Sciences of the United States of America*, vol. 112, no. 5, pp. 1565–1570, Feb. 2015, doi: 10.1073/pnas.1413347112.

[109] J. Gong *et al.*, "Stem cell-derived retinal pigment epithelium from patients with age-related macular degeneration exhibit reduced metabolism and matrix interactions," *STEM CELLS Translational Medicine*, vol. 9, no. 3, pp. 364–376, Mar. 2020, doi: 10.1002/SCTM.19-0321.

[110] G. S. Hageman, P. J. Luthert, N. H. Victor Chong, L. v. Johnson, D. H. Anderson, and R. F. Mullins, "An integrated hypothesis that considers drusen as biomarkers of immune-mediated processes at the RPE-Bruch's membrane interface in aging and age-related macular degeneration," *Progress in Retinal and Eye Research*, vol. 20, no. 6. Elsevier Ltd, pp. 705–732, Nov. 01, 2001, doi: 10.1016/S1350-9462(01)00010-6.

[111] D. H. Anderson *et al.*, "The pivotal role of the complement system in aging and age-related macular degeneration: Hypothesis re-visited," *Progress in Retinal and Eye Research*, vol. 29, no. 2. Pergamon, pp. 95–112, Mar. 01, 2010, doi: 10.1016/j.preteyeres.2009.11.003.

[112] D. H. Anderson, R. F. Mullins, G. S. Hageman, and L. v. Johnson, "A role for local inflammation in the formation of drusen in the aging eye," *American Journal of Ophthalmology*, vol. 134, no. 3, pp. 411–431, Sep. 2002, doi: 10.1016/S0002-9394(02)01624-0.

[113] J. L. Haines *et al.*, "Complement factor H variant increases the risk of age-related macular degeneration," *Science*, vol. 308, no. 5720, 2005, doi: 10.1126/science.1110359.

[114] L. v. Johnson, W. P. Leitner, M. K. Staples, and D. H. Anderson, "Complement activation and inflammatory processes in drusen formation and age related macular degeneration," *Experimental Eye Research*, vol. 73, no. 6, pp. 887–896, 2001, doi: 10.1006/exer.2001.1094.

[115] D. Ardeljan and C. C. Chan, "Aging is not a disease: Distinguishing age-related macular degeneration from aging," *Progress in Retinal and Eye Research*, vol. 37. Elsevier Ltd, pp. 68–89, 2013, doi: 10.1016/j.preteyeres.2013.07.003.

[116] H. Buch, N. v. Nielsen, T. Vinding, G. B. Jensen, J. U. Prause, and M. la Cour, "14-Year incidence, progression, and visual morbidity of age-related maculopathy: The Copenhagen City Eye Study," *Ophthalmology*, vol. 112, no. 5, pp. 787–798, May 2005, doi: 10.1016/j.ophtha.2004.11.040.

[117] M. Rudolf, M. E. Clark, M. F. Chimento, C. M. Li, N. E. Medeiros, and C. A. Curcio, "Prevalence and morphology of druse types in the macula and periphery of eyes with age-related maculopathy," *Investigative Ophthalmology and Visual Science*, vol. 49, no. 3, pp. 1200–1209, Mar. 2008, doi: 10.1167/iovs.07-1466.

[118] C. A. Curcio, J. B. Presley, G. Malek, N. E. Medeiros, D. v. Avery, and H. S. Kruth, "Esterified and unesterified cholesterol in drusen and basal deposits of eyes with age-related maculopathy," *Experimental Eye Research*, vol. 81, no. 6, pp. 731–741, Dec. 2005, doi: 10.1016/j.exer.2005.04.012.

[119] P. Elizabeth Rakoczy, M. J. T. Yu, S. Nusinowitz, B. Chang, and J. R. Heckenlively, "Mouse models of age-related macular degeneration," *Experimental Eye Research*, vol. 82, no. 5. Academic Press, pp. 741–752, May 01, 2006, doi: 10.1016/j.exer.2005.10.012.

[120] L. v. Johnson *et al.*, "Cell culture model that mimics drusen formation and triggers complement activation associated with age-related macular degeneration," *Proceedings of the National Academy of Sciences*, vol. 108, no. 45, pp. 18277–18282, Nov. 2011, doi: 10.1073/PNAS.1109703108.

[121] C. S. Alge, S. M. Hauck, S. G. Priglinger, A. Kampik, and M. Ueffing, "Differential protein profiling of primary versus immortalized human RPE cells identifies expression patterns associated with cytoskeletal remodeling and cell survival," *Journal of Proteome Research*, vol. 5, no. 4, pp. 862–878, Apr. 2006, doi: 10.1021/pr050420t.

[122] L. P. Foltz and D. O. Clegg, "Rapid, directed differentiation of retinal pigment epithelial cells from human embryonic or induced pluripotent stem cells," *Journal of Visualized Experiments*, vol. 2017, no. 128, Oct. 2017, doi: 10.3791/56274.

[123] F. Regent *et al.*, "Automation of human pluripotent stem cell differentiation toward retinal pigment epithelial cells for large-scale productions," *Scientific Reports*, vol. 9, no. 1, Dec. 2019, doi: 10.1038/s41598-019-47123-6.

[124] C. Brandl, "Generation of Functional Retinal Pigment Epithelium from Human Induced Pluripotent Stem Cells," in *Methods in Molecular Biology*, vol. 1834, Humana Press Inc., 2019, pp. 87–94.

[125] T. U. Krohne *et al.*, " Generation of Retinal Pigment Epithelial Cells from Small Molecules and OCT4 Reprogrammed Human Induced Pluripotent Stem Cells ," *STEM CELLS Translational Medicine*, vol. 1, no. 2, pp. 96–109, Feb. 2012, doi: 10.5966/sctm.2011-0057.

[126] C. A. Galloway *et al.*, "Drusen in patient-derived hiPSC-RPE models of macular dystrophies," *Proceedings of the National Academy of Sciences of the United States of America*, vol. 114, no. 39, pp. E8214–E8223, Sep. 2017, doi: 10.1073/pnas.1710430114.

[127] R. Singh *et al.*, "Functional analysis of serially expanded human iPS cell-derived RPE cultures," *Investigative Ophthalmology and Visual Science*, vol. 54, no. 10, pp. 6767–6778, Oct. 2013, doi: 10.1167/iovs.13-11943.

[128] R. Fernandez-Godino, D. L. Garland, and E. A. Pierce, "Isolation, culture and characterization of primary mouse RPE cells," *Nature Protocols*, vol. 11, no. 7, pp. 1206–1218, Jul. 2016, doi: 10.1038/nprot.2016.065.

[129] P. Shang, N. A. Stepicheva, S. Hose, J. S. Zigler, and D. Sinha, "Primary cell cultures from the mouse retinal pigment epithelium," *Journal of Visualized Experiments*, vol. 2018, no. 133, p. 56997, Mar. 2018, doi: 10.3791/56997.

[130] H. Usui *et al.*, "In vitro drusen model – Three-dimensional spheroid culture of retinal pigment epithelial cells," *Journal of Cell Science*, 2019, doi: 10.1242/jcs.215798.

[131] K. Achberger, "Human retinal organoids - Exploration of a human induced pluripotent stem cell-derived in vitro model," Tübingen, 2019.

[132] S. Frank, M. Zhang, H. R. Schöler, and B. Greber, "Small Molecule-Assisted, Line-Independent Maintenance of Human Pluripotent Stem Cells in Defined Conditions," *PLoS ONE*, vol. 7, no. 7, p. e41958, Jul. 2012, doi: 10.1371/journal.pone.0041958.

[133] L. Grupp, H. Wolburg, and A. F. Mack, "Astroglial structures in the zebrafish brain," *Journal of Comparative Neurology*, 2010, doi: 10.1002/cne.22481.

[134] S. T. Wavre-Shapton, I. P. Meschede, M. C. Seabra, and C. E. Futter, "Phagosome maturation during endosome interaction revealed by partial rhodopsin processing in retinal pigment epithelium," *Journal of Cell Science*, vol. 127, no. 17, p. 3852, 2014, doi: 10.1242/JCS.154757.

[135] M. Rudolf and C. A. Curcio, "Esterified cholesterol is highly localized to Bruch's membrane, as revealed by lipid histochemistry in wholemounts of human choroid," *Journal of Histochemistry and Cytochemistry*, vol. 57, no. 8, pp. 731–739, Aug. 2009, doi: 10.1369/jhc.2009.953448.

[136] R. F. Mullins, S. R. Russell, D. H. Anderson, and G. S. Hageman, "Drusen associated with aging and age-related macular degeneration contain proteins common to extracellular deposits associated with atherosclerosis, elastosis, amyloidosis, and dense deposit disease," *The FASEB Journal*, vol. 14, no. 7, pp. 835–846, May 2000, doi: 10.1096/fasebj.14.7.835.

[137] E. Reale, S. Groos, U. Eckardt, C. Eckardt, and L. Luciano, "New Components of 'Basal Laminar Deposits' in Age-Related Macular Degeneration," *Cells Tissues Organs*, vol. 190, no. 3, pp. 170–181, Aug. 2009, doi: 10.1159/000187632.

[138] K. U. Loffler and W. R. Lee, "Basal linear deposit in the human macula," *Graefe's Archive for Clinical and Experimental Ophthalmology 1986 224:6*, vol. 224, no. 6, pp. 493–501, Nov. 1986, doi: 10.1007/BF02154735.

[139] C. A. Curcio, M. Johnson, J.-D. Huang, and M. Rudolf, "Apolipoprotein B-containing lipoproteins in retinal aging and age-related macular degeneration," *Journal of Lipid Research*, vol. 51, no. 3, p. 451, Mar. 2010, doi: 10.1194/JLR.R002238.

[140] C. A. Curcio and M. Johnson, "Structure, Function, and Pathology of Bruch's Membrane," *Retina Fifth Edition*, vol. 1, pp. 465–481, Jan. 2013, doi: 10.1016/B978-1-4557-0737-9.00020-5.

[141] J. Maruotti, K. Wahlin, D. Gorrell, I. Bhutto, G. Lutty, and D. J. Zack, "A Simple and Scalable Process for the Differentiation of Retinal Pigment Epithelium From Human Pluripotent Stem Cells," *STEM CELLS Translational Medicine*, vol. 2, no. 5, 2013, doi: 10.5966/sctm.2012-0106.

[142] S. Reichman *et al.*, "Generation of Storable Retinal Organoids and Retinal Pigmented Epithelium from Adherent Human iPS Cells in Xeno-Free and Feeder-Free Conditions," *STEM CELLS*, vol. 35, no. 5, pp. 1176–1188, May 2017, doi: 10.1002/stem.2586.

[143] K. Ye *et al.*, "Reproducible production and image-based quality evaluation of retinal pigment epithelium sheets from human induced pluripotent stem cells," *Scientific Reports*, vol. 10, no. 1, p. 14387, Dec. 2020, doi: 10.1038/S41598-020-70979-Y.

[144] A. Maminishkis *et al.*, "Confluent Monolayers of Cultured Human Fetal Retinal Pigment Epithelium Exhibit Morphology and Physiology of Native Tissue," *Investigative*

ophthalmology & visual science, vol. 47, no. 8, p. 3612, Aug. 2006, doi: 10.1167/IOVS.05-1622.

[145] A. Al-Ani, S. Sunba, B. Hafeez, D. Toms, and M. Ungrin, "In vitro maturation of retinal pigment epithelium is essential for maintaining high expression of key functional genes," *International Journal of Molecular Sciences*, vol. 21, no. 17, 2020, doi: 10.3390/ijms21176066.

[146] A. Bennis *et al.*, "Stem Cell Derived Retinal Pigment Epithelium: The Role of Pigmentation as Maturation Marker and Gene Expression Profile Comparison with Human Endogenous Retinal Pigment Epithelium.," *Stem Cell Rev and Rep*, vol. 13, pp. 659–669, 2015, doi: 10.1007/s12015-017-9754-0.

[147] F. Michelet, A. Balasankar, N. Teo, L. W. Stanton, and S. Singhal, "Rapid generation of purified human RPE from pluripotent stem cells using 2D cultures and lipoprotein uptake-based sorting," *Stem Cell Research & Therapy 2020 11:1*, vol. 11, no. 1, pp. 1–15, Feb. 2020, doi: 10.1186/S13287-020-1568-3.

[148] I. J. Limnios, Y.-Q. Chau, S. J. Skabo, D. C. Surrao, and H. C. O'Neill, "Efficient differentiation of human embryonic stem cells to retinal pigment epithelium under defined conditions," *Stem Cell Research & Therapy*, vol. 12, no. 1, Dec. 2021, doi: 10.1186/S13287-021-02316-7.

[149] A. Al-Ani, S. Sunba, B. Hafeez, D. Toms, and M. Ungrin, "In Vitro Maturation of Retinal Pigment Epithelium Is Essential for Maintaining High Expression of Key Functional Genes," *International Journal of Molecular Sciences*, vol. 21, no. 17, pp. 1–15, Sep. 2020, doi: 10.3390/IJMS21176066.

[150] J. S. Wade and T. A. Desai, "Planar microdevices enhance transport of large molecular weight molecules across retinal pigment epithelial cells," *Biomedical Microdevices*, vol. 16, no. 4, pp. 629–638, 2014, doi: 10.1007/s10544-014-9865-1.

[151] S. Sonoda, C. Spee, E. Barron, S. J. Ryan, R. Kannan, and D. R. Hinton, "A protocol for the culture and differentiation of highly polarized human retinal pigment epithelial cells," *Nature Protocols*, vol. 4, no. 5, pp. 662–673, 2009, doi: 10.1038/nprot.2009.33.

[152] R. H. Quinn and S. S. Miller, "Ion transport mechanisms in native human retinal pigment epithelium," *Investigative Ophthalmology and Visual Science*, vol. 33, no. 13, 1992.

[153] A. Maminishkis *et al.*, "Confluent monolayers of cultured human fetal retinal pigment epithelium exhibit morphology and physiology of native tissue," *Investigative*

Ophthalmology and Visual Science, vol. 47, no. 8, pp. 3612–3624, Aug. 2006, doi: 10.1167/iovs.05-1622.

[154] S.-C. Lee, O.-W. Kwon, G.-J. Seong, S.-H. Kim, J.-E. Ahn, and E.-D. P. Kay, "Epitheliomesenchymal Transdifferentiation of Cultured RPE Cells," *Ophthalmic Research*, vol. 33, no. 2, pp. 80–86, 2001, doi: 10.1159/000055648.

[155] S. Grisanti and C. Guidry, "Transdifferentiation of retinal pigment epithelial cells from epithelial to mesenchymal phenotype.," *Investigative ophthalmology & visual science*, vol. 36, no. 2, pp. 391–405, Feb. 1995, Accessed: Aug. 12, 2019. [Online]. Available: http://www.ncbi.nlm.nih.gov/pubmed/7531185.

[156] R. Sato *et al.*, "Three-dimensional spheroidal culture visualization of membranogenesis of Bruch's membrane and basolateral functions of the retinal pigment epithelium," *Investigative Ophthalmology and Visual Science*, vol. 54, no. 3, pp. 1740–1749, Mar. 2013, doi: 10.1167/iovs.12-10068.

[157] R. Guymer, P. Luthert, and A. Bird, "Changes in Bruch's membrane and related structures with age," *Progress in Retinal and Eye Research*, vol. 18, no. 1, pp. 59–90, Jan. 1999, doi: 10.1016/S1350-9462(98)00012-3.

[158] E. Keeling *et al.*, "3D-Reconstructed Retinal Pigment Epithelial Cells Provide Insights into the Anatomy of the Outer Retina," *International Journal of Molecular Sciences*, vol. 21, no. 21, pp. 1–16, Nov. 2020, doi: 10.3390/IJMS21218408.

[159] M. J. Hayes, T. Burgoyne, S. T. Wavre-Shapton, T. Tolmachova, M. C. Seabra, and C. E. Futter, "Remodeling of the Basal Labyrinth of Retinal Pigment Epithelial Cells With Osmotic Challenge, Age, and Disease," *Investigative Ophthalmology & Visual Science*, vol. 60, no. 7, p. 2515, Jun. 2019, doi: 10.1167/IOVS.19-26784.

[160] J. C. Booij, D. C. Baas, J. Beisekeeva, T. G. M. F. Gorgels, and A. A. B. Bergen, "The dynamic nature of Bruch's membrane," *Progress in Retinal and Eye Research*, vol. 29, no. 1, pp. 1–18, Jan. 2010, doi: 10.1016/J.PRETEYERES.2009.08.003.

[161] Y. Hirabayashi, O. Fujimori, and S. Shimizu, "Bruch's membrane of the brachymorphic mouse," *Medical Electron Microscopy 2003 36:3*, vol. 36, no. 3, pp. 139–146, Sep. 2003, doi: 10.1007/S00795-003-0218-Z.

[162] H. Ragelle, A. Goncalves, S. Kustermann, D. A. Antonetti, and A. Jayagopal, "Organ-On-A-Chip Technologies for Advanced Blood–Retinal Barrier Models," *Journal of Ocular Pharmacology and Therapeutics*, vol. 36, no. 1, p. 30, Jan. 2020, doi: 10.1089/JOP.2019.0017.

[163] B. Cakir *et al.*, "Development of human brain organoids with functional vascular-like system," *Nature methods*, vol. 16, no. 11, p. 1169, Nov. 2019, doi: 10.1038/S41592-019-0586-5.

[164] R. A. Wimmer *et al.*, "Human blood vessel organoids as a model of diabetic vasculopathy," *Nature*, vol. 565, no. 7740, pp. 505–510, Jan. 2019, doi: 10.1038/S41586-018-0858-8.

[165] G. Inana, C. Murat, W. An, X. Yao, I. R. Harris, and J. Cao, "RPE phagocytic function declines in age-related macular degeneration and is rescued by human umbilical tissue derived cells," *Journal of Translational Medicine*, vol. 16, no. 1, Mar. 2018, doi: 10.1186/s12967-018-1434-6.

[166] J. W. Crabb *et al.*, "Drusen proteome analysis: An approach to the etiology of age-related macular degeneration," *Proceedings of the National Academy of Sciences of the United States of America*, vol. 99, no. 23, pp. 14682–14687, Nov. 2002, doi: 10.1073/pnas.222551899.

[167] C. C. W. Klaver *et al.*, "Genetic association of apolipoprotein E with age-related macular degeneration," *American Journal of Human Genetics*, vol. 63, no. 1, pp. 200–206, Jul. 1998, doi: 10.1086/301901.

[168] C. A. Curcio, J. B. Presley, C. L. Millican, and N. E. Medeiros, "Basal deposits and drusen in eyes with age-related maculopathy: evidence for solid lipid particles," *Experimental Eye Research*, vol. 80, no. 6, pp. 761–775, Jun. 2005, doi: 10.1016/J.EXER.2004.09.017.

[169] Q. Zhang *et al.*, "Highly Differentiated Human Fetal RPE Cultures Are Resistant to the Accumulation and Toxicity of Lipofuscin-Like Material," *Investigative ophthalmology & visual science*, vol. 60, no. 10, pp. 3468–3479, Aug. 2019, doi: 10.1167/iovs.19-26690.

[170] A. Alaimo *et al.*, "Toxicity of blue led light and A2E is associated to mitochondrial dynamics impairment in ARPE-19 cells: implications for age-related macular degeneration," *Archives of Toxicology 2019 93:5*, vol. 93, no. 5, pp. 1401–1415, Feb. 2019, doi: 10.1007/S00204-019-02409-6.

[171] V. M. Parmar, T. Parmar, E. Arai, L. Perusek, and A. Maeda, "A2E-associated cell death and inflammation in retinal pigmented epithelial cells from human induced pluripotent stem cells," *Stem Cell Research*, vol. 27, pp. 95–104, Mar. 2018, doi: 10.1016/j.scr.2018.01.014.

[172] S. Velilla *et al.*, "Smoking and Age-Related Macular Degeneration: Review and Update," *Journal of Ophthalmology*, vol. 2013, p. 11, 2013, doi: 10.1155/2013/895147.

[173] S. Dalvi *et al.*, "Environmental stress impairs photoreceptor outer segment (POS) phagocytosis and degradation and induces autofluorescent material accumulation in hiPSC-RPE cells," *Cell Death Discovery*, vol. 5, no. 1, pp. 1–16, Dec. 2019, doi: 10.1038/s41420-019-0171-9.

[174] O. Arjamaa *et al.*, "Hypoxia and inflammation in the release of VEGF and interleukins from human retinal pigment epithelial cells," *Graefe's Archive for Clinical and Experimental Ophthalmology*, vol. 255, no. 9, pp. 1757–1762, Sep. 2017, doi: 10.1007/s00417-017-3711-0.

[175] P. Mammadzada, P. M. Corredoira, and H. André, "The role of hypoxia-inducible factors in neovascular age-related macular degeneration: a gene therapy perspective," *Cellular and Molecular Life Sciences*, vol. 77, no. 5. Springer, pp. 819–833, Mar. 01, 2020, doi: 10.1007/s00018-019-03422-9.

[176] A. Ly, L. Nivison-Smith, N. Assaad, and M. Kalloniatis, "Fundus Autofluorescence in Age-related Macular Degeneration," *Optometry and Vision Science*, vol. 94, no. 2. Lippincott Williams and Wilkins, pp. 246–259, Feb. 01, 2017, doi: 10.1097/OPX.0000000000000997.

[177] J. Sparrow and T. Duncker, "Fundus Autofluorescence and RPE Lipofuscin in Age-Related Macular Degeneration," *Journal of Clinical Medicine*, vol. 3, no. 4, pp. 1302–1321, Nov. 2014, doi: 10.3390/jcm3041302.

[178] A. D. Marmorstein, L. Y. Marmorstein, H. Sakaguchi, and J. G. Hollyfield, "Spectral profiling of autofluorescence associated with lipofuscin, Bruch's membrane, and sub-RPE deposits in normal and AMD eyes," *Investigative Ophthalmology and Visual Science*, vol. 43, no. 7, 2002.

[179] R. F. Mullins, L. v. Johnson, D. H. Anderson, and G. S. Hageman, "Characterization of drusen-associated glycoconjugates," *Ophthalmology*, vol. 104, no. 2, 1997, doi: 10.1016/S0161-6420(97)30322-4.

[180] T. L. van der Schaft, C. M. Mooy, W. C. de Bruijn, and P. T. V. M. de Jong, "Early stages of age-related macular degeneration: An immunofluorescence and electron microscopy study," *British Journal of Ophthalmology*, vol. 77, no. 10, 1993, doi: 10.1136/bjo.77.10.657.

[181] V. C. Oliveira *et al.*, "Sudan Black B treatment reduces autofluorescence and improves resolution of in situhybridization specific fluorescent signals of brain sections," *Histology and Histopathology*, vol. 25, no. 8, 2010, doi: 10.14670/HH-25.1017.

[182] D. Pauleikhoff, C. A. Harper, J. Marshall, and A. C. Bird, "Aging Changes in Bruch's Membrane: A Histochemical and Morphologic Study," *Ophthalmology*, vol. 97, no. 2, pp. 171–178, Feb. 1990, doi: 10.1016/S0161-6420(90)32619-2.

[183] A. Abdelsalam, L. del Priore, and M. A. Zarbin, "Drusen in age-related macular degeneration: Pathogenesis, natural course, and laser photocoagulation-induced regression," *Survey of Ophthalmology*, vol. 44, no. 1. Elsevier Inc., pp. 1–29, 1999, doi: 10.1016/S0039-6257(99)00072-7.

[184] C. S. Young *et al.*, "A single CRISPR-Cas9 deletion strategy that targets the majority of DMD patients restores dystrophin function in hiPSC-derived muscle cells," *Cell stem cell*, vol. 18, no. 4, p. 533, Apr. 2016, doi: 10.1016/J.STEM.2016.01.021.

[185] D. Hockemeyer and R. Jaenisch, "Induced pluripotent stem cells meet genome editing," *Cell stem cell*, vol. 18, no. 5, p. 573, May 2016, doi: 10.1016/J.STEM.2016.04.013.

[186] Y. Li *et al.*, "Gene therapy in patient-specific stem cell lines and a preclinical model of retinitis pigmentosa with membrane frizzled-related protein defects," *Molecular Therapy*, vol. 22, no. 9, pp. 1688–1697, 2014, doi: 10.1038/mt.2014.100.

[187] S. Pars, K. Achberger, A. Kleger, S. Liebau, and N. Pashkovskaia, "Generation of Functional Vascular Endothelial Cells and Pericytes from Keratinocyte Derived Human Induced Pluripotent Stem Cells," *Cells 2021, Vol. 10, Page 74*, vol. 10, no. 1, p. 74, Jan. 2021, doi: 10.3390/CELLS10010074.

[188] W. Haenseler *et al.*, "A Highly Efficient Human Pluripotent Stem Cell Microglia Model Displays a Neuronal-Co-culture-Specific Expression Profile and Inflammatory Response," *Stem Cell Reports*, vol. 8, no. 6, p. 1727, Jun. 2017, doi: 10.1016/J.STEMCR.2017.05.017.

6 Statement of contributions

Aged Human iPSC-RPE organoid cultures display hallmarks of Drusen formation

L. Mesch*, N. Pashkovskaia*, V. Cora, S. Pars, S. Corti, M. Cipriano, P. Loskill, E. Koertvely, S. Kustermann, M. Mesquida, A. Kleger, S. Liebau and K. Achberger.

In preparation

In this project, we aimed to demonstrate the suitability of hiPSC-derived RPE organoids as in vitro models for AMD, as they contain hallmarks of drusen formation. Figures 3-2 and 3-5 to 3-17 in the current thesis are adapted from this manuscript. For this publication, I contributed in conceptualization and to methodology of all performed experiments, performed imaging and data analysis and wrote the initial draft of the manuscript. N. Pashkovskaia contributed by conceptualization and writing. K. Achberger contributed by conceptualization, writing and supervision of the project.

*shared co-first-authorship

7 Acknowledgements

I sincerely thank Prof. Dr. Stefan Liebau for supervising my thesis. Thank you for the opportunity to contribute my ideas, invaluable advice, and support during the last years. I would like to thank my Advisory Board Committee members Prof. Dr. Peter Loskill and Prof. Dr. Meltem Avci-Adali for their interest in my projects, for many helpful ideas and fruitful discussions.

I would like to thank all my colleagues for the time we spent together. In particular, I thank Dr. Kevin Achberger and Dr. Natalia Pashkovskaia for the patient mentoring; Virginia Cora, Selin Pars, Dr. Serena Corti, Anamaria Bernal-Vergara, Sabine Conrad, Clara Mishbah, Lara Kressing, Dr. Stefanie Klingenstein, Dr. Moritz Klingenstein and Dr. Alfio Milazzo for the pleasant working atmosphere and the constant support. I would also like to thank all students that joined my projects for their contributions and wish them all the best for their scientific careers.

Furthermore, I would like to thank all cooperation partners: Johanna Chuchuy, Dr. Madalena Cipriano and all the members of the µOrgano-Lab; the institute of ophthalmic research; Dr. Deborah Kronenberg-Versteeg from the Hertie-Institute for clinical brain research.

I am very grateful to the Graduate Training Centre of Neuroscience for their help with all administrative duties, outstanding scientific training and activities that helped me to develop myself further scientifically and personally. I would like to express my sincere gratitude to Michael Lehner and Kirsten Wermter for their help with all administrative difficulties.

Finally, I would like to thank my family and my friends: my parents Astrid and Bernd Antkowiak for enabling and supporting my scientific career; my friends for motivating me; my husband Julian Mesch for his continuous support and faith in me.